Chemical Factors Influencing Colloid Mobilization and Th(IV) Transport through Saturated Subsurface Sediment

by

Brian Haliena

A thesis submitted to the Graduate Faculty of
Auburn University
in partial fulfillment of the
requirements for the Degree of
Master of Science

Auburn, Alabama
August 4, 2012

Keywords: Actinide, Thorium(IV), Colloid,
Mobilization, Subsurface, Savannah River

Approved by

Mark O. Barnett, Chair, Malcolm Pirnie Professor of Civil Engineering
Dongye Zhao, Huff Professor of Civil Engineering
Ahjeong Son, Assistant Professor of Civil Engineering

Abstract

In recent years, subsurface colloid mobilization has attracted considerable attention due to its suspected role in enhancing the transport of strongly adsorbing contaminants. Such colloid-facilitated contaminant transport can be induced by changes in groundwater solution chemistry, for example decreases in ionic strength and increases in pH. In this study, colloid mobilization and its effect on the transport of Th(IV), an analog for Pu(IV), were investigated after introducing changes in solution chemistry to saturated columns packed with a heterogeneous, Fe-containing subsurface sand collected from the Savannah River Site (SRS). The SRS is a Department of Energy (DOE) site located in South Carolina that has suffered from significant actinide contamination due to its historical production of nuclear materials for the use in nuclear weapons. Transport experiments in this study were performed by sorption/ mobilization experiments, where Th(IV) was first sorbed to the SRS sediment under conditions minimizing colloid detachment (e.g. high ionic strength) and then mobilized by conditions releasing natural colloids as a result of decreased ionic strength or elevated pH. This method simulated realistic scenarios at DOE waste sites, where groundwater plumes of radioactive waste containing high concentrations of electrolytes have been replaced by infiltrating dilute rainwater from the surface.

After Th(IV) was sorbed to the SRS sediment at a pH of 4, decreases in solution salinity promoted the mobilization of natural colloids from the surface of the SRS sediment, along with significantly enhancing the transport of Th(IV). However, contrary to the original hypothesis,

colloid-facilitated transport played only a minor role in enhancing the transport of Th(IV). Instead, the enhanced transport of Th(IV) was primarily attributed to a decreased pH front accompanying the change in solution salinity, causing higher concentrations of Th(IV) to desorb from the SRS sediment. Results from this study also showed that sorption of Th(IV) had a significant impact on the surface charge of the SRS sediment, affecting the release of colloids. In the absence of Th(IV), colloids were released from the SRS sediment only after increases in influent solution pH, while changes in solution salinity at the lower pH range were ineffective at releasing colloids. In contrast, when Th(IV) was sorbed to the SRS sediment, changes in solution salinity at the lower pH range liberated significant concentrations of colloids.

Acknowledgments

The author would especially like to express his gratitude for the excellent instruction, support, and guidance of his advisor, Dr. Mark Barnett. Without his support, the author would have never had this wonderful opportunity at Auburn University. Additional thanks is expressed to the author's committee members, Dr. Dongye Zhao and Dr. Ahjeong Son, along with the rest of the environmental faculty in the Civil Engineering Department for their inspiring instruction, knowledge, and support during the author's two year term at Auburn University. In addition, the author would like to express his gratitude to Jinling Zhuang for his technical assistance and guidance in the environmental laboratory at Auburn University. His experience in the laboratory, along with his vast knowledge in analytical chemistry made experimentation an accurate, but efficient process. The author would especially like to thank members of his research team, Nathan Melson and Hangping Zheng, for their advice, guidance, and assistance with experiments and other work in the laboratory. Finally, the author would like to thank his family and friends who supported him throughout his studies here at Auburn University. This research was financially supported by the Office of Science's Biological and Environmental Research (BER), U.S. Department of Energy.

Table of Contents

List of Tables

List of Figures

Chapter One.

Introduction

1.1 Problem Statement

Since the 1940's, significant quantities of actinides have accumulated worldwide due to the activities of nuclear weapons programs and nuclear power production (Ahearne, 1997). Unfortunately, improper storage and nuclear weapons testing have released large amounts of actinides into the subsurface, contaminating groundwater aquifers with long-lived, highly toxic, radioactive waste (Ahearne, 1997; Runde, 2000). Some of the highest local concentrations of actinide contamination are found at Department of Energy (DOE) sites, where uranium and plutonium were historically produced and tested for nuclear weapons (Cantrell et al., 2008). Despite the deployment of DOE-funded remediation programs at these sites, significant amounts of subsurface contaminants are likely to remain even after cleanup efforts (Runde, 2000). In addition to these sources, future plans for permanent geological repositories for spent nuclear fuel will potentially introduce much more quantities (up to 70,000 tons) of radioactive waste into the subsurface (Povetko, 2008; Vašíček et al., 2011). The main goal of the repository is to delay the release of radioactive waste until the radiological impacts are within acceptable levels, which could take over ten thousand years (Long et al., 2004). Therefore, the study of actinide biogeochemical transport is extremely important to prevent actinides stored at repositories and waste sites from migrating through the subsurface environment.

Actinides, especially those in the tetravalent oxidation state, tend to have low solubility (below micromolar concentrations) in natural waters due to the precipitation of oxyhydroxide solids (Runde, 2000; Neck et al., 2001; Runde et al., 2002). In addition, they also have strong affinities to many types of aquifer sediments (Runde, 2000; Runde et al., 2002). Therefore, simple aqueous-phase contaminant transport models have predicted actinides to be almost immobile at contaminated DOE sites where many actinides have been released (Kersting et al., 1999). This type of transport model relies on the assumption that the solid aquifer matrix remains immobile, which in many situations is a reasonable assumption. However, several field studies have discovered actinides to be long distances (up to several kilometers) away from their original source (Penrose et al., 1990; Kaplan et al., 1994; Kersting et al., 1999; Novikov et al., 2006). In these studies, a significant fraction of the migrated actinides was associated with colloids, which has led the scientific community to believe that colloid-facilitated transport was responsible for their faster-than-predicted transport.

Colloidal particles are ubiquitous in natural aqueous environments, consisting of inorganic mineral phases and organic biopolymers with diameters less than 10 μm (McCarthy et al., 1989). Due to their small size, they have very large specific surface areas ranging from 10 to 800 m^2/g (Kretzschmar et al., 2005). This property makes colloids very reactive from a physiochemical perspective, allowing them to have high sorption capacities for actinides and other strongly adsorbing contaminants. Therefore, colloids have the potential to carry bound contaminants as they migrate through the groundwater, capable of increasing a contaminant's concentration by several orders of magnitude over the values expected from solubility calculations. In groundwater aquifers, natural colloidal suspensions are formed due to (1) the release of fine particles from the porous media by chemical, physical and biological

disturbances, such as fluctuations in water saturation, flow velocity, biofilm coating, and aqueous solution chemistry (McCarthy et al., 1989; Ryan et al., 1994; Ryan et al., 1994; Seaman et al., 1995; Kaplan et al., 1996; Ryan et al., 1996; Roy et al., 1997; Bunn et al., 2002; McCarthy et al., 2004; Grolimund et al., 2006; Cheng et al., 2010; Li et al., 2012) and (2) *in situ* precipitation of supersaturated mineral phases (Liang et al., 2000; Wan et al., 2004). However, McCarthy et al. (1993) discovered that most colloids existing in groundwater systems appear to be mobilized by changes in solution chemistry, such as decreases in ionic strength and increases in pH. These chemical fluctuations release colloids by increasing the electrostatic repulsive force between colloids and the immobile aquifer grains. Once significant quantities of colloids are released by changes in solution chemistry, they have the potential to enhance the migration of contaminants from waste sites.

In spite of the limited field-scale evidence, many laboratory column transport experiments have confirmed that colloids can enhance the transport of strongly-sorbing contaminants through saturated porous media (Puls et al., 1992; Roy et al., 1997; Um et al., 2002; Mori et al., 2003; Grolimund et al., 2005; Zhang et al., 2007; Cheng et al., 2010; Crancon et al., 2010; Zhou et al., 2011). However, few laboratory studies have demonstrated colloid-facilitated transport of actinide elements. Therefore, further studies are needed to determine whether colloid-facilitated transport is an important mechanism responsible for enhancing the migration of actinides. At many DOE sites, plutonium is one of the main actinides of concern (Cantrell et al., 2008). However, the study of plutonium is extremely complex due to its variable oxidation state behavior, capable of existing in three different oxidation states simultaneously in natural waters (Runde, 2000; Choppin, 2007). This has caused several studies to use Th(IV) as an analog for Pu(IV), along with other complex tetravalent actinides, due to its similar chemical

characteristics in the +IV oxidation state (Choppin, 1999; Guo et al., 2005; Hongxia et al., 2006; Hongxia et al., 2007). In addition, thorium is stable in the tetravalent oxidation sate, which is the most prevalent oxidation state of plutonium in natural groundwater environments (Runde, 2000). However unlike plutonium, the oxidation state of Th(IV) is not a function of its concentration, making it a particularly valuable analog for assessing the behavior of Pu(IV) in the environment (Choppin, 1999). In addition to its use as an analog, thorium contamination could become more relevant in the future due to the use of thorium-based fuels for nuclear power production (Schapira et al., 1999).

1.2 Objectives

The primary objectives of this thesis were 1) to determine if changes in solution chemistry, such as decreases in ionic strength or increases in pH, would promote the *in situ* mobilization of natural colloidal particles from a saturated heterogeneous, Fe-containing subsurface sand collected from the Savannah River Site (SRS), and 2) to determine whether these changes would enhance the transport of Th(IV) sorbed to the SRS sediment. The SRS is a Department of Energy (DOE) site located in South Carolina that has suffered from significant actinide contamination due to its historical production of nuclear materials for the use in nuclear weapons. Saturated column transport experiments were used to meet these objectives. The transport experiments were performed by sorption/mobilization experiments, where Th(IV), an analog for Pu(IV) and other tetravalent actinides, was first sorbed to the SRS subsurface sediment under conditions that minimized colloid detachment (e.g. high ionic strength) and then mobilized by conditions inducing natural colloids to be released as a result of decreased ionic strength or increased pH.

1.3 Organization

The organization of this report follows the guidelines for a publication-style thesis as outlined in the *Guide to Preparation and Submission of Theses and Dissertations* by Auburn University Graduate School. The thesis is broken down into four different chapters. Chapter one identifies the problem and key objectives of the study. Chapter two consists of an in-depth literature review of background material relevant to the study. The materials, methods, results, and discussion from the column transport experiments are presented in chapter three. This chapter is formatted as a draft manuscript, which will later be submitted for publication in a peer-reviewed scientific journal. The final chapter, chapter four, contains the conclusions from the study, as well as recommendations for future work. Supporting information not presented in the body of the thesis is located in the appendices.

.

Chapter Two.

Literature Review

2.1 Radioactive Waste and Contamination

Over the past sixty years, the nuclear fuel cycle has produced large quantities of radioactive waste. In 1990, the estimated accumulations of transuranic actinides in spent nuclear fuel were 472 tons of plutonium, 28 tons of neptunium, 6 tons of americium, and 1.6 tons of curium (Runde, 2000). These transuranic actinides, along with uranium, are long-lived, radioactive, and highly toxic. Currently, the United States stores most of its spent nuclear fuel rods in above-ground temporary storage facilities awaiting the Department of Energy's (DOE) approval for permanent storage in repositories located hundreds of meters underground, such as Yucca Mountain (Ahearne, 1997). However, the use of long-term storage facilities has been delayed due to the public's fear of actinide migration from these sites, potentially contaminating vast areas of land with long-lasting radioactive waste.

Fortunately, the release of radioactive waste into the environment via nuclear energy production has been relatively small in comparison to the amount from nuclear weapons testing, which has contributed to the predominant source of actinide contamination in the environment (Choppin, 2007). A recent estimate by the DOE predicted that over 73 million cubic meters of soil in the United States alone have been contaminated with actinides from nuclear defense programs (Ahearne, 1997). Of the contaminated sites, some of the highest local concentrations of actinides are found at DOE sites where uranium and plutonium were produced and tested for

nuclear weapons, such as the Savannah River Site, Hanford Site, Rocky Flats Environmental Technology Site, Idaho National Laboratory, Los Alamos National Laboratory, Nevada Test Site, and Oak Ridge National Laboratory (Cantrell et al., 2008). Most of these sites are on the Environmental Protection Agency's (EPA) National Priority List (NPL), which has caused them to shift much of their focus to environmental cleanup. Despite the deployment of DOE-funded remediation programs at these sites, significant amounts of subsurface contaminants are likely to remain even after cleanup efforts (Runde, 2000).

2.2 Actinides and the Environment

Along with being very hazardous elements, actinides have some of the most complex chemistry in the periodic table, further complicating their fate and transport through the environment. Actinides are located in the last row of the periodic table, comprising elements with atomic numbers 89 (actinium) to 103 (lawrencium). This group of elements has electrons filling the 5 f orbital, which exposes them far from the nucleus causing many of the actinides to exhibit multiple oxidation states and to form dozens of molecularly distinct species (Clark et al., 1995; Runde, 2000). For instance, in a simple aqueous system, plutonium can exist in three oxidation states simultaneously (Choppin, 1999; Runde, 2000). Like plutonium, uranium and neptunium can also exist in several oxidation states. However, some actinides, such as Am(III), Cm(III), and Th(IV), tend to be present in only one oxidation state (Choppin, 2007). Actinides existing in the same oxidation state, e.g., U(IV), Pu(IV), Np(IV), and Th(IV), tend to have similar chemical characteristics (Choppin, 1999). Therefore, analogs have been used to study the migration of some of the more complex actinides, such as plutonium (Choppin, 1999; Guo et al., 2005; Hongxia et al., 2006; Hongxia et al., 2007).

The concentration of different actinide oxidation states is dependent on pH, E_h and the presence of suspended particulates. Of the different actinide oxidation states, each one has a different chemical behavior, which further complicates the prediction of their migration through the environment (Choppin, 2007). Actinides in the +III and +IV oxidation state exist as simple monotonic cations (An^{+3} and An^{+4}) in solution, while the highly charged actinides in the +V and +VI oxidation states are unstable in aqueous solution and instantly hydrolyze to form linear trans-dioxo cations (AnO_2^{+} and AnO_2^{+2}), or actinyl ions (Choppin, 1999). Since actinides in the +IV oxidation state have the highest effective charge, they form the most stable solution complexes, along with the most stable precipitates with the lowest solubility (Runde, 2000). Therefore, their migration through the environment is strongly hindered by their low solubility. On the contrary, actinides in the +V oxidation state form weak complexes in solution, and their solubility-controlling solids are most soluble, causing them to be more likely to migrate through the environment. Actinide solids generally precipitate as amorphous solids, sometimes in colloidal form, but over time tend to crystallize or age, lowering their solubility (Runde, 2000). Understanding the solution chemistry of actinides is extremely important in developing radioactive waste remediation and long-term management strategies.

2.3 Thorium(IV) as an Analog for Plutonium(IV)

Studies concerning the chemical behavior of plutonium in the environment have been extremely complex due to its variable oxidation state behavior. In addition, plutonium is highly regulated and there are many health hazards involved in working with it. Therefore, many research teams have used oxidation state analogs which mimic the plutonium species to better understand plutonium behavior in the environment. In most ocean and groundwater environments, plutonium's predominant and most stable oxidation state is Pu(IV) (Runde, 2000).

Therefore, in order to simplify the research of Pu(IV), many studies have used Th(IV) as an analog. In a review of plutonium oxidation state analogs, Choppin (1999) states that Th(IV) is the best oxidation state analog for Pu(IV). However, the complexation and hydrolytic tendencies of Th(IV) are somewhat weaker than Pu(IV). Therefore, the use of Th(IV) as a model for Pu(IV) behavior requires adjustment factors, which are calculated based on the ionic radius of Th(IV) being nine percent larger than that of Pu(IV) (Choppin, 1999). The use of these correction factors, allows Th(IV) to accurately be used in modeling the behavior of Pu(IV) in solution.

2.4 General Thorium Mineralogy, Chemistry, and Toxicology

Of the actinide elements, thorium and uranium are the only ones to occur naturally in substantial quantities within the Earth's crust (Clark et al., 1995). However, thorium is about three times more abundant than uranium and occurs at very low concentrations in virtually all rock, soil, and water (Peterson et al., 2007). Therefore, it is also found in plants and animals (EPA, 2011). The average concentration of thorium in soil is about 6 parts per million (ATSDR, 1990). However, minerals such as monazite sand, which is the chief commercial source, can contain higher concentrations up to 3 to 10 percent thorium dioxide (Peterson et al., 2007). Other less common minerals, such as thorite (thorium silicate) and thorianite (mixed thorium and uranium oxides), can contain much greater amounts of thorium (Peterson et al., 2007).

Like all actinide elements, thorium is radioactive. It can exist in more than ten different isotopes. However, 99 percent of natural thorium is in the isotope form of thorium-232, whereas the other isotopes are mostly man-made (ATSDR, 1990). Thorium-232 has a half life of 14 billion years, slowly decaying by alpha emission into radium-228 and radon-220 (EPA, 2011). In its pure form, thorium is a soft, silvery white metal that slowly tarnishes to a black color after

being exposed to air. When heated, thorium oxide glows bright white, which is why it has historically been used in lantern mantles (Peterson et al., 2007). Thorium is the second element in the actinide series with an atomic number 90. In its pure form it has the electron configuration of $[Rn]6d^27s^2$, which causes it to lose four electrons when forming compounds, creating a stable + IV oxidation state.

The Agency for Toxic Substances and Disease Registry (ATSDR) ranked thorium at 102 on the 2011 Priority List of Hazardous Substances (ATSDR, 2011). Although thorium is considered toxic, the main health hazards are attributed to its radioactivity. External exposure to thorium is generally not a health concern, because it emits only small amounts of gamma radiation. Therefore, thorium is usually only a health hazard if it enters the body (Peterson et al., 2007). The main routes of exposure are from ingestion of food or water containing thorium or inhalation of thorium contaminated dust. Once in the body, the ionizing radiation of thorium can cause increased risks of cancer, such as lung and bone cancer. Both the EPA and the ATSDR consider thorium as a known carcinogen (ATSDR, 1990; EPA, 2011). In order to protect the public from radionuclides in drinking water, the EPA has set a Maximum Contaminant Level (MCL) for alpha emitters, such as thorium, at 15 pCi/L or 136 μg-Th/L in drinking water (ATSDR, 1990).

2.5 Th(IV) Aqueous Speciation

In aqueous solutions, many metal ions complex with water and other anions in solution to form multiple chemical species. This distribution of an element among its chemical species is called chemical speciation, which can affect a contaminant's solubility, adsorption properties, and toxicity. Therefore, understanding the speciation of an element is particularly important

when trying to model its behavior in the environment. Several techniques can be used to measure different species in solution, such as potentiometric titration and solvent extraction (Ekberg et al., 2000). In natural environments, hydroxide and carbonate are the most important ligands responsible for metal complexation, which usually form multiple distinct metal species (Runde, 2000).

In aqueous solutions, free metal ions complex with water molecules forming hydrated ions ($M(H_2O)_n^{z+}$). These hydrated metal ions can behave as Lewis acids, causing a proton to be transferred from the hydrated metal to water, forming hydroxide complexes. The process is called metal hydrolysis, which can be seen in the reaction below (Snoeyink et al., 1980).

$$[M(H_2O)_n]^{z+} + H_2O \leftrightarrow [M(H_2O)_{n-1}(OH)]^{(z-1)} + H_3O^+$$

Due to metal hydrolysis, hydrated metal ions can exist as multiple distinct species throughout the pH range.

Thorium undergoes extensive chemical interactions with water and most anions due to its high electric charge (EPA, 1999). However, in comparison with other known tetravalent cations, Th (IV) is the least likely to hydrolyze due to its larger ionic radius (Rand et al., 2008). The hydrolytic behavior of thorium has been studied for over forty years using a variety of ionic background media, including perchlorate (Baes et al., 1965; Grenthe et al., 1991; Ekberg et al., 2000), nitrate (Milić et al., 1982; Brown et al., 1983), and chloride (Šuranji et al., 1981). Nevertheless, its hydrolytic properties are still not fully understood, which can be attributed to the presence of extensive polymerization reactions occurring in a narrow pH range (Ekberg et al., 2000). Therefore, there has been much discrepancy on the agreement of models proposed for its

hydrolysis reactions, causing controversy over which species are formed. In 2008, the Organization for Economic Co-Operation and Development's (OECD) Nuclear Energy Agency (NEA) published a thorium thermodynamic reference book, which has critically reviewed and updated previous thorium thermodynamic data (Rand et al., 2008). The work contributed by the NEA has greatly reduced the uncertainty surrounding thorium solution chemistry and selected the following hydrolytic reactions (Table 2.1) as the most important aqueous species in pure water.

Table 2.1: Aqueous thorium hydrolysis reactions (T=25°C and I=0.0 M) and associated Log K values. Log K constants were calculated from thermodynamic data given by Rand et al. (2008).

Species	Th(IV) Hydroxide Complexation Reactions	Log K
$Th(OH)^{3+}$	$Th^{4+} + H_2O(l) \leftrightarrow H^+ + Th(OH)^{3+}$	-2.500
$Th(OH)_2^{2+}$	$Th^{4+} + 2H_2O(l) \leftrightarrow 2H^+ + Th(OH)_2^{2+}$	-6.200
$Th(OH)_4(aq)$	$Th^{4+} + 4H_2O(l) \leftrightarrow 4H^+ + Th(OH)_4(aq)$	-17.400
$Th_2(OH)_2^{6+}$	$2Th^{4+} + 2H_2O(l) \leftrightarrow 2H^+ + Th_2(OH)_2^{6+}$	-5.900
$Th_2(OH)_3^{5+}$	$2Th^{4+} + 3H_2O(l) \leftrightarrow 3H^+ + Th_2(OH)_3^{5+}$	-6.800
$Th_4(OH)_8^{8+}$	$4Th^{4+} + 8H_2O(l) \leftrightarrow 8H^+ + Th_4(OH)_8^{8+}$	-20.400
$Th_4(OH)_{12}^{4+}$	$4Th^{4+} + 12H_2O(l) \leftrightarrow 12H^+ + Th_4(OH)_{12}^{4+}$	-26.600
$Th_6(OH)_{14}^{10+}$	$6Th^{4+} + 14H_2O(l) \leftrightarrow 14H^+ + Th_6(OH)_{14}^{10+}$	-36.800
$Th_6(OH)_{15}^{9+}$	$6Th^{4+} + 15H_2O(l) \leftrightarrow 15H^+ + Th_6(OH)_{15}^{9+}$	-36.800

As seen in Table 2.1, thorium is capable of forming both mono and polynuclear hydroxide species, where polynuclear species contain more than one thorium atom. Using the thermodynamic data in Table 2.1, a Th(IV) speciation diagram was modeled using Visual MINTEQ in a closed system containing a 0.1 M $NaNO_3$ background solution (Figure 2.1).

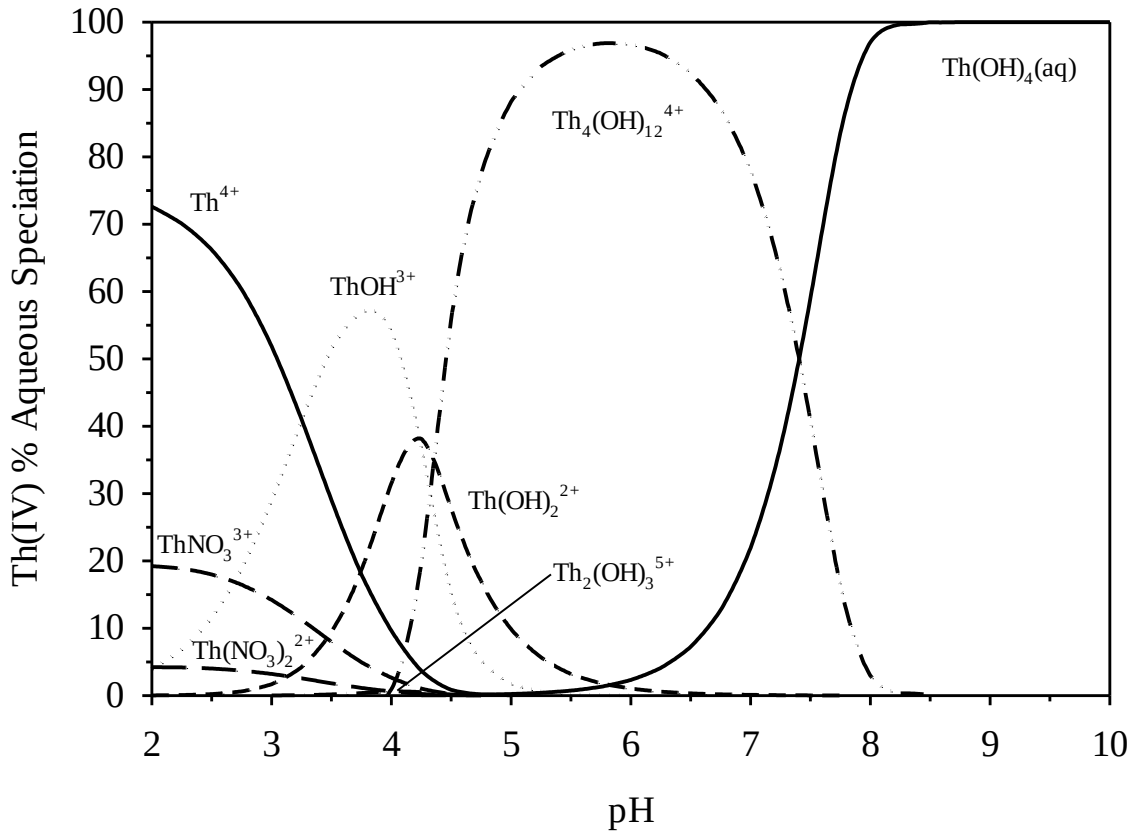

Figure 2.1: Aqueous speciation of 1.14×10^{-5} M Th(IV) as a function of pH. Calculations made on a closed system containing 0.1 M $NaNO_3$ with Visual MINTEQ.

As seen from Figure 2.1, Th(IV) complexes with water and nitrate to form 8 distinct species. In the acidic range (pH<3) the ionic form, Th^{4+}, dominates with the two nitrate species present in lower concentrations (Table 2.2 shows thorium nitrate complexation reactions and their associated Log K constants). From the pH range 3.25 to 4.3, many species are present in significant concentrations, but the $ThOH^{3+}$ is the predominant species. In the pH range of natural waters (4.5<pH<7.5), the polynuclear species, $Th_4(OH)_{12}^{4+}$, has a dominant presence, while the aqueous $Th(OH)_4$ predominates the basic pH range (pH>8).

Table 2.2: Aqueous thorium nitrate complexation reactions (T=25°C and I=0.0 M) and associated Log K values. Log K constants were calculated from thermodynamic data given by Rand et al. (2008).

Species	Th(IV) Nitrate Complexation Reactions	Log K
$\mathbf{ThNO_3^{3+}}$	$\mathbf{Th^{4+} + NO_3^- \leftrightarrow ThNO_3^{3+}}$	1.300
$\mathbf{Th(NO_3)_2^{2+}}$	$\mathbf{Th^{4+} + 2NO_3^- \leftrightarrow Th(NO_3)_2^{2+}}$	2.300

As mentioned previously, carbonate in addition to hydroxide is another important ligand in natural environments that tends to complex with metals. It is considered the most important acid-base system in aqueous solutions, consisting of the following species: gaseous CO_2, CO_2(g), aqueous CO_2, CO_2(aq), carbonic acid, H_2CO_3, bicarbonate, HCO_3^-, carbonate, CO_3^{2-}, and carbonate-containing solids (Snoeyink et al., 1980). Like with many metals, carbonate forms strong complexes with thorium. The effect of the carbonate on thorium solubility and complexation has been studied by either using CO_2(g) at different partial pressures (Östhols et al., 1994; Altmaier et al., 2005), or by using carbonate/bicarbonate buffer solutions, giving constant carbonate concentrations (Felmy et al., 1997; Felmy et al., 1999; Altmaier et al., 2006). However, much like the thorium hydrolysis studies, there has been significant discrepancy between thorium carbonate studies. Therefore, the OECD NEA summarized the literature, selecting the following thorium carbonate complexation reactions in Table 2.3 as the most important (Rand et al., 2008). Using the thermodynamic data in Table 2.3, a thorium speciation diagram (Figure 2.2) was modeled using Visual MINTEQ in an open system (log P_{CO2} = -3.5 atm) containing a 0.1 M $NaNO_3$ background solution. In Figure 2.2, as the pH increases carbonate enters the system from the atmosphere forming several different thorium carbonate

species. The introduction of carbonate strongly affects the speciation of thorium at basic pH ranges (pH>8).

Table 2.3: Aqueous thorium carbonate complexation reactions (T=25°C and I=0.0 M) and associated Log K values. Log K constants were calculated from thermodynamic data given by Rand et al. (2008).

Species	Th(IV) Nitrate Complexation Reactions	Log K
$\mathbf{Th(CO_3)_5^{6-}}$	$\mathbf{Th^{4+} + 5CO_3^{2-} \leftrightarrow Th(CO_3)_5^{6-}}$	31.000
$\mathbf{ThOH(CO_3)_4^{5-}}$	$\mathbf{Th^{4+} + 4CO_3^{2-} + H_2O(l) \leftrightarrow H^{+} + ThOH(CO_3)_4^{5-}}$	21.600
$\mathbf{Th(OH)_2(CO_3)_2^{2-}}$	$\mathbf{Th^{4+} + 2CO_3^{2-} + 2H_2O(l) \leftrightarrow 2H^{+} + Th(OH)_2(CO_3)_2^{2-}}$	8.800
$\mathbf{Th(OH)_4(CO_3)^{-2}}$	$\mathbf{Th^{4+} + CO_3^{2-} + 4H_2O(l) \leftrightarrow 4H^{+} + Th(OH)_4(CO_3)^{2-}}$	-15.600

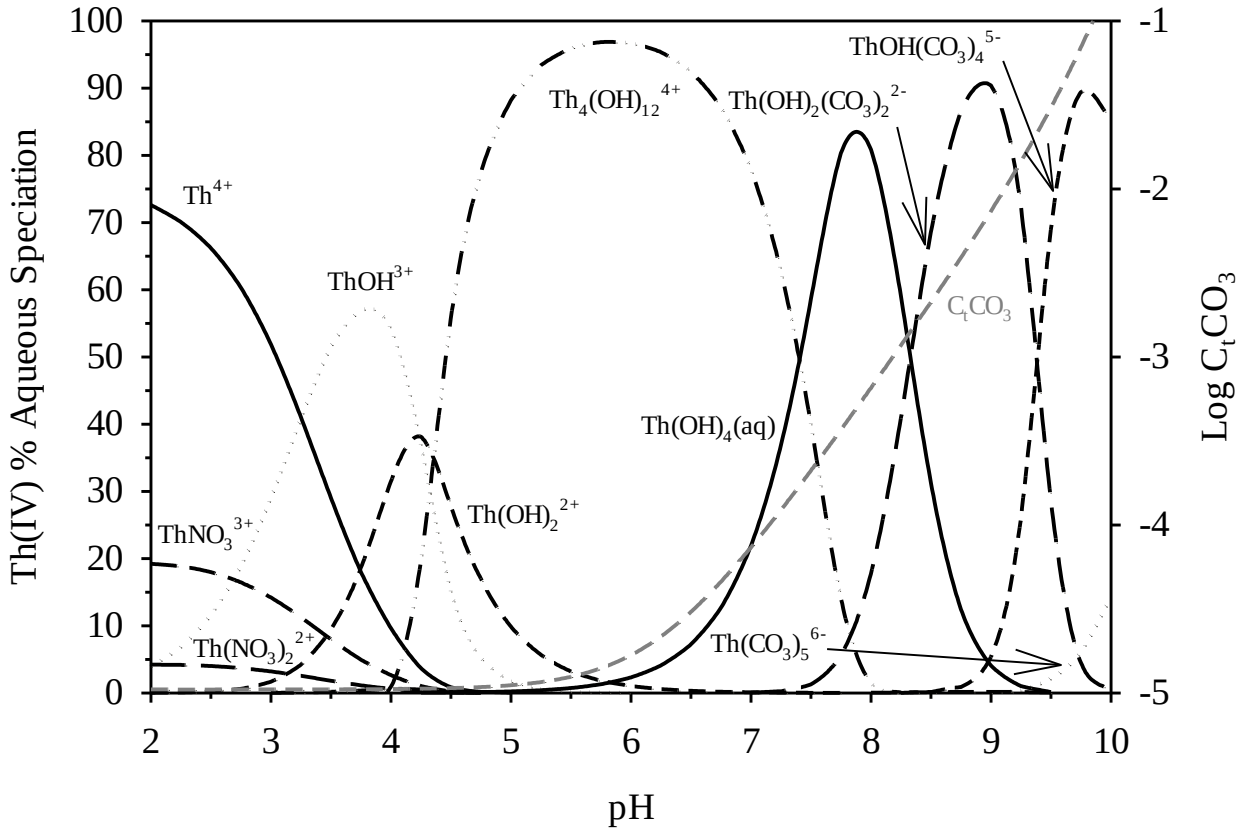

Figure 2.2: Aqueous speciation of $1.14x10^{-5}$ M Th(IV) and Log total dissolved carbonate concentration (dashed line) as a function of pH. Calculations made on an open system with Log P_{CO2} = -3.5atm containing 0.1M $NaNO_3$ with Visual MINTEQ.

2.6 Th(IV) Solubility

In terms of environmental engineering, solubility quantifies how much of a contaminant (solid) can be dissolved in aqueous solutions. It is a very important property in the study of contaminant fate and transport, because it can be a limiting factor for the migration of a contaminant through the environment. The solubility of a substance can be dependent on many factors, including temperature, ionic strength, pressure, polarity, and particle size. The dissolution of a solid at equilibrium can be calculated by using the solubility product, K_{so}, which is derived from thermodynamic data. The solubility product is an equilibrium constant that describes the reaction by which a solid dissolves in pure water to form its simplest chemical species, as seen below (Snoeyink et al., 1980).

$$A_xB_y(s) \leftrightarrow xA^{y+} + yB^{x-}$$

The concentration of the soluble chemical species can be calculated by using the equilibrium constant equation, K_{so}, seen below.

$$K_{so} = \frac{\{A^{y+}\}^z\{B^{z-}\}^y}{\{A_zB_{y(s)}\}} = [A^{y+}]^z[B^{z-}]^y * \left(\gamma_{Ay+}\right)^z(\gamma_{Bz-})^y$$

The solubility constant can be written in terms of activity or concentration by using activity coefficients, or gamma (Snoeyink et al., 1980).

Much like the hydrolytic properties of thorium, many studies have also concentrated on better understanding the solubility of thorium. The majority of the solubility studies have been conducted by adding appropriate amounts of solid crystalline, microcrystalline, or amorphous thorium oxides to a solution and achieving equilibrium from the direction of undersaturation

(Östhols et al., 1994; Neck et al., 2002; Altmaier et al., 2004). Additional Th(IV) solubility studies have been accomplished by titrating a constant concentration of acidic thorium solution until the formation of solid precipitate or colloids are observed (Bundschuh et al., 2000; Neck et al., 2002). Although numerous studies have been conducted, significant discrepancies on thorium solubility still exist (Neck et al., 2002). The OECD NEA has reviewed and summarized the solubility studies found in the literature, providing more reliable thorium solubility data. The NEA has concluded that thorium participates in the following thermodynamic dissolution reactions shown in Table 2.4 (Rand et al., 2008).

Table 2.4: Th(IV) solubility reactions (T=25°C and I=0.0 M) and associated Log K_{so} values. Log K_{so} constants were calculated from thermodynamic data given by Rand et al. (2008).

Precipitate	Th (IV) Solubility Reactions	Log K_{so}
ThO_2(am, hyd, fresh)	**$Th^{4+} + 2H_2O(l) \leftrightarrow 4H^+ + ThO_2$(am, hyd, fresh)**	-9.300
ThO_2(am, hyd, aged)	**$Th^{4+} + 2H_2O(l) \leftrightarrow 4H^+ + ThO_2$(am, hyd, aged)**	-8.500
ThO_2(cr)	**$Th^{4+} + 2H_2O(l) \leftrightarrow 4H^+ + ThO_2$(cr)**	-1.766

As seen in Table 2.4, thorium can form both amorphous and crystalline solids. However, when thorium begins to precipitate from solution, the solid is considered to be an amorphous thorium hydroxide "$Th(OH)_4$(am)" or a hydrous oxide "ThO_2*xH_2O(am)", which is not a well-defined compound (Rand et al., 2008). Unlike the regular repeating patterns of crystalline solids, amorphous solids have considerable disorder in their structure. Over time, the amorphous thorium hydroxides gain crystallinity, eventually transforming into the less soluble crystalline thorium dioxide, a process enhanced by increased temperature (Rai et al., 2000). However, at room temperature the transformation is a relatively slow process, taking about 270 days (Prasad et al., 1967). Therefore, the thermodynamically stable crystalline thorium dioxide is not expected to control the solubility in natural systems (Rand et al., 2008). Using Visual MINTEQ,

the solubility of the three precipitates in Table 2.4 were modeled as a function of pH based on their thermodynamic solubility products (Figure 2.3).

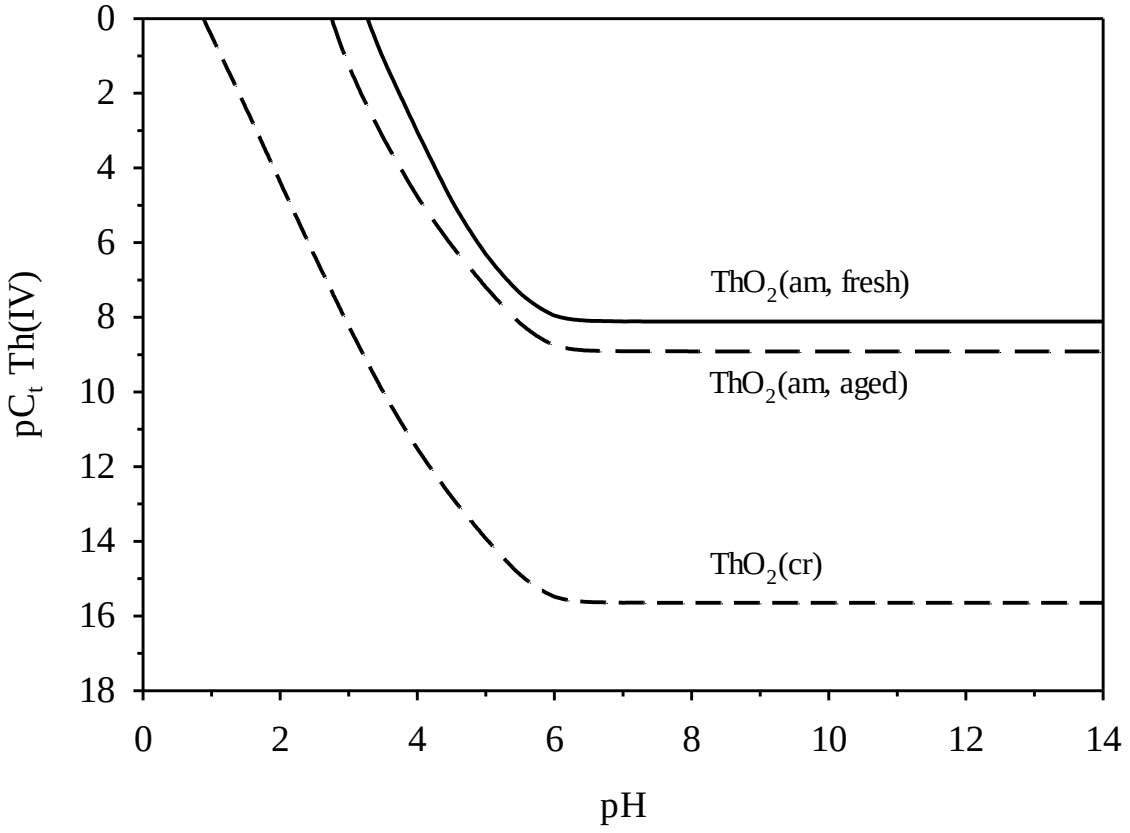

Figure 2.3: Solubility of Th(IV) precipitates as a function of pH. Calculations made on a closed system containing 0.1 M $NaNO_3$ with Visual MINTEQ using Log K_{so} constants from Rand et al. (2008).

As seen from the modeled thermodynamic solubility data, there is a vast difference in solubility between the crystalline thorium dioxide and amorphous thorium hydroxide, up to 8 orders of magnitude. These solubility differences between the two solids are mainly attributed to the particle size or surface hydration (Rand et al., 2008). According to the equations developed by Schindler (1967), the solubility product of oxide and hydroxide particles less than 300 nm

depends significantly on the particle size, because of the difference in Gibbs free energy between small particles and large crystals suspended in solution. Therefore, thorium amorphous solids with crystallite sizes around 3 to 8 nm have significantly greater solubility than the large thorium dioxide crystals with negligible molar surface. However, several studies have shown that the experimental solubility data of crystalline ThO_2(cr) does not reflect the thermodynamic data seen in Figure 2.3 (Moon, 1989; Neck et al., 2003). Experimental data provided by Neck et al. (2003) determined that the solubility of ThO_2(cr) at pHs greater than 2.5 exceed the thermodynamic calculated solubility. At near neutral solutions, the experimental solubility is independent of pH and exceeds the thermodynamic calculation by 6 orders of magnitude, approaching the solubility of thorium hydroxide amorphous solids (Neck et al., 2003). The experimental findings by Neck are thought to be caused by the dissolution of small amounts of amorphous solids present in the crystalline solid, which remain dissolved as hydrolyzed species. The slow dissolution of the crystalline solid followed by the fast hydrolysis reactions of Th(IV) is considered to cause an irreversible dissolution reaction, which reaches equilibrium around the amorphous solid's solubility limit. This can be demonstrated by the following dissolution reaction seen below (Neck et al., 2003).

$$ThO_2 \rightarrow Th_x(OH)_y{}^{4x-y}(aq) \leftrightarrow Th(OH)_4(am)$$

The experimental results from thorium solubility studies demonstrate that thermodynamic data derived from calorimetric measurements with well-prepared crystalline solids (not formed in aqueous solutions) can considerably underestimate the maximum thorium concentrations as well as other tetravalent actinide concentrations (Fanghanel et al., 2002). Therefore, the OECD NEA recommends the use of amorphous thorium hydroxide solubility constants for modeling

thorium solubility in natural systems (Rand et al., 2008). In addition, they classify the $Th(OH)_4(am)$ solid as either being fresh or aged, providing solubility constants for each. This distinction is based on the lower solubility of aged amorphous solid, which is caused by larger particle size. Over time, the fresh amorphous solids increase in particle size by surface recrystallization. The aging effects of the amorphous solid phase is best demonstrated by Higashi (1959), who showed thorium concentrations decreasing over time, eventually reaching the solubility limit of the aged amorphous thorium hydroxide. Although there is no exact borderline between the solubility data for the two amorphous thorium hydroxides, the review by OCED NEA suggests that an equilibrium time of less than 25 days should be used to describe the fresh amorphous solids, while an equilibrium time of greater than 70 days should be used to describe aged amorphous solids (Rand et al., 2008).

As mentioned previously, carbonate forms strong complexes with thorium in aqueous solutions. Consequently, the presence of carbonate can affect the solubility of Th(IV), causing it to become more soluble at neutral to basic pH ranges. Figure 2.4 shows the solubility of Th(IV) precipitates as a function of pH modeled with Visual MINTEQ in an open system with Log P_{CO2}=-3.5 in 0.1 M $NaNO_3$ solution. As seen in Figure 2.4, the thorium solubility begins to increase as carbonate enters the system from the atmosphere, forming thorium carbonate complexes. Therefore, thorium migration could be enhanced in groundwater systems with significant carbonate concentrations.

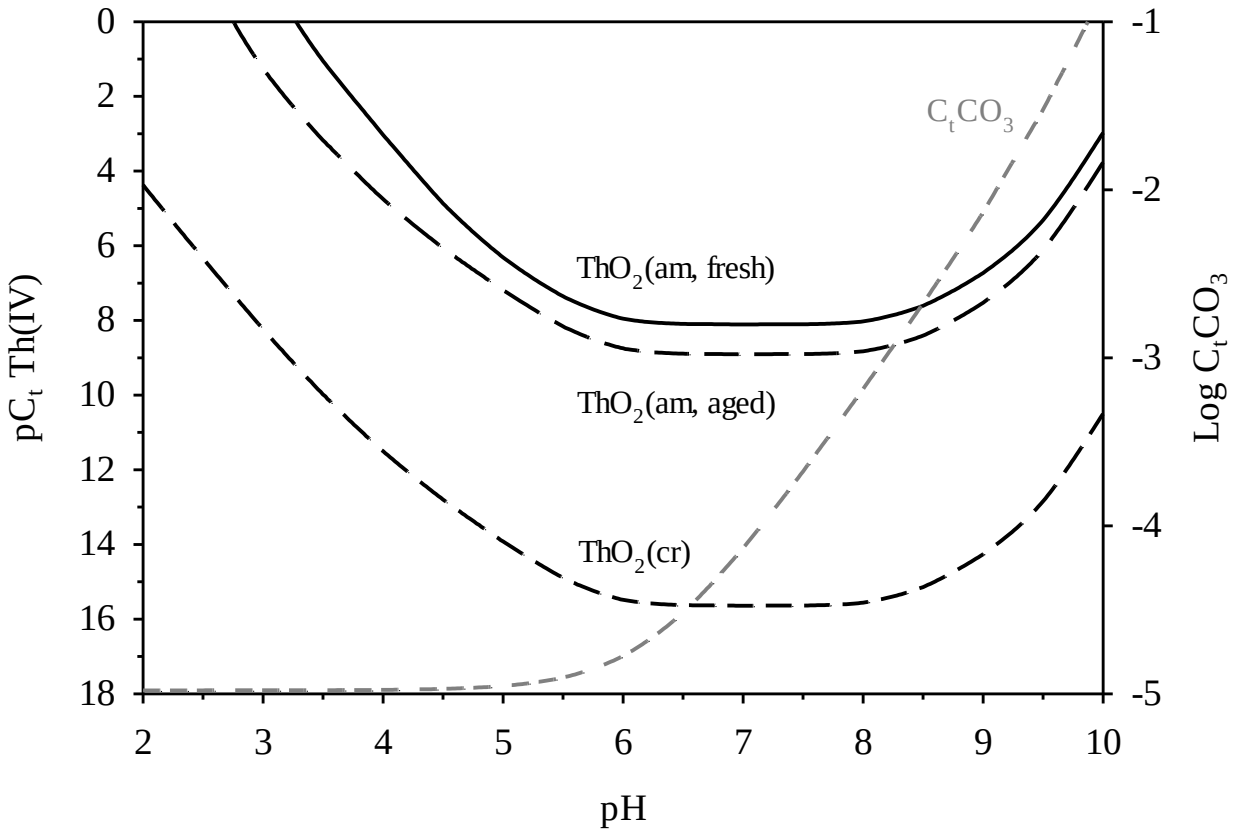

Figure 2.4: Solubility of Th(IV) precipitates and Log total dissolved carbonate concentration (dashed line) as a function of pH. Calculations made on an open system with Log P_{CO2} = -3.5atm containing 0.1 M $NaNO_3$ with Visual MINTEQ using Log K_{so} constants from Rand et al. (2008).

2.7 Sorption of Th(IV) onto Homogenous Metal Oxide and Clay Minerals

The solubility of Th(IV) provides an upper limit to thorium concentration in solution and is considered to be the first barrier to its migration or transport through the environment. Once dissolved in solution, the sorption of thorium onto the surface of surrounding soil particles is expected to act as a secondary barrier. Sorption is a physicochemical process, which can be contributed to physical adsorption, ion exchange, surface complexation (chemisorption), and surface precipitation, all of which attach the adsorbate to a mineral surface, preventing its

transport. Several factors affect the sorption of actinides onto the surface of minerals, including the actinide's concentration and speciation, the groundwater flow rate and aqueous chemistry, and the mineral composition of the surrounding soil (Runde, 2000). Sorption characteristics are typically studied by performing batch adsorption experiments, where the solute is allowed to come into contact with the geomedia of interest until equilibrium is reached. After equilibrium, the difference between the remaining and initial solute concentrations equals the amount adsorbed to the geomedia. Understanding sorption characteristics of actinides can help to predict how they will migrate through the groundwater environment.

2.7.1 Sorption of Th(IV) onto Metal Oxides

Since Th(IV) is an analog for actinides in the IV oxidation state, many sorption experiments have been conducted with thorium onto various types of geomedia. The majority of the Th(IV) sorption studies have been performed with iron oxides, due to the potential use as metallic storage containers for radioactive materials and their abundance in the earth's crust. Of the various iron oxides, Th(IV) sorption has been studied onto magnetite (Rojo et al., 2009; Seco et al., 2009), ferrihydrite (Rojo et al., 2009; Seco et al., 2009), goethite (Hunter et al., 1988; Reiller et al., 2002; Yan et al., 2011), and hematite (Cromieres et al., 1998; Murphy et al., 1999; Reiller et al., 2002; Reiller et al., 2005). The previous studies showed that iron oxides have a strong tendency to adsorb Th(IV) from solution. Th(IV) sorption was pH dependent, increasing from 0 to 100 percent adsorbed over the pH range of 1 to 4. However the studies showed that the sorption was independent of ionic strength, indicating that strong chemical bonds or surface complexation reactions were primarily responsible for the sorption of Th(IV) onto the surface of iron oxides.

In addition to iron oxides, Th(IV) sorption studies have also been conducted with other homogeneous minerals, such as silica (Östhols, 1995; Östhols et al., 1997; Li et al., 2002; Reiller et al., 2003; Chen et al., 2007), aluminum oxides (Li et al., 2002; Guo et al., 2005; Hongxia et al., 2006), titania (Anna-Maria, 1999; Zhijun et al., 2005; Tan et al., 2007), and manganese oxides (Hunter et al., 1988). The following studies determined that thorium was significantly adsorbed onto the various metal oxides with sharp sorption edges in the pH ranges of 1 to 4.5. Similar to the iron oxide studies, most of these studies also demonstrated that Th(IV) sorption was independent of ionic strength. However, two studies showed that thorium adsorption was sensitive to ionic strength, causing lower ionic strengths to have greater adsorption (Guo et al., 2005; Zhijun et al., 2005). Both of these studies tested the effect of ionic strength during single pH adsorption isotherms, while the majority of the studies tested the effect of ionic strength during pH sorption edges. Therefore, Zinjun et al. (2005) states that the effect of ionic strength on the adsorption of metals onto oxides can be dependent on the concentration of the metal, the ionic strength range, and the cation and anion background solution.

2.7.2 Sorption of Th(IV) onto Clay Minerals

In addition to metal oxides, several studies have also conducted Th(IV) adsorption experiments with several types of common clays, including bentonite (Zhao et al., 2008), montmorillonite (Chen et al., 2006; Pshinko et al., 2009), and kaolinite (Banik et al., 2007). The previous studies have shown that Th(IV) is strongly adsorbed to the various clays with sorption edges between pH values of 1 to 3, indicating that surface complexation reactions dominate the sorption mechanism. However, Zhao et al. (2008) suggested that Th(IV) sorption to bentonite was partially attributed to electrical forces or cation exchange, due thorium's adsorption sensitivity to ionic strength. In his study, Th(IV) adsorption to bentonite decreased with

increasing ionic strength (Zhao et al., 2008). In conclusion, the literature seems to reveal that thorium has a stronger affinity to clays than metal oxides. For instance, Banik et al. (2007) demonstrated that 85 percent of Th(IV) was adsorbed onto kaolinite at a pH of 1. However, both the clay and metal oxide studies showed significant Th(IV) adsorption. Therefore, since most soils are composed of these common minerals and clays, Th(IV) migration in the environment is likely to be significantly retarded due to adsorption.

2.7.3 Effects of Groundwater Chemistry on Th(IV) Sorption

In addition to mineral composition, the aqueous chemistry of surrounding groundwater can also affect the adsorption of metals. Therefore, many Th(IV) adsorption studies have also evaluated the effect of common groundwater solutes on thorium's adsorption. As seen in Figure 2.2, thorium forms complexes with carbonate increasing its solubility at pH ranges above 7. Studies have shown that the presence of carbonate leads to reduced Th(IV) adsorption at relatively high pH values (pH>6.5) (LaFlamme et al., 1987; Banik et al., 2007). The decrease in Th(IV) adsorption is attributed to competition from carbonate ions for surface sites and increased dissolved thorium carbonate complexes, enhancing thorium's migration through the environment. In addition to carbonate, many studies have also evaluated the effect of phosphate on Th(IV) adsorption onto alumina (Guo et al., 2005), silica (Hongxia et al., 2007), goethite (Yan et al., 2011), titania (Zhijun et al., 2005), and gibbsite (Hongxia et al., 2006). The previous studies demonstrated that the presence of phosphate in solution significantly enhances the sorption of Th(IV) onto the various geomedia at pH<4. For instance, Guo et al. (2005) showed that at a pH of 1.5, Th(IV) adsorption onto alumina in the presence of phosphate was 67 percent, whereas in the absence of phosphate adsorption was 10 percent. The positive effects of

phosphate on the adsorption of Th(IV) can be attributed to the formation of ternary surface complexes and precipitates involving Th(IV) and phosphate (Hongxia et al., 2006).

The presence of natural organic material (NOM) has also shown to affect the sorption of Th(IV) onto various minerals and clays. NOM enters the groundwater through the degradation of plants and animals into the form of particulate, dissolved and colloidal organic carbon. However, it is widely heterogeneous, composed of hundreds of amphiphilic compounds including proteins, polysaccharides, lipids, humic acids and fulvic acids complicating its behavior (Murphy et al., 1999). The reactive nature of NOM is due to the presence of acidic carboxyl, phenolic, and alcoholic functional groups, causing it to disassociate at different pHs (Tan et al., 2007). NOM in groundwater is predominately composed of humic substances, which are classified as: humin, insoluble at all pHs; humic acids (HA), soluble above a pH of 3.5; and fulvic acids (FA), soluble at all pH values (Chang et al., 2007). The affect of humic substances on the adsorption of Th(IV) has been studied onto a variety of clays and metal oxides (Reiller et al., 2002; Reiller et al., 2003; Reiller et al., 2005; Chen et al., 2006; Hongxia et al., 2006; Banik et al., 2007; Chang et al., 2007; Chen et al., 2007; Tan et al., 2007; Pshinko et al., 2009). The previous studies have determined that Th(IV) adsorption is enhanced in the presence of HA/FA at pH values below 4 due to ternary surface complexation reactions. However, several studies have shown the presence of HA/FA to decrease Th(IV) adsorption at pH values above 6 (Reiller et al., 2002; Chang et al., 2007; Chen et al., 2007; Pshinko et al., 2009). This reduction in Th(IV) adsorption onto geomedia is caused by the formation of stable aqueous (HA/FA)-Th complexes at high pH values, increasing thorium's solubility in solution (Chen et al., 2007). Therefore, groundwater containing humic substances can further complicate the behavior of Th(IV) in the environment.

2.8 Sorption of Th (IV) onto Savannah River Site Subsurface Soil

Most of the literature regarding Th(IV) adsorption has been conducted onto homogenous minerals and clays. However, not many studies have used heterogeneous soil from contaminated sites, which can provide more accurate predictions of Th(IV) behavior at these sites. Therefore, preceding research by Melson (2011) through Auburn University's Civil Engineering Department conducted Th(IV) batch adsorption experiments onto heterogeneous iron-containing subsurface soil from the U.S. Department of Energy's Savannah River Site (SRS) located in South Carolina. SRS was utilized by the U.S. military to produce Pu-239 for use in nuclear weapons during the Cold War (Dai et al., 2002). Due to the production of Pu-239, parts of the site have suffered from historic actinide contamination. The sediment used for Th(IV) batch adsorption (Melson, 2011) and column transport (current research) studies was collected from actinide free soil located in the E-Area Low-Level Waste Disposal Site. The sediments collected from this site were classified as subsurface clay and subsurface sand. Both sediments were air dried and stored in plastic bags in the dark at room temperature. The SRS soil characteristics can be seen in Table 2.5.

Table 2.5: SRS soil characteristics

Soil	Subsurface Clay	Subsurface Sand
% sand (>53 µm)	57.9	97
% silt (53 – 2 µm)	40.6	2.9
% clay (<2 µm)	1.6	0.2
Textural classification	Silty clay	Sand
pH	4.55	5.1
% OM	8.8	0
CEC (cmol/kg)	1.09 ± 0.31	-0.35 ± 0.22
AEC (cmol/kg)	1.58 ± 0.61	0.06 ±0.19
BET surface area (m^2/g)	15.31	1.27
Single point surface area (m^2/g)	15.07	1.24
CDB extractable Fe (mg/g)	15.26	7.06
Al (ppm)	63.59	16.64
Na (ppm)	42.91	34.69
Mg (ppm)	144.05	98.76
Ca (ppm)	64.41	24.62
K (ppm)	182.87	92.97
Mineralogy	Kao > goeth > Hem (no qtz or 14 A)	Kao > goeth >musco/14A (no qtz)

After conducting Th(IV) batch adsorption kinetic experiments onto SRS sandy subsurface soil, Melson (2011) determined that equilibrium was reached after 48 hours, at which no further Th(IV) concentration loss was observed due to adsorption to the soil. Therefore, he used 48 hours for all of his batch adsorption experiments to ensure equilibrium was reached. Both the sandy and clayey SRS sediments showed significant Th(IV) adsorption. However, the clayey sediment showed increased adsorption of Th(IV), which can be seen in the experimental Th(IV) adsorption pH edges for SRS sandy (Figure 2.5) and clayey (Figure 2.6) subsurfaces. Melson et al. (2012) also conducted an experiment in the absence of soil at various pH values to determine Th(IV) removal by precipitation mechanisms, which can be seen in Figure 2.7.

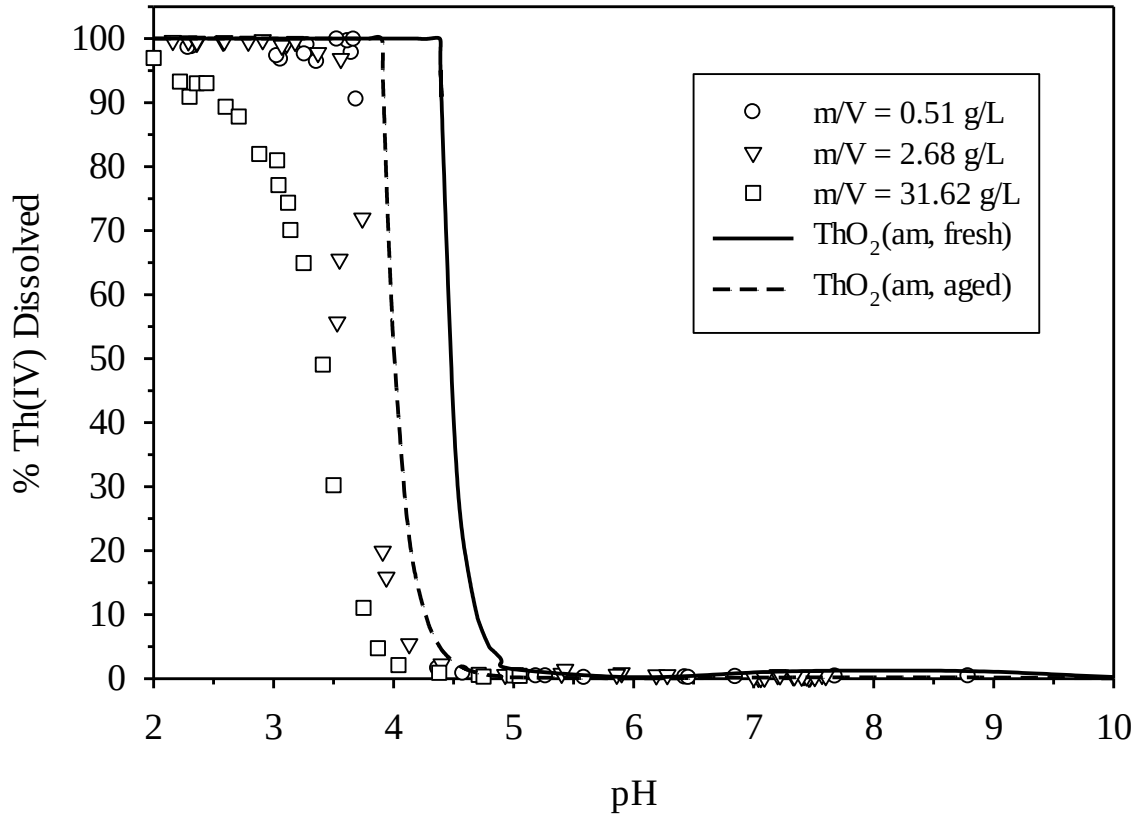

Figure 2.5: Percent Th(IV) dissolved vs. pH for different solid-solution ratios of SRS sandy subsurface soil compared to theoretical solubility values of ThO_2(am, fresh) and ThO_2(am, aged) precipitates ($C_{0(Th\ (IV))}$ = 3.34 x 10^{-5}M, I=0.09M $NaNO_3$/0.01M $NaHCO_3$, T=26±1°C). Adapted from Melson (2011).

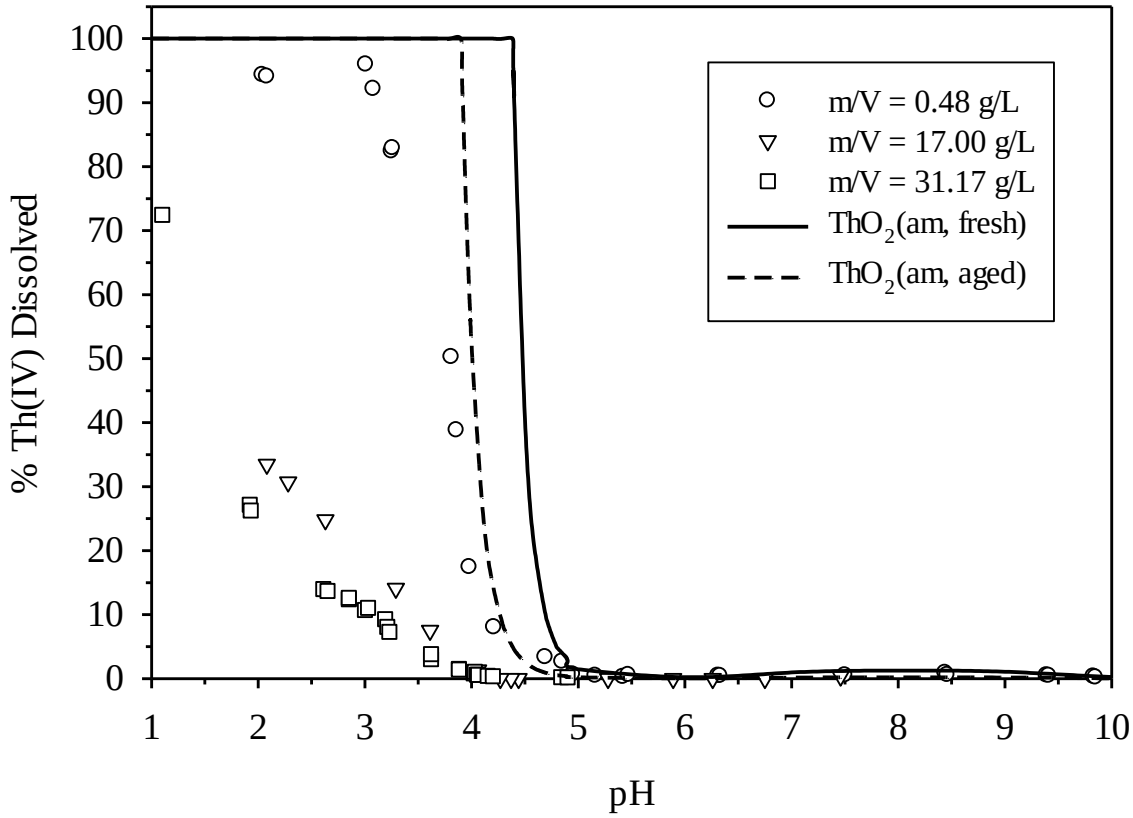

Figure 2.6: Percent Th(IV) dissolved vs. pH for different solid-solution ratios of SRS clayey subsurface soil compared to theoretical solubility values of ThO_2(am, fresh) and ThO_2(am, aged) precipitates ($C_{0(Th\ (IV))}$ = 3.30 x 10^{-5}M, I=0.09M $NaNO_3$/0.01M $NaHCO_3$, T=26±1°C). Adapted from Melson (2011).

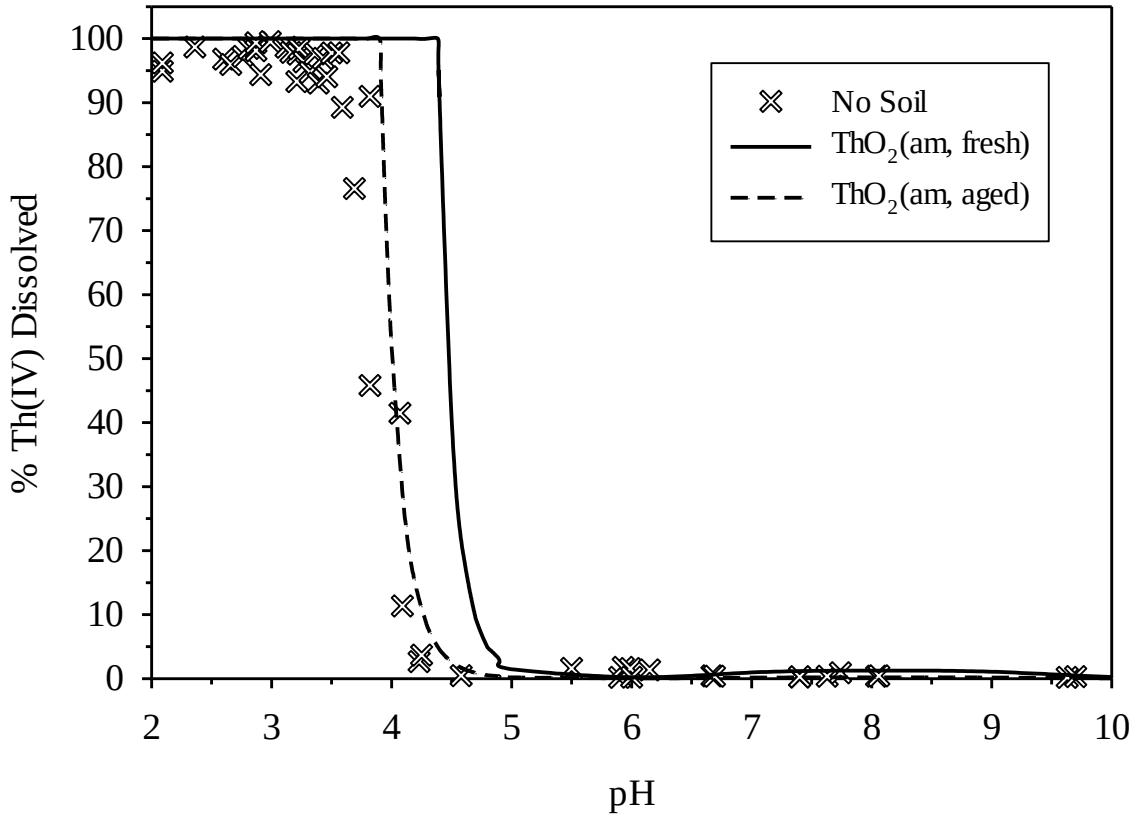

Figure 2.7: Percent Th(IV) dissolved vs. pH for samples containing no soil compared to theoretical solubility values of ThO_2(am, fresh) and ThO_2(am, aged) precipitates ($C_{0(Th\ (IV))}$ = 3.31 x 10^{-5}M, I=0.09M $NaNO_3$/0.01M $NaHCO_3$, T=26±1°C). Adapted from Melson et al. (2012).

As seen from Figures 2.5 and 2.6, the SRS clayey subsurface sediment had a stronger affinity for Th(IV) than the sandy sediment. At low solid-solution ratios, Th(IV) removal from solution in the presence of SRS sandy subsurface sediment seemed to be due to precipitation of thorium amorphous oxides. However, the adsorption edge shifted at a solid-solution ratio of 31.62 g/L of SRS sandy soil, signifying Th(IV) adsorption to the surface of the soil. The stronger adsorption of Th(IV) onto the clayey subsurface was most likely due to the significantly larger BET surface area (15.31 m^2/g) of the sediment in comparison to the sandy subsurface (1.27 m^2/g). In addition, the subsurface clay had twice the extractable iron content of the

subsurface sand, which could also contribute to greater Th(IV) affinity. Melson's experiments had similar locations of adsorption edges in comparison to Th(IV) adsorption experiments to metal oxides and clays in the literature. Therefore, the adsorption is assumed to be predominately attributed to surface complexation reactions, due to the hydrolysis of Th(IV) species. As seen from Figure 2.7, Melson demonstrated that the solubility of Th(IV) in the absence of soil was around the ThO_2(am, aged) solubility limits, which is contrary to previous studies in the literature stating it should be around the solubility of ThO_2 (am, fresh) at equilibrium times less than 25 days (Rand et al., 2008). This result could be contributed to adsorption of Th(IV) to the walls of Teflon sample tubes.

As seen in Table 2.5, X-ray diffraction studies showed the mineralogy of the two SRS subsurface soils (particles <2μm) to be composed mainly of kaolinite and goethite. Therefore, Melson (2011) also conducted Th(IV) adsorption studies with homogeneous kaolinite and goethite minerals. His experiments showed strong adsorption to both of these minerals, which can be seen in Figures 2.8 and 2.9. Melson's Th(IV) adsorption edge onto goethite was very similar to studies in the literature (Hunter et al., 1988; Reiller et al., 2002; Yan et al., 2011). In comparison to the goethite, Melson showed that kaolinite had a significantly stronger affinity for Th(IV) at lower pH values. However, at pH values between 5 and 11 Th(IV) was oversaturated in respect to the theoretical solubility of the amorphous fresh solid in the presence of kaolinite. In addition, Th(IV) solubility increased with increasing solid-solution ratio of kaolinite. The dissolved Th(IV) concentration at pH values between 6 and 11 was about 2 orders of magnitude greater than the theoretical solubility of ThO_2 (am, Aged). This strange result at alkaline pH values could have been attributed to Th(IV) adsorption to hydroxy aluminumsilicate (HAS) colloids, forming Th(IV) pseudocolloids (Banik et al., 2007). During centrifugation, HAS

colloids may have remained in solution, giving higher false thorium concentrations. Therefore, the thorium concentrations may be lower in the absence of colloids. Another explanation for this phenomenon could be attributed to the increased solubility of kaolinite at pH values greater than 8. The soluble kaolinite species could have potentially formed aqueous complexes with Th(IV), increasing its solubility. In a similar study, Banik et al. (2007) also found Th(IV) adsorption onto kaolinite to decrease at pH values greater than 8.5. However, he attributed the decrease in Th(IV) adsorption to the formation of negatively charged aqueous thorium carbonate species, which would less likely adsorb to the negatively charged kaolinite (Banik et al., 2007). However, this theory does not explain Melson's results because the dissolved thorium concentration was significantly higher than the theoretical solubility of the amorphous thorium solid.

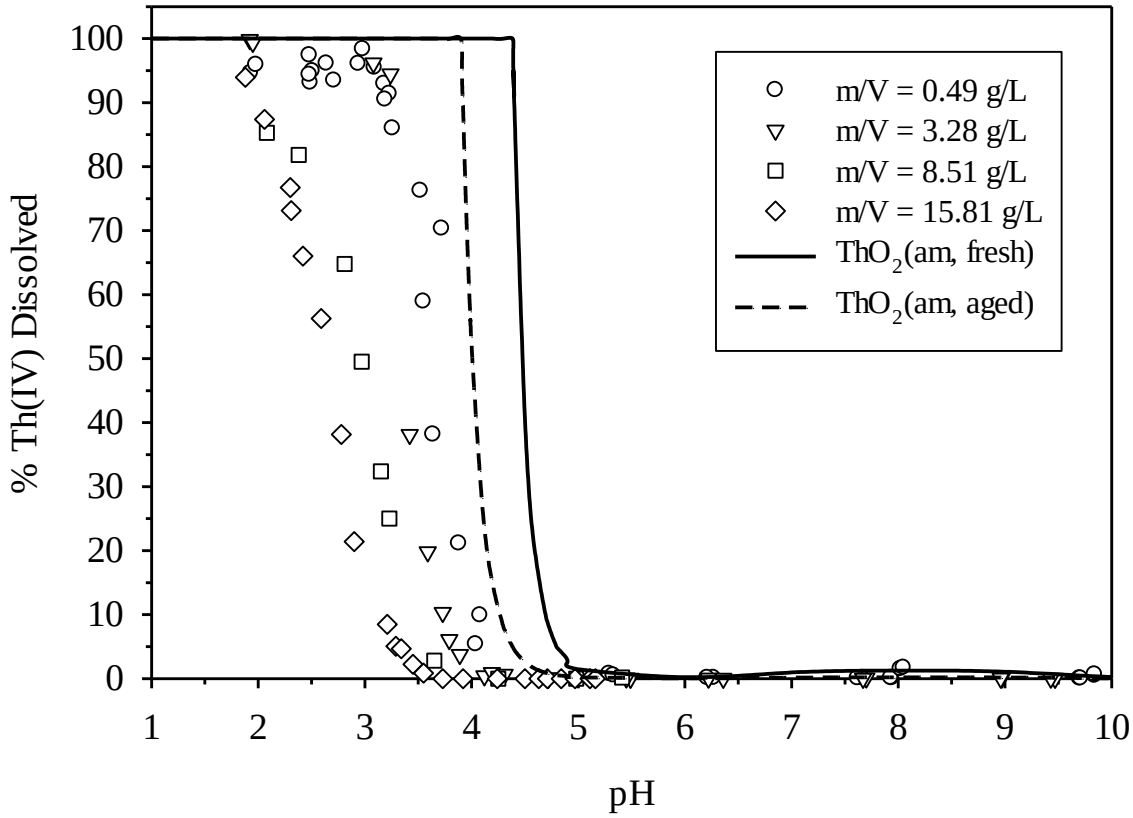

Figure 2.8: Percent Th(IV) dissolved vs. pH for different solid-solution ratios of goethite compared to theoretical solubility values of ThO_2(am, fresh) and ThO_2(am, aged) precipitates ($C_{0(Th\ (IV))}$ = 3.34 x 10^{-5}M, I=0.09M $NaNO_3$/0.01M $NaHCO_3$, T=26±1°C). Adapted from Melson (2011).

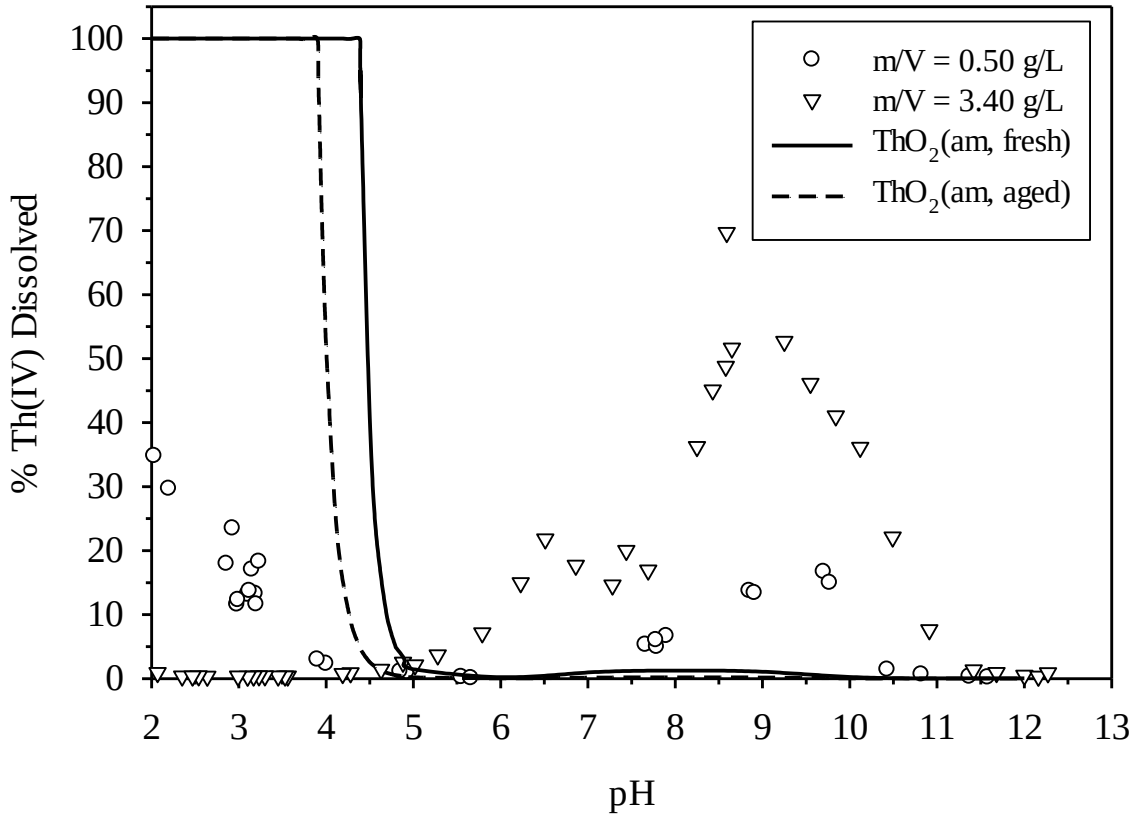

Figure 2.9: Percent Th(IV) dissolved vs. pH for different solid-solution ratios of kaolinite compared to theoretical solubility values of ThO_2(am, fresh) and ThO_2(am, aged) precipitates ($C_{0(Th\ (IV))}$ = 3.34 x 10^{-5}M, I=0.09M $NaNO_3$/0.01M $NaHCO_3$, T=26±1°C). Adapted from Melson (2011).

2.9 Colloid-Facilitated Contaminant Transport

Until 25 years ago, the mobility of contaminants in groundwater aquifers was believed to be dependent on their distribution between a two-phase system in which solutes partition between an immobile solid aquifer matrix and a mobile aqueous groundwater phase (Sen et al., 2006). Using this system, strongly adsorbing contaminants, such as radionuclides, were thought to be relatively immobile in the subsurface, presenting little threat to groundwater supplies. However, the unexpected transport of low-solubility contaminants far from known sources has

led to the examination of a third phase consisting of mobile colloids (McCarthy et al., 1989; Ryan et al., 1996; Sen et al., 2006). In a three-phase system, colloids can adsorb relatively insoluble contaminants forming pseudo-colloids and become mobilized in the aqueous phase, enhancing the migration contaminants through the subsurface (Kim, 1991). This contaminant transport mechanism is referred in the literature as colloid-facilitated transport (Sen et al., 2006). Figure 2.10 compares the two and three-phase contaminant transport models.

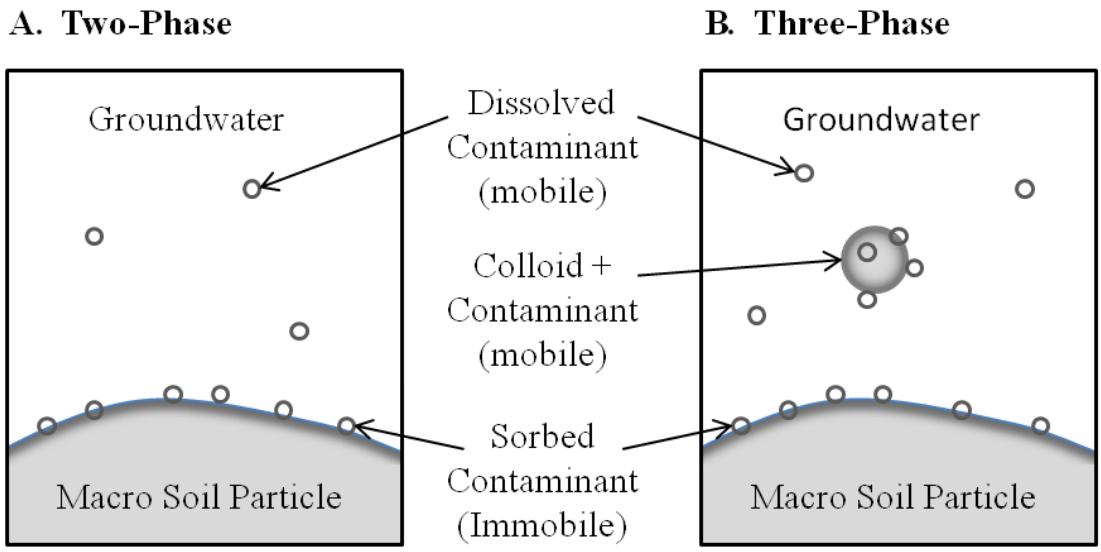

Figure 2.10: Comparison of two and three-phase contaminant transport models in groundwater. Adapted from McCarthy et al. (1989).

Notable field studies at hazardous waste sites (Buddemeier et al., 1988; Penrose et al., 1990; Kaplan et al., 1994; McCarthy et al., 1998; Kersting et al., 1999; Novikov et al., 2006) and natural uranium deposits (Airey, 1986; Short et al., 1988) have concluded that colloid-facilitated transport is responsible for the unexpectedly rapid movement of trace metals and radionuclides from their source. For instance, Kersting et al. (1999) discovered that plutonium had migrated 1.3 kilometers from an underground nuclear test conducted 30 years ago at the Nevada Test Site.

This rapid transport of plutonium from its origin severely underestimated the predicted migration of plutonium, suggesting colloid-facilitated transport must have played an important role (Kersting et al., 1999). In a similar instance, plutonium activities of 0.16 Bq/L were detected 3 kilometers from one of the worst contaminated nuclear sites in the world, the Mayak nuclear waste reprocessing plant located in Russia (Novikov et al., 2006). A field study by Novikov et al. (2006) confirmed that 70 to 90 percent of the plutonium detected was associated with colloids, which were thought to be iron oxides ranging from 1 to 15 nm. In addition to field studies, many laboratory experiments testing colloid-facilitated transport have also confirmed that colloids can enhance the transport of strongly sorbing contaminants through saturated porous media (Puls et al., 1992; Roy et al., 1997; Um et al., 2002; Mori et al., 2003; Grolimund et al., 2005; Zhang et al., 2007; Cheng et al., 2010; Crancon et al., 2010; Zhou et al., 2011). Therefore, the use of simple two-phase contaminant transport models of the past can significantly underestimate the migration of low-solubility contaminants through groundwater aquifers where colloids are present.

2.9.1 Sources of Colloidal Particles in the Groundwater

Colloidal particles are ubiquitous in natural aqueous environments, including surface waters, shallow vadose zones, and deep groundwater aquifers (Kretzschmar et al., 2005). They are classified as migratory particles with dimensions between 1 nm and 10 μm (Figure 2.11) (McCarthy et al., 1989). Due to their small sizes, colloids have a high specific surface area in the range of 10 to 800 m^2/g, giving them a high capacity to adsorb trace metals (Kretzschmar et al., 2005). Most colloids in groundwater systems originate from the mobilization of existing fine particle-sized minerals contained within naturally present aquifer sediments (McCarthy et al., 1989). However, colloidal particles can also be generated by *in situ* precipitation of

supersaturated mineral phases. This colloidal formation process is less common in most natural environments, but is more likely to occur in environments near high-level radioactive waste repositories (Ryan et al., 1996). In these contaminated environments, supersaturated actinides, along with aqueous mineral phases, can undergo hydrolysis and form intrinsic colloids or eigencolliods by precipitation, enhancing their migration through the subsurface due to the nature of their size (Ryan et al., 1996; Fanghanel et al., 2002; Runde et al., 2002). In addition, colloids can also be introduced into groundwater systems through man-made waste management procedures, such as landfills, septic tanks, and groundwater recharge (Sen et al., 2006). Colloids within groundwater environments can consist of a variety of inorganic and organic materials, including clay minerals, rock fragments, mineral precipitates (predominately iron, aluminum, manganese, or silica oxides, hydroxides, carbonates, and phosphates), macromolecules of natural organic matter and biocolloids (such as microorganisms and viruses) (McCarthy et al., 1989; Kretzschmar et al., 2005; Sen et al., 2006). These submicron-sized particles can be released from groundwater aquifers in the form of colloids by fluctuations in physical and chemical groundwater conditions, which can have a significant impact on the migration of strongly sorbing trace metals (Kretzschmar et al., 2005).

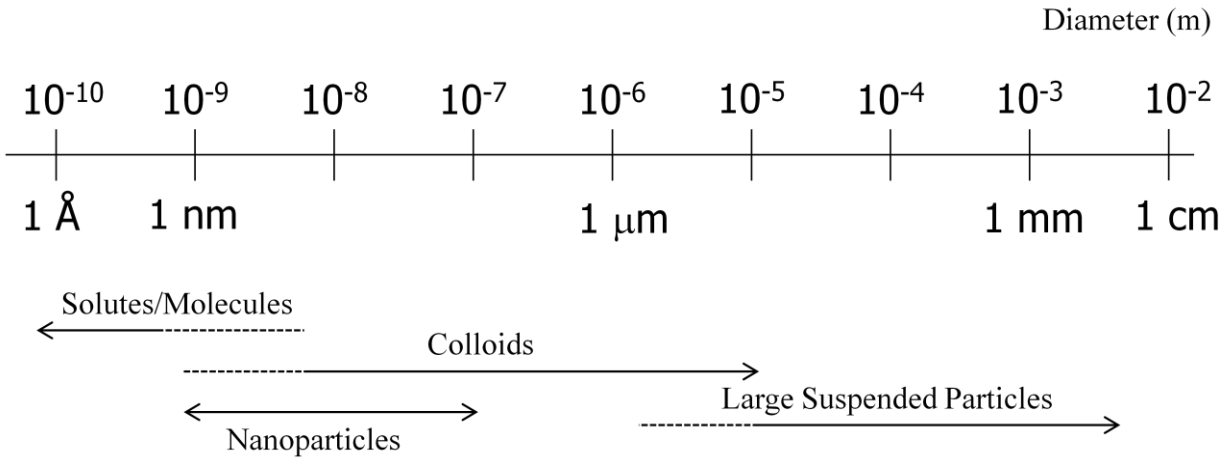

Figure 2.11: Size spectrum of waterborne particles. Adapted from McCarthy et al. (1989).

2.9.2 Colloid Release Mechanisms

As mentioned earlier, most groundwater sediments contain submicron-sized particles that are normally immobile under stable physical and chemical conditions (McCarthy et al., 1989). However, these fine particles can be released from the aquifer matrix by fluctuations in water saturation, flow velocity, and aqueous solution chemistry (Ryan et al., 1996; Kretzschmar et al., 2005; Sen et al., 2006). For instance, high flow rates can cause particle release due to the hydraulic shear stress on larger particles (Sharma et al., 1992; Kaplan et al., 1993). However, in natural subsurface aquifers, the flow rates are generally low. Therefore, colloid release is more likely to occur due to changes in solution chemistry, such as decreases in ionic strength, increases in pH, variations in redox potentials, and adsorption of solutes that alter mineral surface charges (McCarthy et al., 1989). In most groundwater aquifers, drastic changes in solution chemistry are usually unlikely, but they can be greatly influenced by man-made conditions near contaminated sites. In a review, Ryan et al. (1996) states that the most common change in groundwater chemistry is the decrease in ionic strength. This perturbation can be

triggered by the infiltration of dilute freshwater from natural rain events, irrigation, or artificial groundwater recharge (Ryan et al., 1996). During these events, groundwater aquifers containing solutions of higher ionic strength are replaced by solutions of lower salinity, which can induce the detachment of colloidal fines from sediments. This effect is particularly important at DOE radioactive waste sites, where high concentrations of electrolytes (>5M Na^+) and radionuclides have been leaking from storage tanks into groundwater aquifers (Gephart et al., 1998). Over time these hypersaline solutions can be diluted by infiltrating solution from the surface, potentially enhancing colloid-facilitated transport of radionuclides (Blume et al., 2005).

The effect of aqueous solution chemistry on the detachment of colloidal particles has been studied in many laboratory columns using a variety of porous media (Seaman et al., 1995; Roy et al., 1997; Bunn et al., 2002; Um et al., 2002; Blume et al., 2005; Grolimund et al., 2005; Zhang et al., 2007; Crancon et al., 2010; Zhou et al., 2011). In addition, this phenomena has also been observed in several field studies ranging from the reduction of hydraulic conductivity at coastal (Goldenberg, 1985), agricultural (Abu-Sharar et al., 1995), and oil recovery sites (Khilar et al., 1984; Kia et al., 1987) to groundwater turbidity caused by artificial recharge (Nightingale et al., 1977). The chemically induced detachment and mobilization of colloids is attributed to the alteration of forces between the surface of the colloids and the sediment surface to which they are attached (Ryan et al., 1996). These intersurface forces include both London-van der Waals attractive forces that promote colloidal aggregation and the double layer electrostatic repulsive forces that drive particles apart (McCarthy et al., 1989).

The net effect of the attractive and repulsive forces between particle surfaces over their separation distance is described by the DLVO (Derjaguin, Landau, Verwey, and Overbeek)

Theory (Sen et al., 2006). The attractive van der Waals forces are only effective within close distances of the charged particle and are independent of changes in solution chemistry (Reynolds et al., 1996). Therefore, the chemically induced mobilization of colloids primarily occurs by the alteration of the double layer potential energy between the colloid surface and the surface of the aquifer sediment (Ryan et al., 1996). If a change in solution chemistry alters the double layer potential energy enough, the repulsive forces between the attached colloids and grains will overcome the attractive forces, causing colloids to be released. This double layer electrostatic potential surrounding the surface of a colloid arises from the particle's charge, which attracts clouds of counterions around its surface to neutralize the electrostatic charge (Priesing, 1962). In many models, the electrostatic field is conceptually divided into two layers, hints the name "double layer". Figure 2.12 depicts the electrostatic field of a negatively charged colloid and the relative concentration gradient of counterions within each layer.

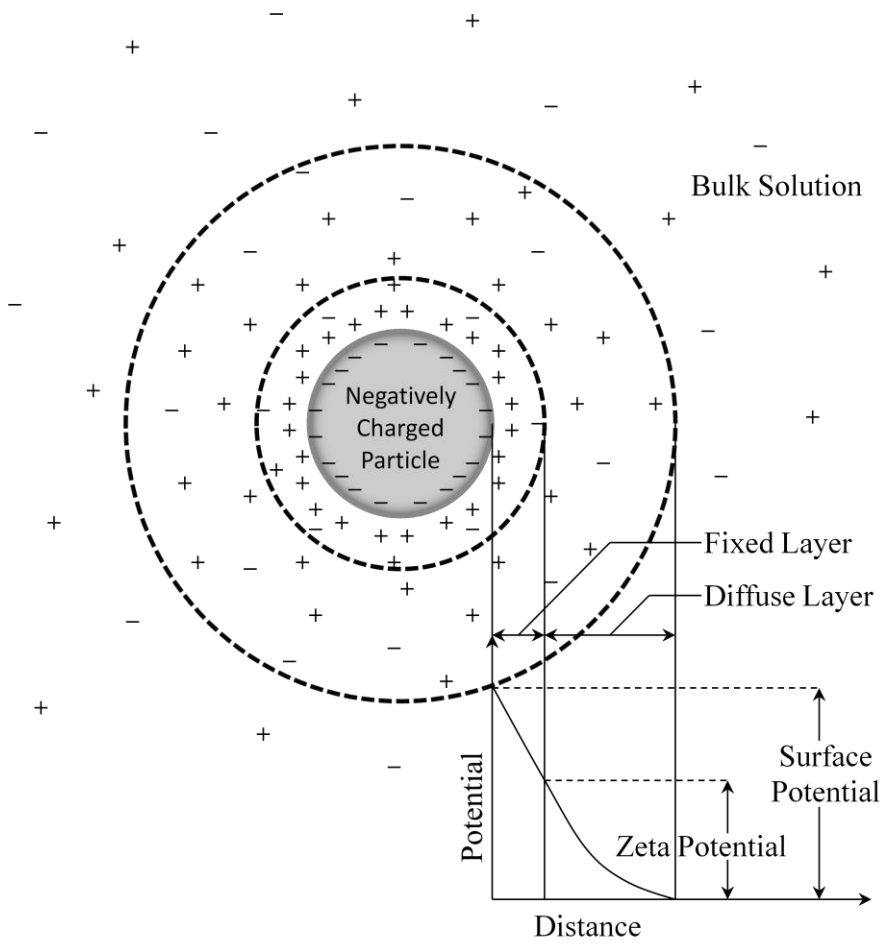

Figure 2.12: Electrostatic field of a negatively charged colloidal particle. Adapted from Priesing (1962).

Since surface potentials of particles cannot be directly measured, zeta potentials, as portrayed in Figure 2.12, are usually used to determine the double layer potential energy between particles (Ryan et al., 1996). The zeta potential measures the particle charge at a distance from the particle's surface known as the shear plane (Priesing, 1962). Depending on the interacting charged surfaces, the double layer potential energy between particles is either a repulsive force (like-charges) or an attractive force (opposite charges). The distance the double layer extends from the charged surface of particles is controlled by the ionic strength of the aqueous solution (Ryan et al., 1996). At high ionic strengths, the surface charge is be balanced by a thin,

compressed double layer due to the high concentration of ions near the charged surface of the particle. While at low ionic strengths, the double layer is expanded. Therefore, when ionic strength of the aqueous solution decreases, the double layers around the like-charged colloids and grains expand, increasing the repulsive interaction and promoting colloid detachment (Sen et al., 2006). The reverse effect occurs during the traditional coagulation process of water treatment facilities. During coagulation, a multivalent cation is added to solution to increase the solution ionic strength. This causes the repulsive double layers between colloidal suspensions to compress and allows the attractive van der Waals forces to dominate the potential energy profile, promoting particle aggregation. Figure 2.13 shows the interparticle forces acting between two particles within aqueous solutions containing high and low concentrations of electrolytes.

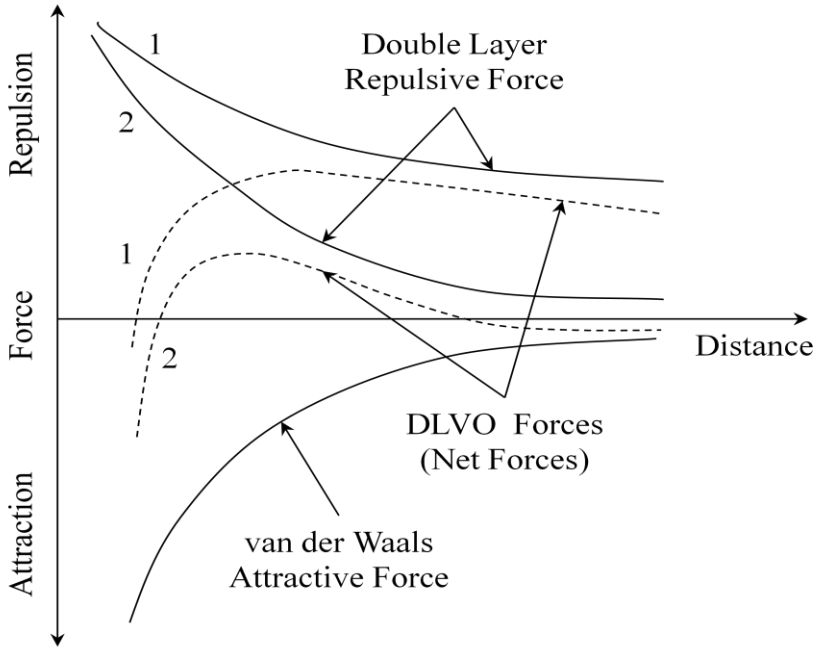

Figure 2.13: Interparticle forces vs. distance at low electrolyte concentrations (1) and high electrolyte concentrations (2). Adapted from Pitts (1995).

In order to further understand the colloidal release phenomena caused by decreases in solution salinity, many studies have focused on the critical salt concentration (CSC), which is the concentration of electrolytes at which fine particles begin to release from aquifer sediments (Sen et al., 2006). CSCs have been experimentally determined for many types of aquifer sediments, including Berea sandstone (Khilar et al., 1984; Kia et al., 1987), silty loam soil (Quirk et al., 1955; Grolimund et al., 1998), Hanford sediment (Blume et al., 2005), homogeneous iron oxide-coated sand (Blume et al., 2005), and other natural heterogeneous soil containing various clay contents. Traditionally, CSC values are determined through column experiments by initiating stepwise decreasing salt concentrations to an aquifer media until particles are released (Blume et al., 2005). However, Blume et al. (2005) used batch experiments in addition to column experiments to determine CSCs values for aquifer sediments, which had similar results. Not only do CSCs differ between types of porous media, but they also depend on the valence and size of the solubilized salt's cation, the pH of the solution, and the temperature of system (Blume et al., 2005).

Multivalent salts tend to have much lower CSC values due to their multiple charges per ion, allowing them to more efficiently screen the repulsive surface interaction energies between colloids and grain surfaces (Sen et al., 2006). For instance, divalent salts such as Ca^{2+}, usually show no particle release until their CSC is less than 0.0001 M, whereas a monovalent salt, such as sodium, start releasing particles around a CSC value of 0.07 M (Blume et al., 2005). In addition to sodium, Kilhar and Folger (1984) determined CSCs of Berea sandstone for a variety of other monovalent salts. Their study concluded that CSCs of soils depend on the size of the solublized cation in solution, giving the following order of CSCs from high to low:

$Na^+ > Li^+ > K^+ > NH_4^+ > Cs^+$ (Khilar et al., 1984). Since natural groundwater systems usually have mixtures of cations in solution, CSCs of natural aquifers can be more difficult to predict.

In addition to decreases in solution salinity, increases in pH can also promote colloid mobilization. As mentioned earlier, a change in ionic strength alters the distance the diffuse layers extend between colloids and grains, which either strengthens or weakens the electrostatic forces between particle surfaces. However, changes in ionic strength cannot drastically alter the surface charges of particles. Therefore, a decrease in solution salinity only mobilizes colloids when the colloids and grains have like-charged surfaces, or repulsive interactive forces. When colloids and grains are oppositely charged, ionic strength has no effect on colloid mobilization (Sen et al., 2006). Unlike changes in ionic strength, changes in solution pH can drastically alter or reverse the surface charge of particles by exchanging protons from solution with the particle's surface functional groups. Most minerals have a positive surface charge at low pH values and a negative charge at high pH values. The pH at which a mineral has a zero charge is called the zero point charge, or pH_{pzc} (Ryan et al., 1996). Surface charge properties of colloids and grains within natural aquifers can vary drastically depending on their chemical composition. For instance, natural metal oxide minerals have pH_{pzc} values ranging from 2 for quartz to 8 for iron oxides.

Since surface charges of particles are influenced by pH, changes in pH can cause colloids to become mobilized by altering and sometimes reversing a particle's surface charge. Many colloids found in natural aquifers are composed of clays, which usually have negatively charged surfaces. These negatively charged clay particles are typically attached to positively charged grains, such as iron-coated sand. Increasing the pH past the grain's point zero charge

($pH>pH_{pzc}$) causes the grain's surface charge to reverse from a positive charge to a negative charge, inducing the interactive forces between the grains and colloids to become repulsive. Once the double layer repulsive force is strong enough to overcome the attractive London-van der Waals forces, the fine clay particles detach and become mobilized in the groundwater.

Much like changes in pH, the adsorption of ions and surfactants can also alter the surface charge of colloids and grains within aquifers (Ryan et al., 1996). In some cases, this alteration of surface charges can also mobilize colloids. For instance, Ryan and Gschwend (1994) studied the effect of dodecanoic acid, a negatively charged surfactant, on the mobilization of colloids from iron-coated sand. Their results showed that the surfactant reversed the charge on the surface of the goethite, which caused the detachment of colloids (Ryan et al., 1994). Although this situation is unlikely to occur in natural aquifer environments, it could occur in aquifers near land that has been altered by man-made events.

2.9.3 Colloid Stabilization and Filtration

Once colloids are released into groundwater aquifers by either chemical or physical fluctuations, they can travel significant lateral distances depending on their colloidal suspension stability. Colloidal transportation through various types of saturated subsurfaces has been demonstrated by both field studies (Harvey et al., 1989; Higgo et al., 1993) and laboratory column experiments (Grolimund et al., 1998; Lenhart et al., 2003; Loveland et al., 2003; Zhou et al., 2011). These studies, along with many others, have shown that the stability of colloidal suspensions are governed by a combination of physical and chemical conditions, such as groundwater flow rate, density, size, and concentration of suspended colloids, size and connectivity of the porous structure, surface charge chemistry, and groundwater solution

chemistry (Kretzschmar et al., 2005). Depending on these conditions, suspended colloids can either remain stable or be removed from solution by aggregation, settling, readhesion to pore surfaces, or entrapment at pore constrictions (McCarthy et al., 1989). The interdependency of these factors makes it difficult to predict the distance colloids will flow through the porous media.

Since individual colloids are typically submicron sized particles, they can travel long distances due to their extremely low settling velocities. In addition, their small size also prevents filtration by straining while traveling through the porous media. In fact, several studies have found colloids to travel faster than conservative tracers through aquifers (Harvey et al., 1989; Grolimund et al., 1998; Sirivithayapakorn et al., 2003). These studies attributed the faster transport to size exclusion effects, which cause colloids to be excluded from smaller pore spaces and more tortuous flow paths within the soil medium (Ryan et al., 1996).

However, the transport of colloids is dramatically affected by the tendency for them to aggregate or attach to the porous media by physical-chemical forces (Kretzschmar et al., 2005). Aggregation causes colloids to form larger flocks, which enhances filtration by the porous media. Much like the factors controlling colloid release, colloid aggregation and deposition is also primarily controlled by the balance of electrostatic interaction forces and attractive van der Waals forces acting between the colloids themselves and the porous surface (Kretzschmar et al., 2005). Therefore, aggregation occurs when the attractive forces between colloids overcome the repulsive electrostatic energy barrier. This destabilization of colloidal suspensions can be influenced by increased ionic strength, presence of multivalent counter ions, change in pH, and

the adsorption of oppositely charged ions to the surface of colloids (McCarthy et al., 1989; Kretzschmar et al., 2005).

In addition, coagulation kinetics is also a function of particle concentration, particle size, and particle size distribution (McCarthy et al., 1989). These physical characteristics can influence the extent of particle-particle collisions within groundwater systems, thus affecting the rate of aggregation. Once colloidal suspensions become destabilized, they are much more likely to be removed by the porous media through surface deposition and filtration by straining (Sen et al., 2006).

Even when the groundwater chemistry promotes colloid stability, particles can still be filtered from solution by physical straining and physical-chemical collection by attractive surfaces of the immobile aquifer matrix (McCarthy et al., 1989). However, filtration by physical straining is usually ineffective in many porous media due to the relatively small size of colloids (usually 1μm or less). Therefore, the primary removal of stable colloids is by physical-chemical collection, which is controlled by electrostatic, chemical, or van der Waals forces (McCarthy et al., 1989). This filtration process is similar to the particle-particle interactions involved in aggregation, but involves colloids associating with the mineral or organic surfaces of the immobile aquifer media instead of other suspended particles. Colloidal suspensions are attracted to oppositely charged aquifer matrices, causing rapid deposition that is usually irreversible as long as the surface charge of the colloids and aquifer grains remain unchanged (Kretzschmar et al., 2005). Since many groundwater aquifers carry a net negative charge, negatively charged colloids are usually considered more mobile than colloids with positive surface charges (McCarthy et al., 1989).

However, many groundwater aquifers are composed of heterogeneous grains with varying surface charges. Therefore, measured net surface charges of heterogeneous soils can be somewhat irrelevant to colloid transport predictions (McCarthy et al., 2004). For instance, an aquifer dominated by negatively charged surfaces might have small patches of positively charged surfaces that can effectively remove negatively charged colloids (Kretzschmar et al., 2005). This problem was demonstrated by Elimelech et al. (2000), who created a heterogeneously charged soil by treating negatively charged quartz grains with aminosilane, producing a positive surface charge. Mixing varying proportions of treated and untreated quartz created a heterogeneously charged soil, which they used for colloid transport experiments. The results showed that the soils containing more positively charged grains reduced the breakthrough of the negatively charged silica colloids. However, the experimental results substantially differed from the predicted results based on the average surface charge of the media. This study further illustrated the complexities of predicting colloid transportation through heterogeneous porous media. The main processes controlling the mobility of colloids through water-saturated porous media can be seen in Figure 2.14.

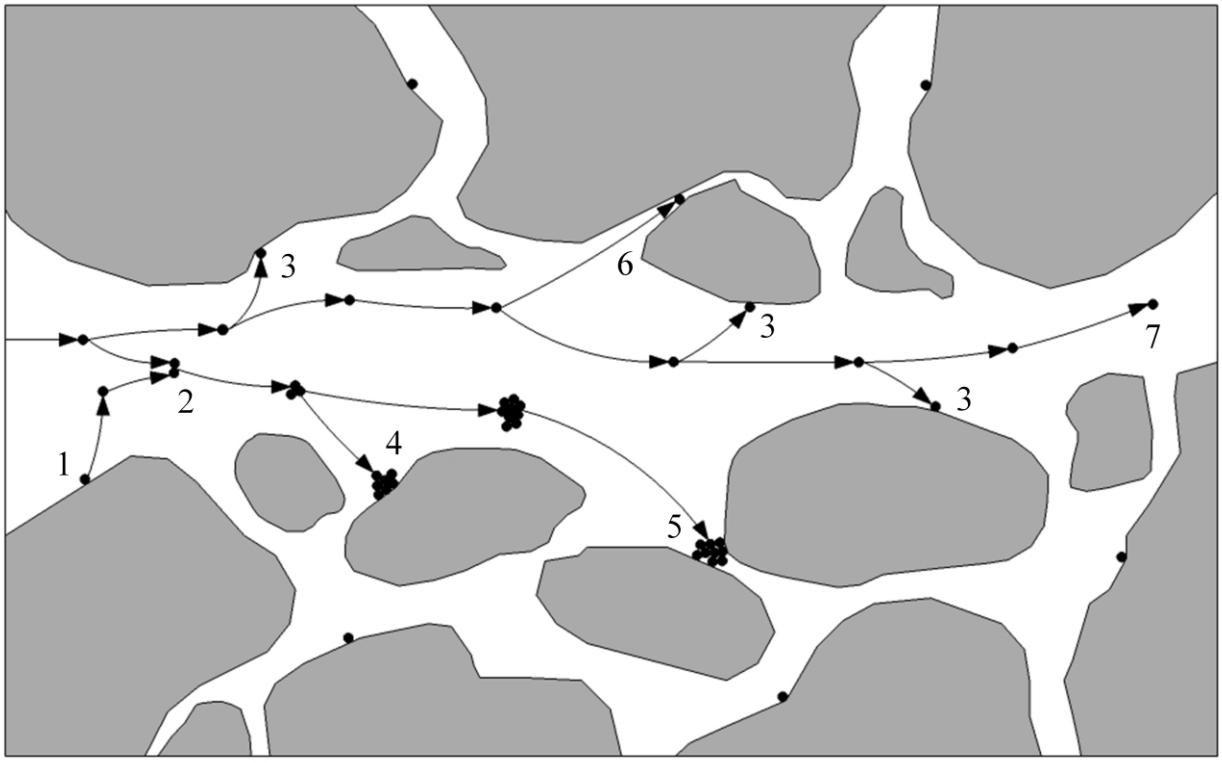

Figure 2.14: Processes controlling the mobility of colloidal particles in water-saturated porous media: (**1**) Colloid detachment from aquifer matrix, (**2**) Aggregation of colloids, (**3**) Immobilization by physical-chemical collection, (**4**) Immobilization by gravitational settling of flocks, (**5**) immobilization by straining of flocks, (**6**) Immobilization by straining of single particle, (**7**) Transport of dispersed colloids over long distances by flowing groundwater. Adapted from Kretzschmar et al. (2005).

Chapter Three.

Chemical Factors Influencing Colloid Mobilization and Th(IV) Transport through Saturated Subsurface Sediment

This chapter serves as a draft manuscript. It will later be submitted for publication in a peer-reviewed scientific journal article.

3.1 Introduction

Since the 1940's, significant quantities of actinides have accumulated worldwide due to the activities of nuclear weapons programs and nuclear power production (Ahearne, 1997). Unfortunately, improper storage and nuclear weapons testing have released large amounts of this waste into the subsurface, contaminating groundwater aquifers with long-lived, highly toxic, radioactive waste (Ahearne, 1997; Runde, 2000). Some of the highest local concentrations of actinide contamination are found at Department of Energy (DOE) sites where uranium and plutonium were produced and tested for nuclear weapons, such as the Savannah River Site, Hanford Site, Rocky Flats Environmental Technology Site, Idaho National Laboratory, Los Alamos National Laboratory, Nevada Test Site, and Oak Ridge National Laboratory (Cantrell et al., 2008). Despite the deployment of DOE-funded remediation programs at these sites, significant amounts of subsurface contaminants are likely to remain even after cleanup efforts (Runde, 2000). In addition to these sources, future plans of permanent geological repositories for spent nuclear fuel will potentially introduce much more quantities (up to 70,000 tons) of radioactive waste into the subsurface (Povetko, 2008; Vašíček et al., 2011). The main goal of the repository is to delay the release of radioactive waste until the radiological impacts are within acceptable levels, which could take over ten thousand years (Long et al., 2004). Therefore, the

study of actinide biogeochemical transport is extremely important to prevent actinides from migrating through the subsurface environment.

Actinides, especially those in the tetravalent oxidation state, tend to have low solubility (below micromolar concentrations) in natural waters due to the precipitation of oxyhydroxide solids (Runde, 2000; Neck et al., 2001; Runde et al., 2002). In addition, they also have strong affinities to many types of aquifer sediments (Runde, 2000; Runde et al., 2002). Therefore, aqueous-phase contaminant transport models have predicted actinides to be almost immobile at contaminated DOE sites where many actinides have been released (Kersting et al., 1999). This type of transport model relies on the assumption that the solid aquifer matrix remains immobile, which in many situations is a reasonable assumption. However, several field studies have discovered actinides to be long distances (up to several kilometers) away from their contaminated sites (Penrose et al., 1990; Kaplan et al., 1994; Kersting et al., 1999; Novikov et al., 2006). In all of these studies, a significant fraction of the actinides was determined to be associated with colloids, which has led the scientific community to believe that colloid-facilitated transport was responsible for their faster-than-predicted transport.

Colloidal particles are ubiquitous in natural aqueous environments and consist of inorganic mineral phases and organic biopolymers with diameters less than 10 μm (McCarthy et al., 1989). Due to their small size, they have very large specific surface areas ranging from 10 to 800 m^2/g (Kretzschmar et al., 2005). This property makes colloids very reactive from a physiochemical perspective, allowing them to have high sorption capacities for contaminants. Therefore, colloids have the potential to carry bound contaminants as they migrate through the groundwater, a process often referred to as “colloid-facilitated contaminant transport” (McCarthy

et al., 1989). This transport mechanism is especially important for the movement of contaminants with low solubility and high affinity for solid interfaces, such as radionuclides, heavy metals, and nonpolar organics (Roy et al., 1997; Zhuang et al., 2003; Crancon et al., 2010; Zhou et al., 2011). Colloid-facilitated transport can significantly increase the concentration of these types of contaminants by several orders of magnitude over the values expected from solubility calculations through the formation of pseudo-colloids, or colloids with sorbed contaminants (Kim, 1991).

In groundwater aquifers, natural colloidal suspensions are formed due to (1) the release of fine particles from the porous media by chemical, physical and biological disturbances, such as fluctuations in water saturation, flow velocity, biofilm coating, and aqueous solution chemistry (McCarthy et al., 1989; Ryan et al., 1994; Ryan et al., 1994; Seaman et al., 1995; Kaplan et al., 1996; Ryan et al., 1996; Roy et al., 1997; Bunn et al., 2002; McCarthy et al., 2004; Grolimund et al., 2006; Cheng et al., 2010; Li et al., 2012) and (2) *in situ* precipitation of supersaturated mineral phases (Liang et al., 2000; Wan et al., 2004). However, McCarthy et al. (1993) discovered that most colloids existing in groundwater systems appear to be mobilized by changes in solution chemistry, such as decreases in ionic strength and increases in pH. These chemical fluctuations release colloids by increasing the electrostatic repulsive force between colloids and the immobile aquifer grains. In most groundwater aquifers, drastic changes in solution chemistry are atypical, but they can be produced by man-made conditions near contaminated sites. In a review, Ryan et al. (1996) state that the most common change in groundwater chemistry is the decrease in ionic strength. This perturbation can be triggered by the infiltration of dilute freshwater from natural rain events, irrigation, or artificial groundwater recharge. During these events, groundwater aquifers containing solutions of higher ionic strength are replaced by

solutions of lower salinity, potentially inducing the detachment of colloidal fines from sediments. This effect is particularly important at DOE radioactive waste sites, where high concentrations of electrolytes (>5M) and radionuclides have been leaking from storage tanks into groundwater aquifers (Gephart et al., 1998). Over time these hypersaline solutions can be diluted by infiltrating solution from the surface, potentially enhancing colloid-facilitated transport of radionuclides (Blume et al., 2005).

In spite of the limited field-scale evidence, many laboratory column experiments testing colloid-facilitated transport have confirmed that colloids can enhance the transport of strongly-sorbing contaminants through saturated porous media (Puls et al., 1992; Roy et al., 1997; Um et al., 2002; Mori et al., 2003; Grolimund et al., 2005; Zhang et al., 2007; Cheng et al., 2010; Crancon et al., 2010; Zhou et al., 2011). However, few studies have demonstrated colloid-facilitated transport of actinide elements. Therefore, the primary objectives of this study were 1) to determine if changes in solution chemistry would promote the *in situ* mobilization of natural colloidal particles from a saturated subsurface sediment collected from the Savannah River Site (SRS), and 2) to determine whether these changes would enhance the transport of Th(IV) sorbed to the SRS sediment. The Savannah River Site was historically used by the DOE to produce nuclear materials for their use in nuclear weapons (Seaman et al., 2007). Therefore, the SRS sandy sediment served as a particularly relevant subsurface material for conducting transport experiments due to the site's historic actinide disposal and subsurface contamination. The column experiments were performed by sorption/mobilization experiments, where Th(IV) was first adsorbed to the Savannah River Site sandy soil under conditions that minimized colloid detachment (e.g. high ionic strength) and then mobilized by conditions inducing natural colloids to be released as a result of decreased ionic strength or increased in pH. This method simulates

realistic scenarios at DOE sites, where plumes of radioactive waste containing high concentrations of electrolytes are replaced by infiltrating solutions of dilute rainwater from the surface. Th(IV) was chosen as the actinide for this transport study due to its similar chemical properties to Pu(IV), an actinide of concern at many DOE sites (Choppin, 1999). In addition, thorium is stable in the tetravalent oxidation state, which is the prevalent oxidation state of plutonium in most groundwater environments (Runde, 2000). Unlike plutonium, the oxidation state of Th(IV) is not a function of its concentration. Therefore, it is a particularly valuable analog assessing the behavior of Pu(IV) in the environment. In addition to its use as an analog, thorium contamination could also become more relevant in the future due to the use of thorium fuels for nuclear power production (Schapira et al., 1999)

3.2 Materials and Methods

3.2.1 Chemical Solutions

All chemicals used in this study were ACS grade or better and obtained from VWR International LLC. The Th(IV) stock solution was prepared by dissolving solid $Th(NO_3)_4 \cdot 4H_2O(s)$, obtained from International Bio-Analytical Industries Inc, in 0.07 M HNO_3. Aqueous Th(IV) standards were prepared by diluting a Th(IV) atomic absorption standard from Sigma-Aldrich with a 0.1 M HNO_3 solution containing similar background ionic strength of the samples. $NaNO_3(s)$ was used to adjust the ionic strength of the background electrolyte. Solution pH was adjusted with 0.1 M HNO_3 or 0.07 M NaOH. For solutions with pH greater than 6, CO_2 absorption was prevented by purging with N_2.

3.2.2 Sediment Description

A heterogeneous, Fe-containing subsurface sandy sediment was used as the packing material for column experiments. The sand was collected from the U.S. Department of Energy Savannah River Site (SRS), located in western South Carolina on the upper Atlantic Coastal Plain. This site was established in the 1950's to produce and refine a variety of nuclear materials, mainly ^{239}Pu and ^{3}H, for the use in nuclear weapons (Seaman et al., 2007). Although the SRS has discontinued the production of radionuclides, parts of the site have suffered from significant actinide contamination. However, the soil sample used in this study was collected from a trench located in an uncontaminated portion of the E-Area Low Level Waste Disposal Site at a depth of 9.5 m. This sediment is part of the Tobacco Road formation, which is a major formation in the lower vadose zone and water table aquifer at the SRS (Li et al., 2012). In order to preserve the undisturbed subsurface sediment, the sample was collected horizontally from the trench by first removing disturbed surface sediment. Once collected, the soil sample was air-dried, homogenized, and passed through a #10 sieve, removing any coarse grains larger than 2 mm.

The SRS sediment was texturally classified as sand and had size characteristics of 97% sand, 2.9% silt, and 0.2% clay. The pH of the soil was 5.1 (Allen, 1989) and the Fe content was measured to be 7.06 mg/g via citrate-dithionite-bicarbonate extraction (CDB), which represents free amorphous and crystalline Fe oxyhydroxides. Scanning transmission X-ray microscopy (STXM) analysis of the sediment determined that the sand grains were predominately composed of quartz, while X-ray diffraction data showed the mineralogy of the clay-sized fraction (<2 μm) consisted of mostly of kaolinite and goethite with lesser fractions of muscovite. Using a

scanning electron microscope (SEM), Li et al. (2012) observed that these fine particle minerals occurred as coatings on the quartz grain surfaces.

3.2.3 Column Transport Experiments

Transport experiments were conducted in 1 cm and 2.5 cm diameter Omnifit glass columns at room temperature. Only one column experiment (SRS # 4) used the larger scale column, which allowed for larger effluent sample volumes. This enabled both dissolved and total Th(IV) concentrations to be effectively analyzed. Each column was dry-packed with an average mass of 8.5 g (1-cm-dia.) and 54.5 g (2.5-cm-dia.) of Savannah River Site sandy soil to a height of 7 cm. The bottom of each column was retained with a fixed end piece fitting, while the top had an adjustable end piece that was adjusted until the plunger was snuggly in place with the soil. In addition, each column was fitted with 30 μm PTFE frits at both ends, which retained the soil but also allowed for the passage of mobile colloids into sampling test tubes. After dry-packing, the average bulk density of the SRS sandy sediment was 1.58 ± 0.03 g/cm^3, which assuming an average particle density of 2.65 g/cm^3 for the quartz-dominated sediment, corresponds to an average porosity of 0.40 ± 0.01. This porosity gave an average pore volume of 2.18 mL for the small scale columns and 14 mL for 2.5 cm column.

The transport experiments were performed in two phases, consisting of a sorption phase and a desorption/mobilization phase. Prior to the transport experiments, a background solution containing 0.1 M $NaNO_3$ at a pH of 4 was introduced into the column until air spaces were no longer visible and the pH had stabilized at 4. A low pH was used in these experiments due to thorium's low solubility at the neutral pH range, which was below the detection limits of the ICP-OES. Influent solutions were injected upward from the bottom of the vertically positioned

columns at a constant flow of 0.1 mL/min (1-cm-dia.) and 0.61 mL/min (2.5-cm-dia.) by HPLC pumps. These flow rates were chosen so that the 1-cm-dia. and 2.5-cm-dia. columns would have similar Darcy velocities, 1.83 m/day and 1.79 m/day respectfully, corresponding to an average retention time of 22 minutes. Column hydrodynamic properties were determined by conducting bromide tracer tests, yielding dispersion coefficients ranging from 8.34 to 2.61 cm^2/hr (column Peclet Numbers ranging from 16 to 48).

After the columns were saturated with background solution, the sorption phase was initiated, allowing Th(IV) to adsorb to the SRS sediment under conditions minimizing colloid detachment by the use of high electrolyte concentrations. During this phase, a step input of Th(IV) at an average concentration of 2.60 mg/L ($1.12x10^{-5}$ M) was introduced to each of the columns. Effluent samples were collected by a fraction collector at fixed time intervals. This phase was run until the effluent Th(IV) concentration reached at least 70% of the initial influent concentration. At this point, the desorption/mobilization phase was initiated by introducing a Th(IV)-free influent solution containing a change in solution chemistry to encourage colloid release from the SRS sediment. During this phase, several of the column experiments were subjected to multiple changes in solution chemistry. The conditions for all of the column experiments are shown in Table 3.1.

Table 3.1: Column transport experiment conditions

Column ID	Change in Solution Chemistry	Composition of Influent Solution	
		During Sorption	**During Desorption/Mobilization**
SRS # 1	Ionic Strength and pH - Multiphase	Th(IV)-Free, 0.1 M $NaNO_3$, pH 4.0	1) 0.001 M $NaNO_3$, pH 4.0 2) DI Water, pH 11.0
SRS # 2	Ionic Strength	$1.14x10^{-5}$ M $Th(NO_3)_4$, 0.1 M $NaNO_3$, pH 4.0	0.001 M $NaNO_3$, pH 4.0
SRS # 3	No Change	$1.13x10^{-5}$ M $Th(NO_3)_4$, 0.1 M $NaNO_3$, pH 4.0	0.1 M $NaNO_3$, pH 4.0
SRS # 4	Ionic Strength - Multiphase	$1.14x10^{-5}$ M $Th(NO_3)_4$, 0.1 M $NaNO_3$, pH 4.0	1) 0.05 M $NaNO_3$, pH 4.0 2) 0.01 M $NaNO_3$, pH 4.0 3) 0.001 M $NaNO_3$, pH 4.0 4) DI Water, pH 4.0
SRS # 5	Ionic Strength and pH - Multiphase	$1.10x10^{-5}$ M $Th(NO_3)_4$, 0.1 M $NaNO_3$, pH 4.0	1) 0.1 M $NaNO_3$, pH 11.0 2) DI Water, pH 11.0 3) DI Water
SRS # 6	Ionic Strength and pH - Multiphase	$1.11x10^{-5}$ M $Th(NO_3)_4$, 0.1 M $NaNO_3$, pH 4.0	1) 0.001 M $NaNO_3$, pH 4.0 2) DI Water, pH 11.0 3) DI Water

3.2.4 Turbidity, pH, and Th(IV) Concentration

Within 1 day of collection, effluent samples were agitated for 20 s using a vortex mixer and analyzed for turbidity with a Hach 2100N Laboratory Turbidimeter. Turbidity was then correlated to colloid concentration by utilizing a colloid calibration curve developed from the gravimetric analysis of 10 colloid effluent samples released from the SRS sediment by means of laboratory column experiments. This correlation has been conducted in several other studies but only provides an approximation of the true colloid concentration due to variations in scattered light by heterogeneous colloids of different size and composition (Roy et al., 1997; Bunn et al., 2002; Li et al., 2012). After analyzing turbidity, effluent pH was measured using a pH meter and combination electrode (Thermo Orion Model 410 A+) calibrated with standard buffer solutions. A Varian 710-ES ICP-OES was used to analyze the total Th(IV) concentration (dissolved and colloid-associated). Before analyzing with the ICP, each effluent sample was acidified with

0.625% by volume of 16 M HNO_3, giving a 0.1 M HNO_3 concentration and ensuring minimal Th(IV) was adsorbed to colloids and sample tube walls. In addition to total Th(IV), column experiment SRS # 4 also analyzed dissolved Th(IV) for selected effluent samples. Dissolved Th(IV) was measured by the ICP after filtering with a 0.2 μm water-wettable PTFE syringe filter (Pall Corporation) and then acidifying with HNO_3. This type of syringe filter was chosen due to its minimal adsorption of Th(IV), yielding 98% recovery. Teflon tubes were used for collecting effluent samples that were analyzed for dissolved Th(IV) to minimize Th(IV) loss by adsorption to tube walls.

3.2.5 Point of Zero Salt Effect

The batch potentiometric titration method by Zelazny et al. (1996) was used to estimate the net surface charge of the SRS sediment as a function of pH at two different ionic strengths. This method determined the point of zero salt effect (PZSE), which is the pH where the net proton surface charge density is unaffected by changes in ionic strength. In addition to PZSE, the crossover point of the two titration curves at different ionic strengths also represents the pH where the soil exhibits a zero net surface charge, or pH_{pzc}.

In order to conduct this method, soil samples weighing 3 g were suspended in 30 mL of 0.1 M and 0.005 M $NaNO_3$ and the pH was adjusted to a range between 2.5 and 11.5 with HNO_3 and NaOH. For each soil suspension at different pH values, an identical 30 mL blank solution (no soil) was prepared containing the same ionic strength and amounts of HNO_3 and NaOH. Both the blanks and soil sample suspensions were placed in 40 mL Teflon vials and rotated on an end-over-end tumbler for a 2 day period to equilibrate. After this period of time, pH values of the soil sample supernatants and the pure solutions were recorded. These pH values were then

plugged into a modified equation from Zelazny et al. (1996) to calculate surface charge, which can be seen in the appendix. The equation was modified due to conversion errors in the original equation.

3.2.6 SRS Colloid Characteristics

Synchrotron-based scanning transmission X-ray microscopy (STXM) at Lawrence Berkley National Laboratory's (LBNL) Advanced Light Source (ALS) facility was used to characterize Th(IV)-free colloids liberated from the SRS sandy sediment. The colloidal samples were collected from laboratory column transport experiments after being released by elevated pH. Before sending to LBNL, the colloid suspensions were filtered with 0.1 μm Polyvinylidene Difluoride (PVDF) membranes manufactured by Millipore. STXM combined with X-ray absorption near edge structure (XANES) spectroscopy was used to characterize the morphology, composition, and heterogeneity of the dried SRS colloids. XANES spectroscopy measurements were performed at the C K-edge, O K-edge, Fe L-edge, Al K-edge, and Si K-edge to identify various minerals and organic compounds contained within the colloids.

In addition to STXM analysis, ζ-potentials of Th(IV)-free colloidal suspensions mobilized from column experiment SRS # 1 were measured as function of pH and ionic strength using a Zetasizer Nano ZS (Malvern Instruments Ltd.). These measurements were conducted to determine the isoelectric point (IEP) of the SRS colloids, along with their stability as a function of pH and ionic strength. Before measuring ζ-potentials, 0.5 mL samples of the effluent colloidal suspensions were diluted to 17 mL solutions containing 0.1 M, 0.005 M, and 0.001 M $NaNO_3$, while the pH was adjusted to a range between 2.5 and 11.5 with HNO_3 and NaOH. Once suspensions of varying pH and ionic strength were prepared, they were then shaken with a

vortex mixer for 30 s and placed into a disposable folded capillary cell for measurement of ζ-potential. The Zetasizer calculated ζ-potential by determining electrophoretic mobility and then applying the Smoluchowski equation, $\mu = \varepsilon\zeta/\eta$, where μ is the electrophoretic mobility, ε is the dielectric constant, ζ is the zeta potential, and η is the viscosity. In addition to ζ-potential, particle size distributions of the effluent colloidal suspensions were also measured with the Zetasizer, using a technique called Dynamic Light Scattering. This technique produced a particle size distribution, along with a mean value for size based off of signal intensity.

3.3 Results and Discussion

3.3.1 SRS Colloid Characteristics

Figure 3.1 displays the results from the STXM analysis of the liberated SRS colloids. The elemental maps (columns I and II) from the STXM analysis showed strong response from carbon, oxygen, iron, aluminum, and silicon. The XANES spectrum measurements (column III) determined that the SRS colloids were composed of ferric oxyhydroxide and aluminosilicate minerals. The Fe L-edge spectral shape was very similar to hematite and goethite. However, the pre-edge low energy spectral shape of the O K-edge was more characteristic of goethite than hematite. The aluminosilicate found within the colloids was very similar to kaolinite, evident from the spectral shapes of the O K-edge, Al K-edge, and Si K-edge. The presence of kaolinite and goethite in the STXM results were consistent with the results found from XRD analysis of the clay-sized soil fractions. In addition, a similar study conducted by Li et al. (2012) released colloids from columns packed with a SRS soil collected from the same location. These colloids were determined to be composed of goethite and kaolinite by XRD and EDX (energy dispersive X-ray spectroscopy), giving very similar colloid composition to this study (Li et al., 2012).

Along with the presence of goethite and kaolinite, the XANES spectrum at the C K-edge yielded a significant amount of carbon.

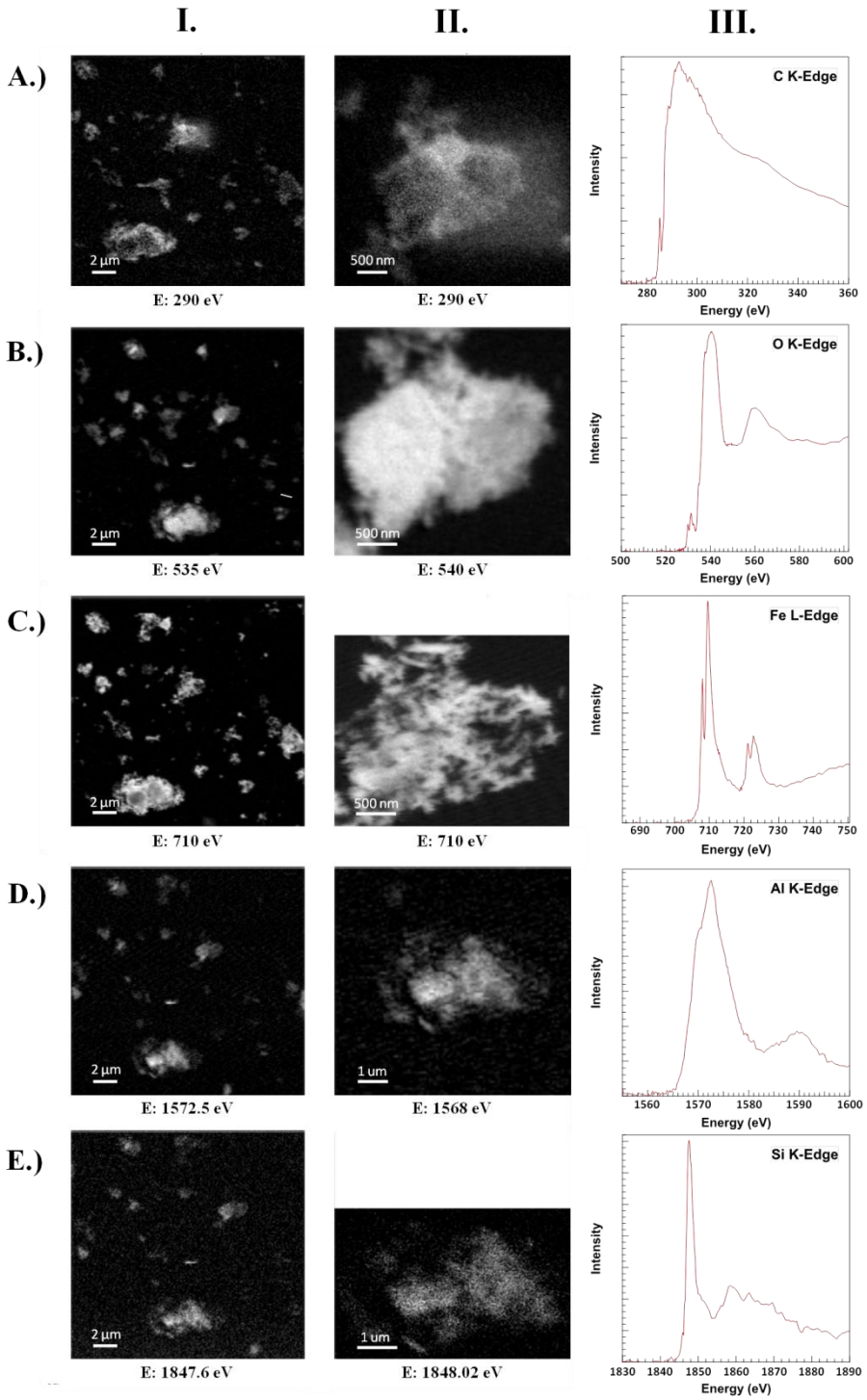

Figure 3.1: Scanning transmission X-ray microscopy (STXM) elemental maps of thorium-free SRS colloids liberated from column transport experiments (columns I and II) along with XANES spectrum measurements (column III) of carbon (A), oxygen (B), iron (C), aluminum (D), and silicon (E).

In addition to STXM analysis, ζ-potentials of Th(IV)-free colloidal suspensions were determined as a function of pH at three different ionic strengths (Figure 3.2). As seen from the arrow in Figure 3.2, the isoelectric point (IEP) is around a pH of 4.75. This value falls between measured IEP values for goethite (8.1) and kaolinite (4.1), (Appel et al., 2003), which were the predominate minerals detected within the colloids from the STXM analysis. As expected, the SRS colloids were much more stable at lower ionic strengths, giving higher absolute values for ζ-potentials. The mean size of effluent colloid samples mobilized from column transport experiments ranged from 185 to 600 nm. However, colloid samples that were titrated to lower pH ranges for measurement of ζ-potentials had much larger mean sizes, ranging up to 1700 nm. The largest sized colloids were measured around their IEP, where the colloids were less stable. Therefore, the large size was most likely due to aggregation.

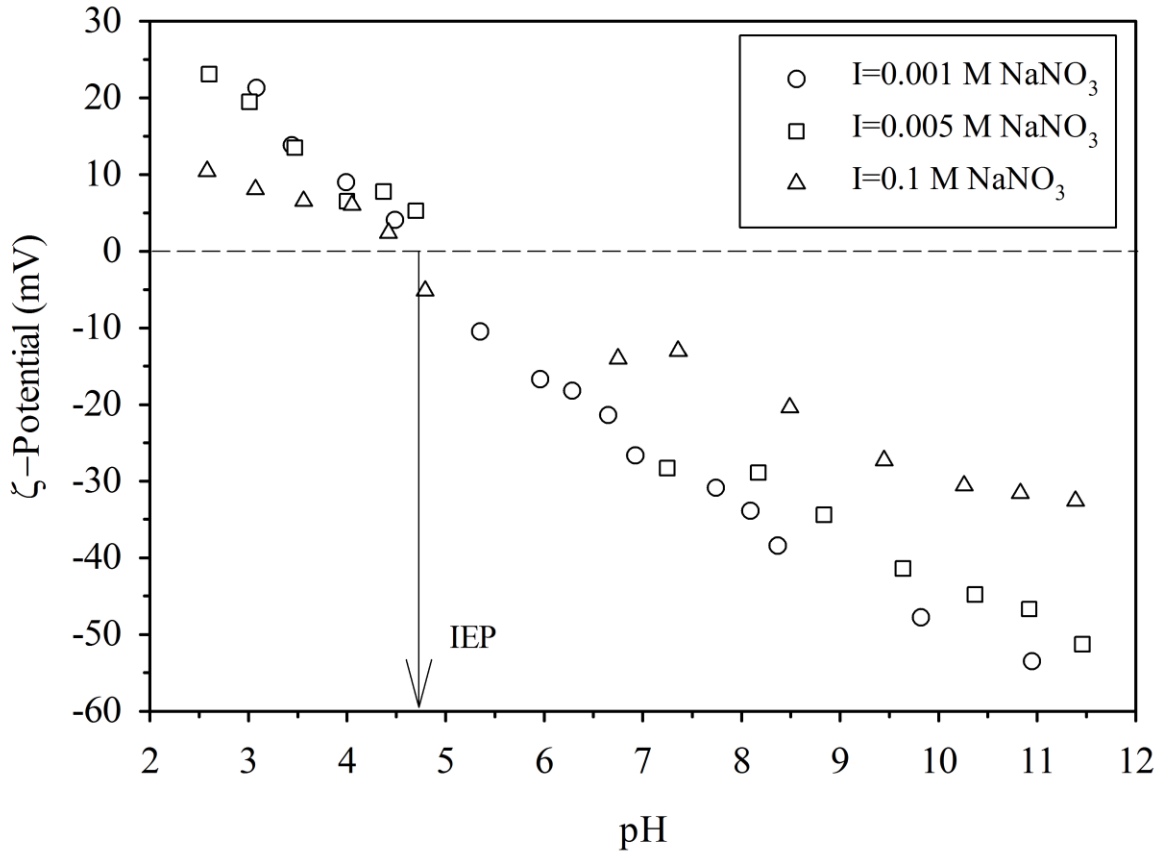

Figure 3.2: ζ-potentials of thorium-free SRS soil colloids released from column transport experiments as a function of pH at different ionic strength conditions. Arrow represents the approximate isoelectric point (IEP) of the colloids.

The net surface charge of the bulk uncontaminated SRS soil was also analyzed as a function of pH by conducting potentiometric titrations at two different ionic strengths (Figure 3.3). As seen from the arrow in Figure 3.3, the PZSE is approximately at a pH of 5.6. At this point, the net proton surface charge is unaffected by changes in ionic strength. As pH deviates from the PZSE, the absolute value of the net surface charge increases with increasing ionic strength. The PZSE also represents the point of zero charge (pH_{pzc}), or the pH where the soil exhibits a zero net surface charge. Although the SRS sand is predominately composed of quartz,

which has a measured pH_{pzc} of 2.3 (Taubaso et al., 2004), the presence of kaolinite and goethite on the surface of the quartz alters the pH_{pzc} to a higher value.

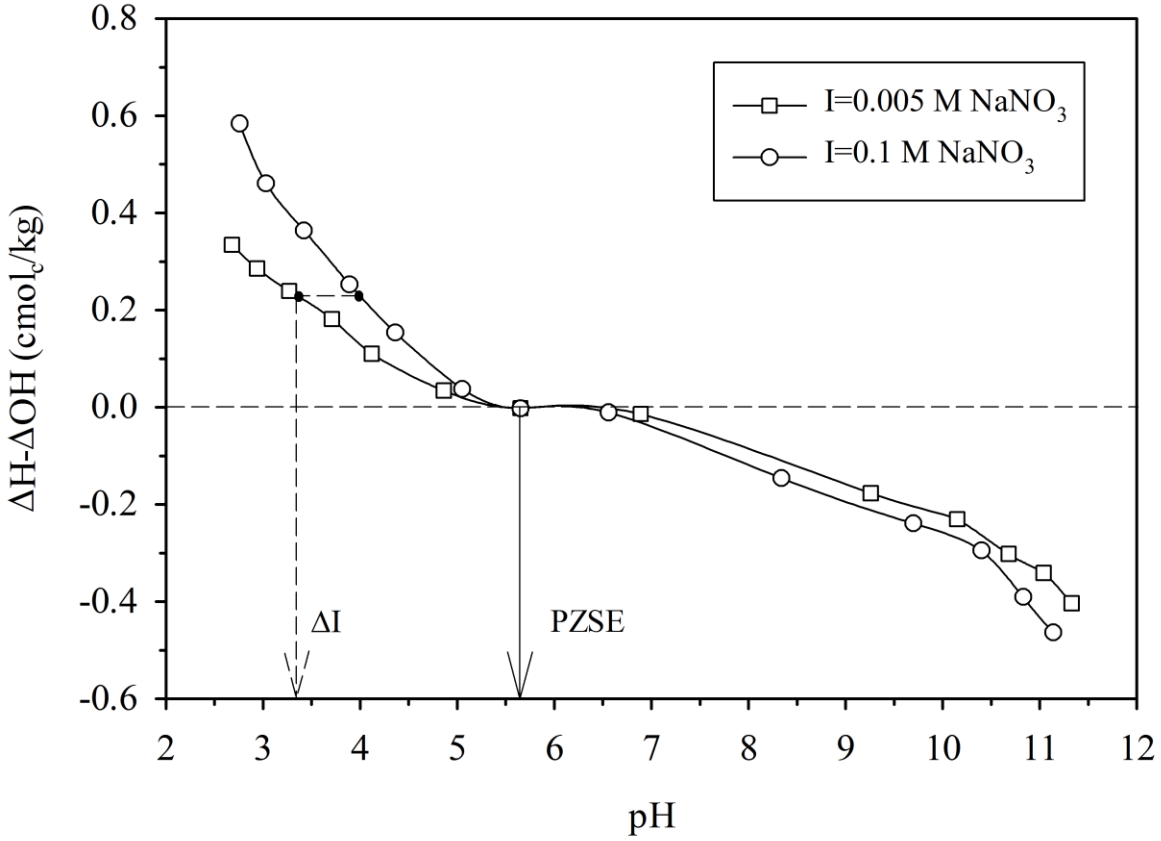

Figure 3.3: Potentiometric titrations of SRS sediment as a function of pH at two different ionic strengths. Solid arrow represents point of zero salt effect (PZSE), while dashed arrow represents the change in pH induced by decreases in solution ionic strength at a pH of 4.

3.3.2 Chemical Factors Influencing Colloid Mobilization from SRS Sandy Sediment in the Absence of Th(IV)

Since Th(IV) is a multivalent cation, its sorption could significantly influence the surface charge of the SRS sediment, impacting colloid detachment. Therefore, before Th(IV) transport experiments were performed, the first column experiment, SRS # 1, was conducted to determine

the effect of changes in solution chemistry on the release of colloids from the SRS sandy sediment in the absence of Th(IV).

Column experiment SRS # 1 was conducted by first introducing a step input solution containing a high ionic strength (I=0.1 M $NaNO_3$) at a pH of 4. This was the same background solution later used in the sorption phase of the Th(IV) transport experiments. During this phase of the experiment, no colloid mobilization was observed in the effluent solutions. The effluent pH and colloid concentration breakthrough curves for SRS # 1 are shown in Figure 3.4. After running this high ionic strength step feed for 330 pore volumes, the first mobilization phase was initiated by introducing a low ionic strength (I=0.001 M $NaNO_3$) influent solution at the same pH. However, this decrease in solution salinity was ineffective at mobilizing natural colloids from the surface of the SRS sediment. This result was somewhat surprising, because low electrolyte concentrations are commonly known to cause colloid mobilization (Nightingale et al., 1977; Khilar et al., 1984; Roy et al., 1996; Lenhart et al., 2003). However, several other studies using similar ferric oxyhydroxide coated sands observed similar results (Ryan et al., 1994; Seaman et al., 1995; Bunn et al., 2002). A decrease in solution salinity is only effective in mobilizing colloids when the colloids and grains have like-charged surfaces, or repulsive interactive forces. In the case of the SRS sediment at a pH of 4, the fine particles (kaolinite and goethite) attached to the surface of the immobile quartz grains had opposite charges. As seen in Figure 3.2, the heterogeneous SRS colloids had a positive charge at a pH of 4, while the immobile quartz grains had a negative charge in reference to its pH_{pzc} around 2.3 (Taubaso et al., 2004). Therefore, it is hypothesized that lower ionic strength would actually increase the electrostatic attractive force between the colloids and grains, further preventing detachment.

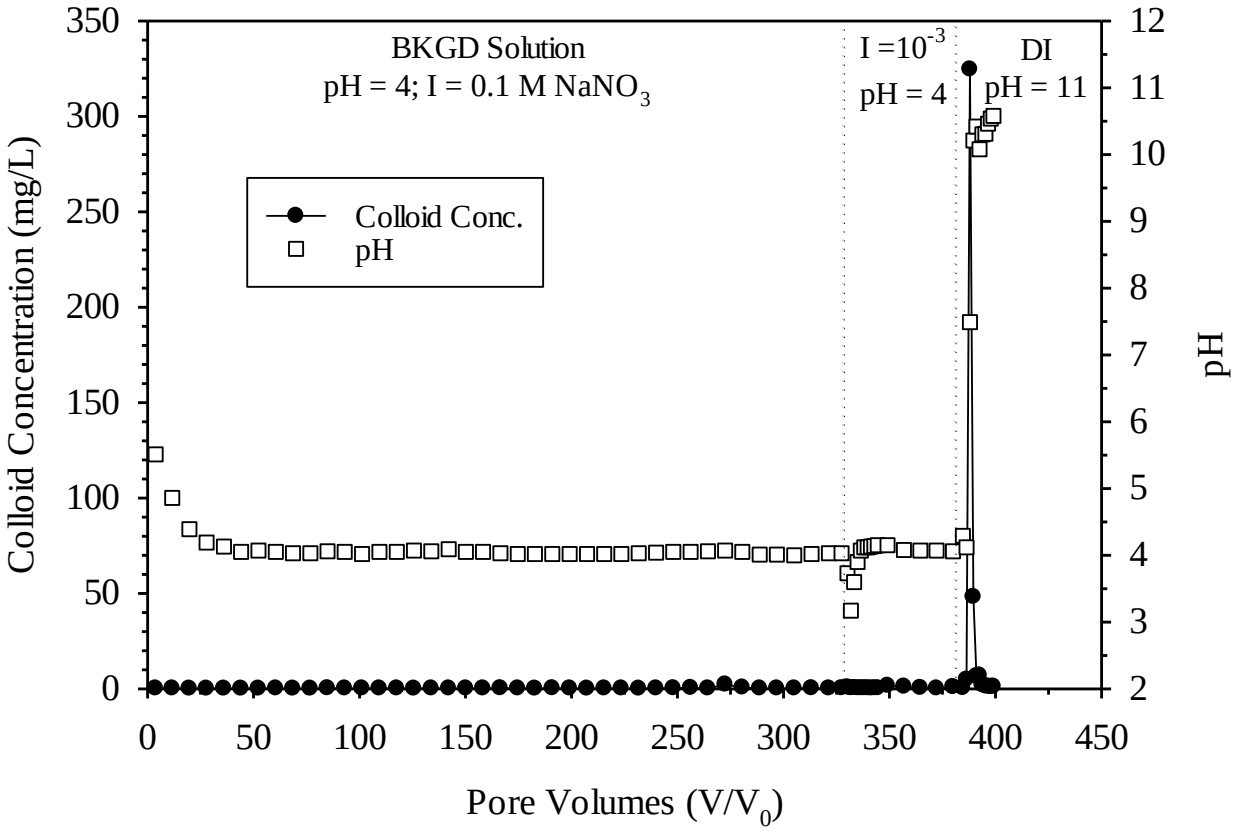

Figure 3.4: Effluent colloid concentration and pH for SRS # 1 (Th(IV)-free transport experiment, Temp=26±1°C, Q=6 mL/hr). Dotted lines indicate changes in influent solution chemistry.

Another surprising result in the first mobilization phase of SRS # 1 was the decreased pH front induced by changes in solution salinity. Once falling to a minimum pH of 3.17, the effluent pH increased back to 4 after approximately eight PVs. This phenomenon can be explained by the surface charge density of the soil at different electrolyte concentrations (Figure 3.3). During a significant decrease in ionic strength, the surface charge of the solid phase must remain constant by adjusting the solution pH (via ion exchange) to the value that corresponds to the same charge density at the lower salinity, as seen in Figure 3.3 (Scheidegger et al., 1994). For

instance in SRS # 1, the decreased salinity front at the low pH of 4 triggered the following anion exchange reaction to occur at the sediment surface, X:

$$NO_3^- X + OH^- \leftrightarrow OH^- X + NO_3^-$$

This ion exchange reaction kept the surface charge of the sediment constant by exchanging nitrate for hydroxide, causing a non-retarded decrease in effluent solution pH. Such pH fronts will always accompany changes in solution salinity unless the initial pH corresponds to the point where the surface charge of the sediment is independent of the electrolyte concentration, or PZSE.

Since no significant colloid concentration was detected after the first mobilization phase in SRS # 1, a second phase was initiated after 383 PVs, introducing a solution containing a high pH. In contrast to the first phase, the second phase promoted the mobilization of natural colloids from the surface of the SRS sediment. In fact, the colloidal front could actually be seen moving within the glass column (Figure 3.5). The colloid concentration peaked at 324 mg/L before plugging the column, causing leaks at tubing connections. The column was most likely plugged by multiparticle bridging at the column frit due to the extremely high concentrations of colloids mobilized from the SRS sediment. Several studies using similar iron oxyhydroxide coated sands also observed comparable colloid mobilization upon the introduction of elevated pH solutions (Ryan et al., 1994; Bunn et al., 2002; Li et al., 2012).

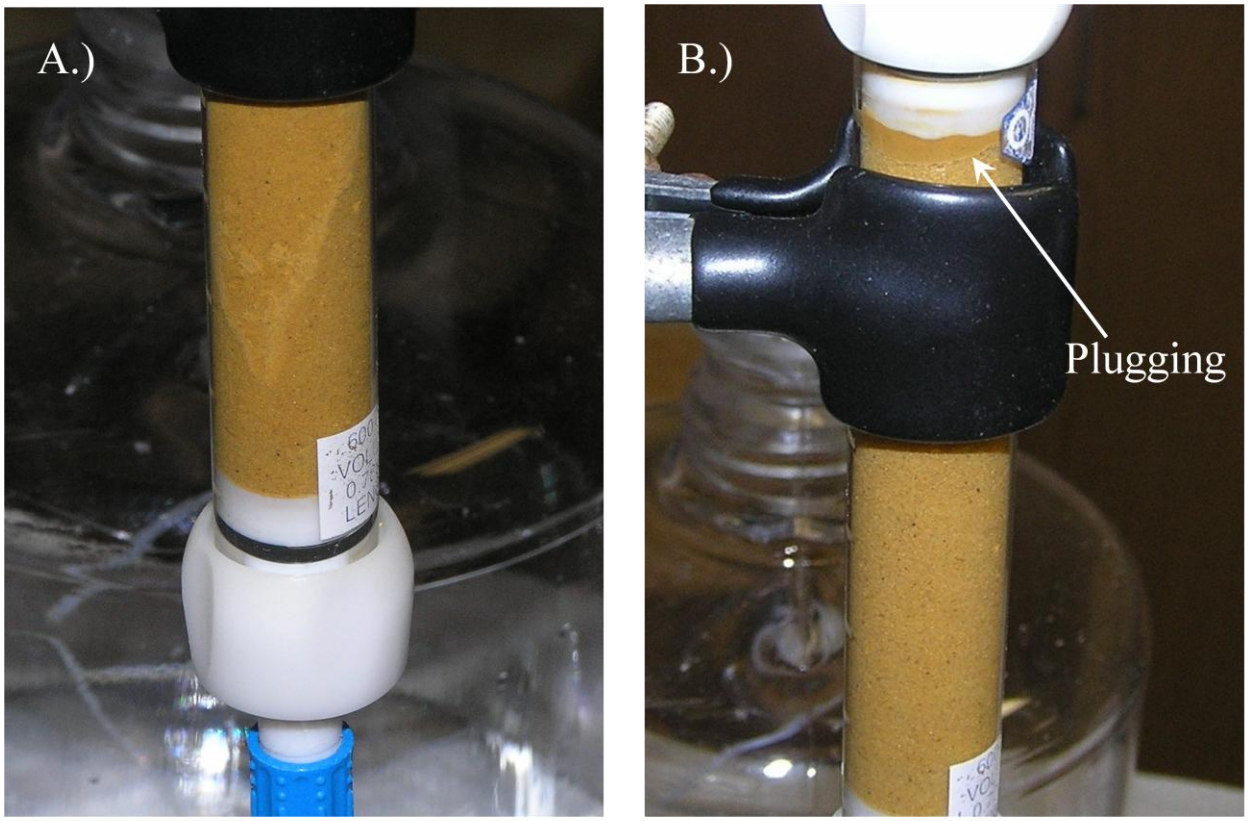

Figure 3.5: Colloid mobilization front in SRS # 1 after the infiltration of an elevated pH solution (A) and column plugging due multiparticle bridging at the column frit (B).

During natural aquifer conditions at the Savannah River Site, the positively charged goethite particles coating the SRS sediment act as a cementing agent, holding kaolinite and itself onto the surface of immobile quartz grains by electrostatic attraction (Li et al., 2012). However, the introduction of the high pH solution in the second mobilization phase caused the surface charge on the goethite to reverse, releasing both kaolinite and goethite colloids from the surface of the quartz grains. The highly negative ζ-potential of the heterogeneous SRS colloids at a pH of 11 shown in Figure 3.2 further demonstrates the surface charge reversal caused by elevated pH. Figure 3.6 shows an illustration of the two mobilization phases conducted in SRS # 1.

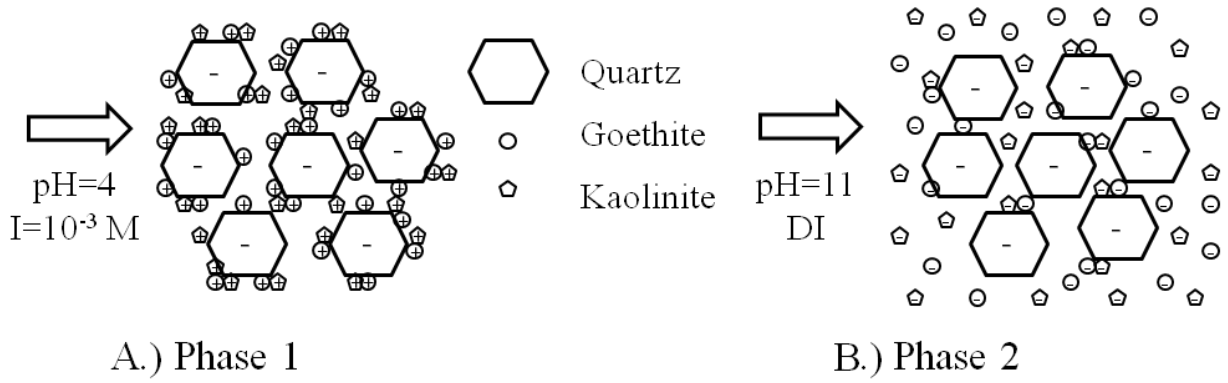

Figure 3.6: Illustration of colloid release from SRS # 1 mobilization phases, where phase 1 was ineffective at releasing colloids (A) and phase 2 promoted colloid mobilization (B).

3.3.3 Effect of Decreased Ionic Strength on Th(IV) Transport

Column experiments SRS # 2 and SRS # 3 were conducted to compare the effects of a system that experiences a drastic decrease in influent ionic strength to a system that experiences no change in solution chemistry during desorption. Both of these column experiments had identical procedures up to the desorption phase. At this point, the only difference between the two columns was that SRS # 2 had a decrease in influent solution salinity from 0.1 M $NaNO_3$ to 0.001 M $NaNO_3$, while the ionic strength of SRS # 3 remained constant at 0.1 M $NaNO_3$.

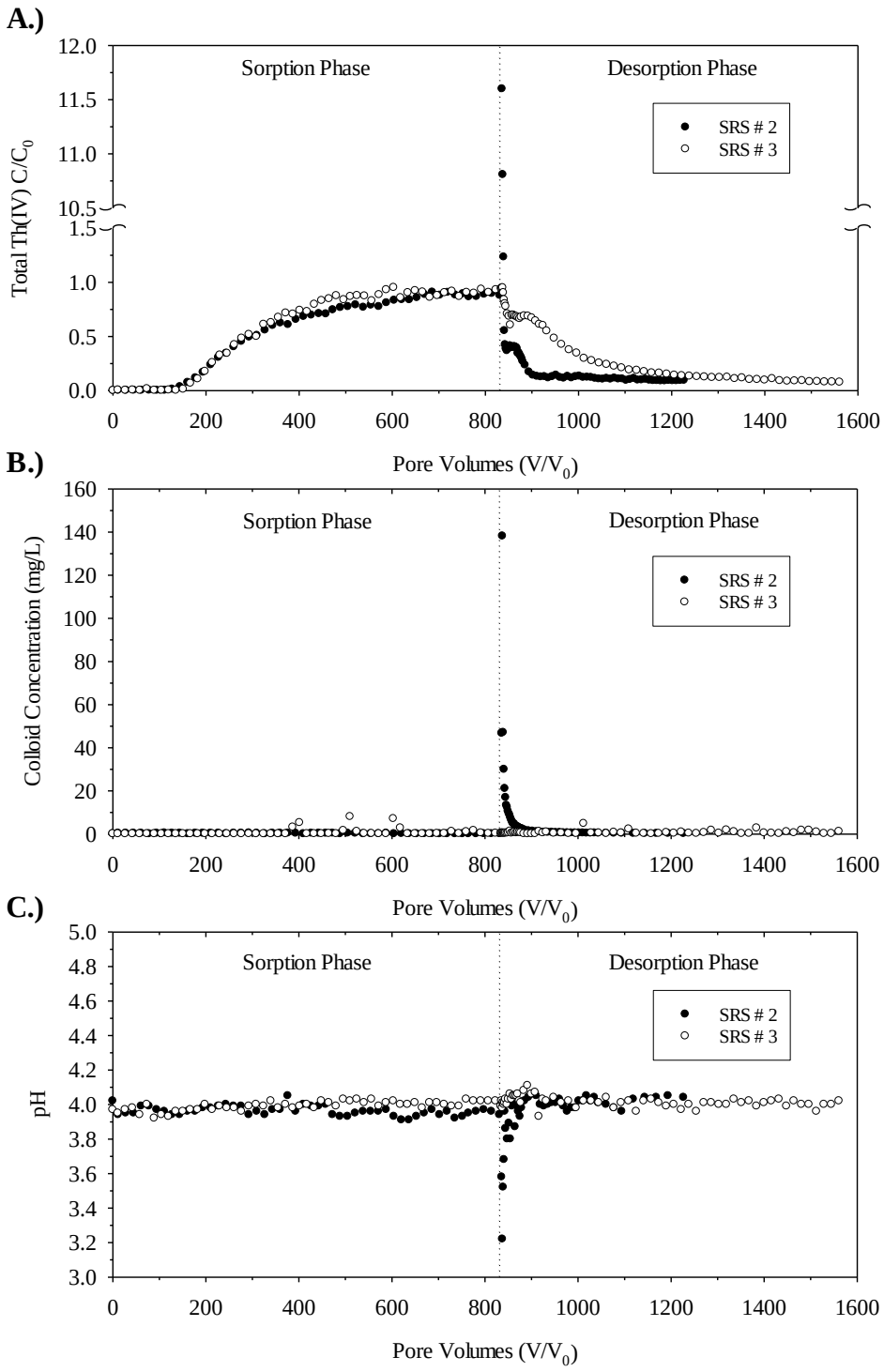

Figure 3.7: Effluent total Th(IV) concentration (A.), colloid concentration (B.), and pH (C.) for SRS # 2 and SRS # 3 (C_0=2.64 mg/L, pH=4, log P_{CO2}=-3.5, Temp=26±1, Q=6 mL/hr). Dotted line indicates change from sorption phase to desorption phase.

Figure 3.7 displays the total Th(IV) concentrations, colloid concentrations, and pH of the effluent solutions for SRS # 2 and SRS # 3. As seen from Figure 3.7A., the SRS sandy soil significantly retarded the transport of Th(IV) during the sorption phase, taking over 100 PVs before any Th(IV) was detected in the effluent solutions. After 100 PVs, Th(IV) had a traditional breakthrough curve, which began to plateau around 400 PVs. Due to the long period of time for Th(IV) to fully breakthrough, the desorption/mobilization phase was initiated when the Th(IV) concentration was greater than 90% of the influent concentration, which occurred around 830 PVs.

Once the desorption phase was initiated, the breakthrough curve in SRS # 2 experienced major differences compared to SRS # 3. The decrease in solution salinity in SRS # 2 significantly affected the transport of Th(IV), the release of colloids, and the effluent pH. Contrary to SRS # 1, which was conducted in the absence of Th(IV), the decrease in ionic strength in SRS # 2 caused significant concentrations of colloids to be released, peaking at 138 mg/L. Therefore, the sorption of Th(IV) may have impacted the surface charge on the SRS sediment. Several studies have shown that the adsorption of multivalent ions and surfactants can alter the surface charge of minerals (Omenyi et al., 1986; Schramm et al., 1991; Ryan et al., 1994; Roy et al., 1997; Alkan et al., 2005). For instance, one study conducted by Omenyi et al. (1986) determined that low concentrations of Th(IV) (10^{-6} to 10^{-5} M) strongly affected the electrophoretic mobility of quartz and other minerals to the point where its sorption reversed the surface charge of the minerals at an approximate pH of 5.6. Therefore, it is hypothesized that the sorption of Th(IV), a tetravalent cation, reversed the negative surface charge of the predominately quartz sediment, causing repulsive electrostatic forces between the colloids and

grains. These repulsive forces were further increased after the decrease in solution salinity, promoting colloid mobilization.

Coinciding with increases in colloid concentration, the total Th(IV) effluent concentration peaked at 11.5 times the influent concentration immediately after the change in solution chemistry in SRS # 2. Therefore, it was initially hypothesized that colloid-facilitated transport was responsible for the increase in Th(IV) effluent concentrations. However, the pH also dropped after the decrease in ionic strength, similar to SRS # 1. Previous batch sorption pH edges conducted by Melson et al. (2012) showed that Th(IV) has less affinity to the SRS sandy subsurface soil at lower pH values. Therefore, the drop in pH may also be responsible for the enhanced mobilization of Th(IV).

In comparison to SRS # 2, SRS # 3 had a typical Th(IV) desorption breakthrough curve, releasing no significant concentration of colloids and experiencing no change in pH (Figure 3.7). On the contrary, SRS # 2 breakthrough curve had an initial peak in Th(IV) concentration, followed by a sharp drop in concentration, where it plateaued around 10% of the initial Th(IV) concentration. The percent recovery of Th(IV) for SRS # 2 was around 69%, while the recovery for SRS # 3 was around 80%. In order to accurately compare the percent recoveries of the two experiments, the breakthrough curve in SRS # 2 had to be extrapolated, because SRS # 3 was carried out for an additional 330 pore volumes. The lower percent recovery in SRS # 2 can be easily seen by comparing the desorption breakthrough curves of the two experiments in Figure 3.7A. Although Th(IV) transport in SRS # 2 was immediately enhanced after the decrease in ionic strength, it was later retarded relative to the breakthrough curve of SRS # 3. The exact cause of this lower percent recovery was not evident, but two possible events may have

attributed to the retarded Th(IV) transport. The first explanation is colloid-associated retardation due to the plugging phenomenon (Sen et al., 2002). This process retards the transport of contaminants by increasing the accessibility of adsorption sites after colloids that have been mobilized are later removed from solution by aggregation, settling, readhesion to pore surfaces, or entrapment at pore constrictions. In addition to this possible factor, several studies demonstrated that Th(IV) adsorption onto metal oxides was sensitive to ionic strength, causing Th(IV) to have greater adsorption in lower ionic strength solutions (Guo et al., 2005; Zhijun et al., 2005). This Th(IV) adsorption property could also help explain why Th(IV) was retarded in SRS # 2.

3.3.4 Th(IV) Mobilization Mechanism during Decreases in Ionic Strength

In order to determine whether the drop in pH or the mobilization of colloids was responsible for the enhanced Th(IV) migration in SRS # 2, SRS # 4 was conducted. This column transport experiment was conducted in a larger scale column to allow for the analysis of both dissolved and total Th(IV) concentrations. Since the two previous experiments showed that Th(IV) took long periods of time to fully breakthrough during the sorption phase, SRS # 4 initiated the mobilization phases when the Th(IV) effluent concentration was around 80% of the influent concentration. In this experiment, multiple mobilization phases were initiated, each with decreasing influent solution ionic strength at a constant pH of 4 (Table 3.1).

Both the total and dissolved Th(IV) concentrations, along with colloid concentrations and pH of the effluent solutions for SRS # 4 are shown in Figure 3.8. Each sequential drop in solution salinity enhanced the transport of Th(IV), causing the concentration to peak above the influent concentration. In addition to peaks in Th(IV) concentration, the pH also dropped after

each decrease in solution ionic strength. However, colloids were not detected in effluent samples until after the influent solution ionic strength dropped to 0.01 M $NaNO_3$ in the second mobilization phase. Therefore, it is hypothesized that a critical salt concentration (CSC) of approximately 0.01 M $NaNO_3$ must be reached before colloids begin releasing from this system. The highest concentration of colloids was released when the ionic strength was dropped to 0.001 M $NaNO_3$ in the third mobilization phase. At this point, the colloid concentration peaked at 240 mg/L and the pH dropped to a minimum of 3.49. This phase also experienced the largest peak in Th(IV) concentration, nine times the influent concentration.

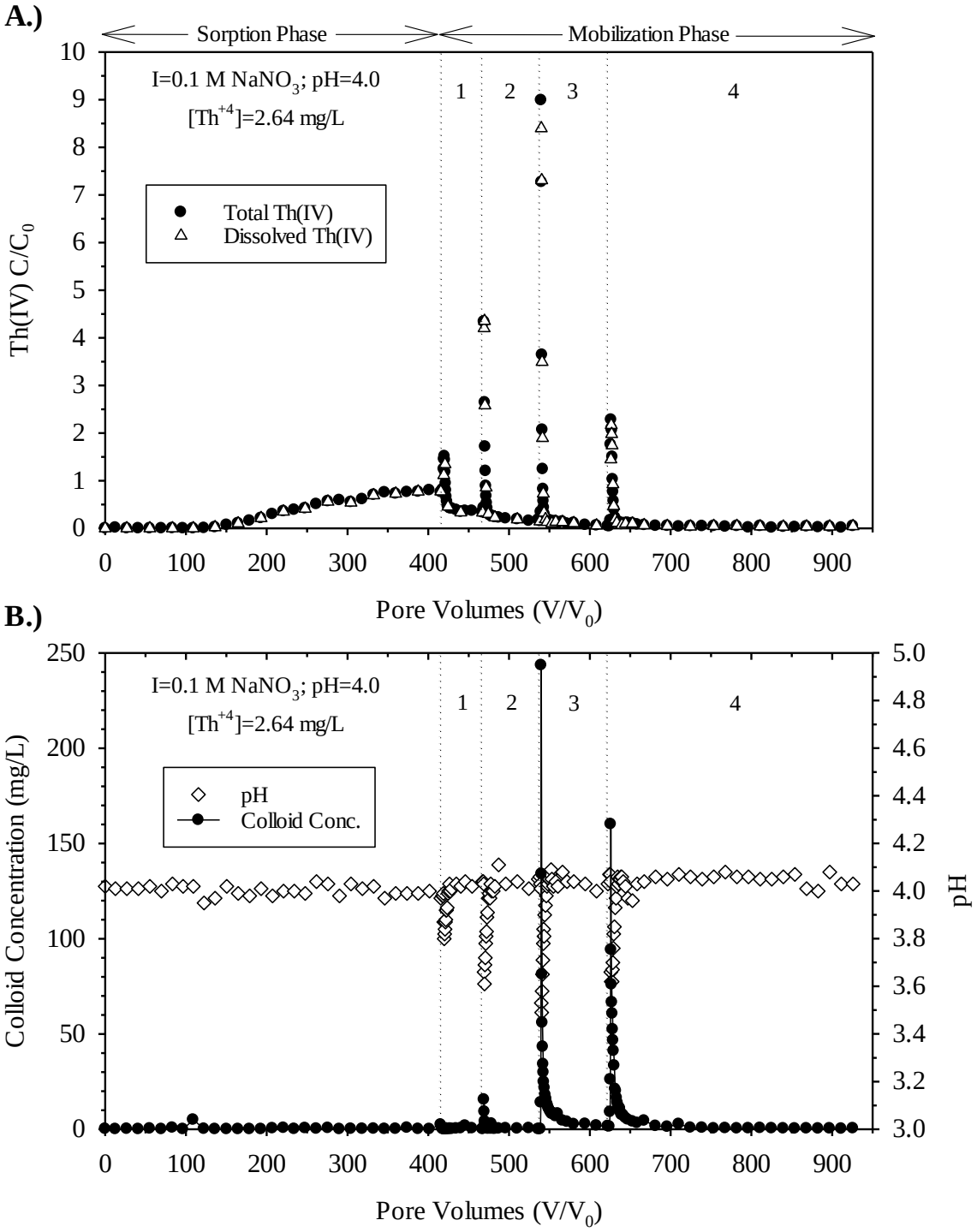

Figure 3.8: Effluent total and dissolved Th(IV) concentrations (A.), colloid concentrations, and pH (B.) for SRS # 4 (pH=4, log P_{CO2}=-3.5, Temp=26±1, Q=36.6 mL/hr). Dotted lines indicate each mobilization phase containing the following decreased solution salinities, 0.05 M (1), 0.01 M (2), 0.001 M (3), and DI (4) at pH=4.

Dissolved Th(IV) concentrations were determined after filtration with 0.2 μm membrane filters. After this filtration process, minimal turbidity (< 0.2 NTU) was detected in the samples. Therefore, it was assumed that the majority of the SRS colloids were removed from solution. As seen in Figure 3.8 A, the dissolved Th(IV) concentrations were very similar to the total Th(IV) concentrations, averaging around 93% of the total concentrations. Therefore, it was concluded that colloid-facilitated transport only played a minor role in enhancing the transport of Th(IV). Instead, the decreased pH fronts associated with the changes in solution salinity were primarily responsible for the enhanced Th(IV) migration. The results from the first mobilization phase further solidify this conclusion. This phase experienced peaks in Th(IV) concentrations without the release of colloids. Therefore the decreased pH front, falling to a minimum of 3.8 in this phase, must have desorbed higher concentrations of Th(IV) from the surface of the SRS sandy sediment.

3.3.5 Effects of Increased pH on Th(IV) Transport

In addition to the effects of decreased solution salinity, the effects of elevated pH on Th(IV) transport were also investigated in this study. Similar to the previous experiments, SRS # 5 adsorbed Th(IV) to the SRS sediment before initiating mobilization phases. However, this experiment initiated mobilization phases by increasing the influent solution pH (Table 3.1). The results from SRS # 5 are shown in Figure 3.9.

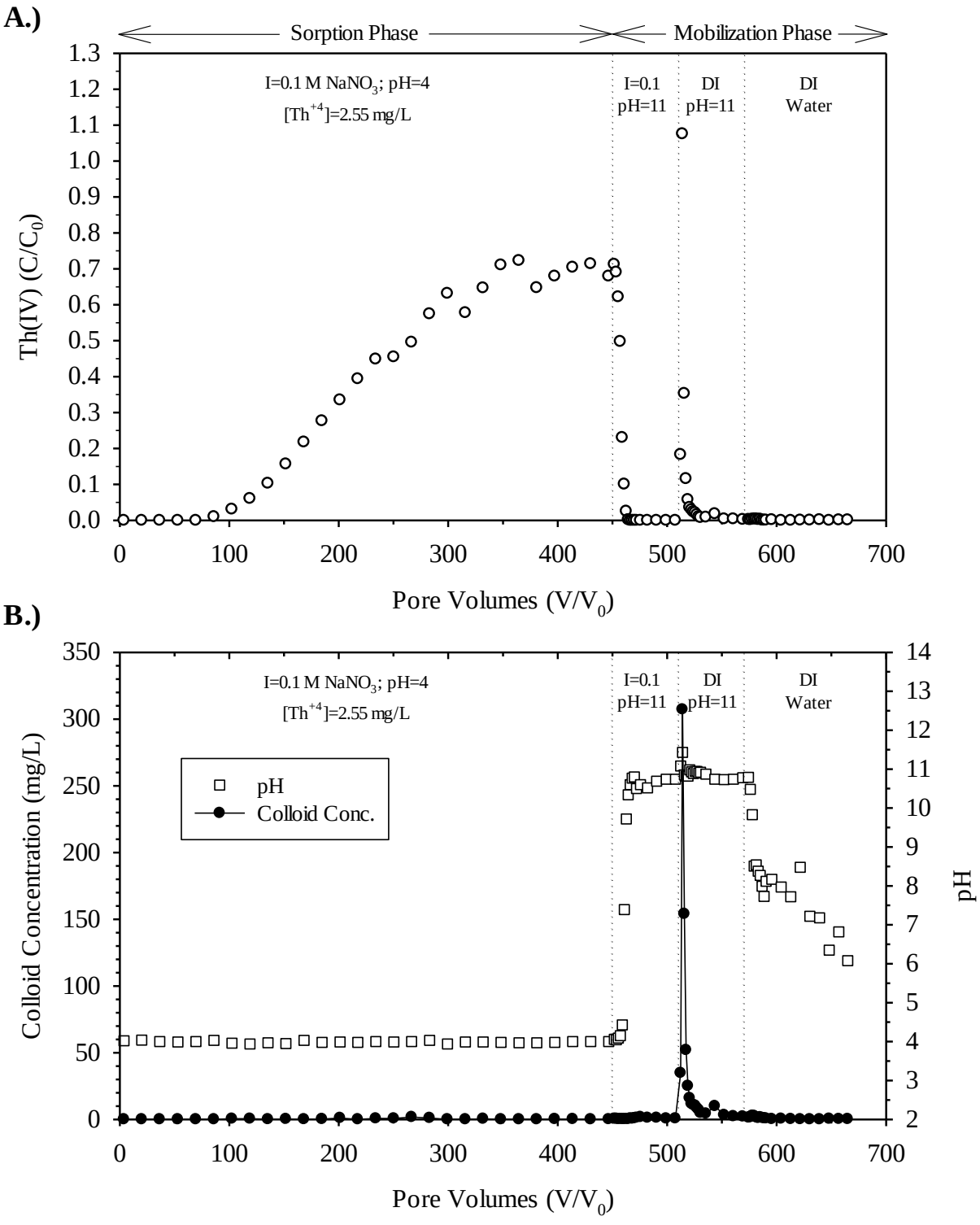

Figure 3.9: Effluent total Th(IV) concentrations (A.), colloid concentrations, and pH (B.) for SRS # 5 (Temp=26±1, Q=6 mL/hr). Dotted lines indicate changes in solution chemistry.

As seen in Figure 3.9A, the first mobilization phase caused the total effluent Th(IV) concentration to quickly fall below the detection limits of the ICP-OES. This drastic drop in Th(IV) concentration was due to the infiltration of the basic influent solution. Previous experiments by Melson et al. (2012) have shown that the solubility of Th(IV) is controlled by the formation of ThO_2 (am, aged) precipitates. As seen in Figure 3.10, the influent Th(IV) concentration becomes oversaturated with respect to the formation of amorphous thorium hydroxide solid slightly above a pH of 4.

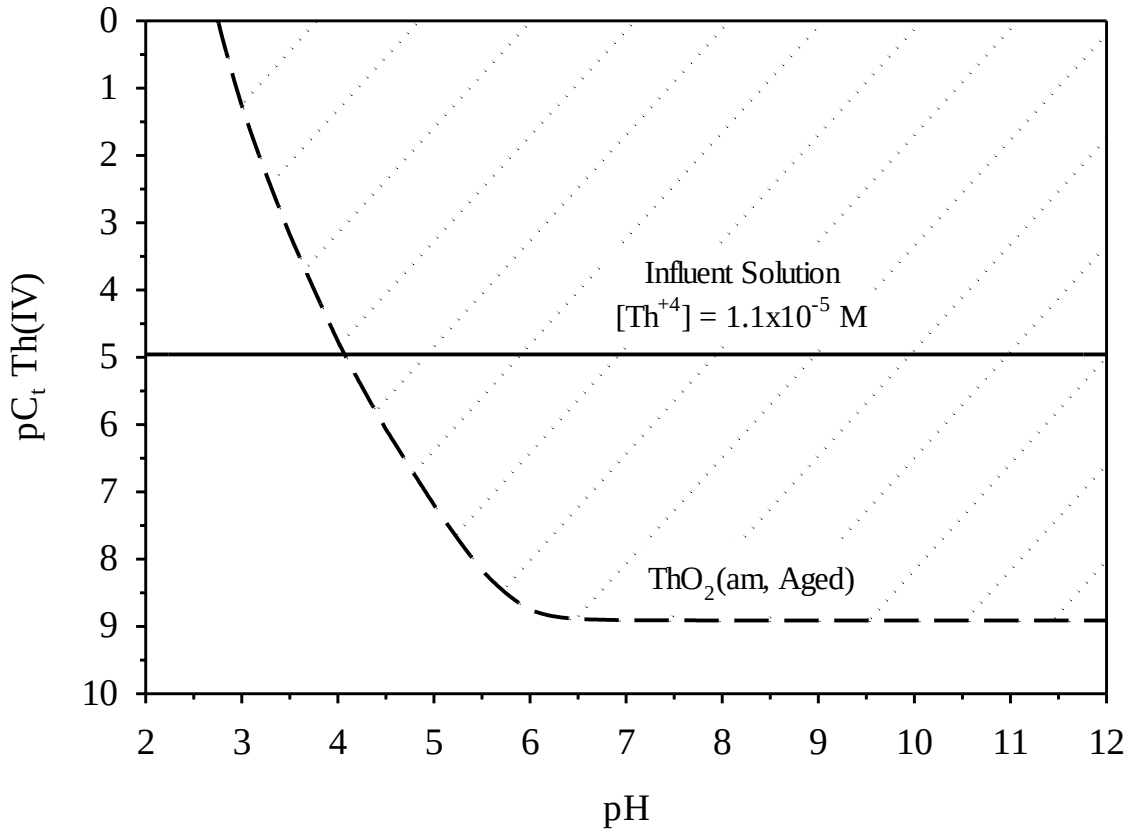

Figure 3.10: Solubility of ThO_2 (am, Aged) precipitate as a function of pH. Solid line indicates the Th(IV) concentration in the influent solution of SRS # 5. Dotted lines indicate region of oversaturation. (Solubility calculation made on closed system containing 0.1 M $NaNO_3$ with Visual MINTEQ)

As seen in Figure 3.9B, the increase in pH alone in the first mobilization phase was ineffective in mobilizing colloids from the SRS sediment. This result was somewhat surprising, because the ζ-potentials of uncontaminated SRS colloids were determined to be negative at high pH values, as seen in Figure 3.2. Therefore, it was believed that the high pH alone would have induced a strong enough repulsive force to release the colloids from the surface of the SRS sediment. However, the high ionic strength (I=0.1 M $NaNO_3$) and the sorption of Th(IV) in this phase may have prevented their release. After the ionic strength was decreased in the second phase, colloids were mobilized from the SRS sediment, peaking at 307 mg/L. In addition to colloid release, this phase also enhanced the transport of Th(IV), where effluent Th(IV) concentrations coincided directly with increased colloid concentrations detected in the effluent samples. The measured Th(IV) effluent concentrations were also oversaturated with respect to the solubility calculations of the ThO_2 (am, aged) solid. Therefore, it was concluded that colloid-facilitated transport was responsible for the enhanced migration of Th(IV) in this experiment. After the decrease in solution salinity, the effluent Th(IV) concentration peaked at 108 % of the influent Th(IV) concentration. This peak in Th(IV) concentration was observed in the same effluent sample containing the peak in colloid concentration. The average concentration of Th(IV) sorbed onto the surface of the mobilized SRS colloids in this phase was 24 μmol of Th(IV)/g of colloids. Although colloid-facilitated transport significantly enhanced the migration of Th(IV) in this experiment, it was much less effective in comparison to the previous Th(IV) transport experiments inducing changes in solution salinity at the lower pH range. The final mobilization phase in SRS # 5 introduced an influent solution containing deionized water.

However, no significant concentrations of colloids nor Th(IV) were detected in the effluent solutions during this phase.

3.3.6 The Impact of Th(IV) on Colloid Detachment from SRS Sediment

As demonstrated from the column transport experiments conducted in this study, the sorption of Th(IV) had a significant impact on the mobilization of natural colloids from the SRS sediment. To further demonstrate this, SRS # 6 replicated the mobilization phases in SRS # 1, but in the presence of Th(IV). The results for SRS # 6 are shown in Figure 3.11.

Comparing the results of SRS # 1 to SRS # 6 further concludes that Th(IV) sorption altered the surface charge of the SRS sediment. In the absence of Th(IV) (SRS # 1), colloids were mobilized from the SRS sediment only after increases in influent solution pH, while changes in solution salinity at the lower pH range were ineffective at releasing colloids. In contrast, changes in solution salinity at the low pH range in SRS # 6 promoted the mobilization of colloids from the SRS sediment, as seen in Figure 3.11. In addition, the sorption of Th(IV) also appeared to hinder the mobilization of colloids once the pH was increased in the second phase. The elevation in pH in this phase released very low concentrations of colloids in comparison to the Th(IV)-free experiment. This was probably attributed to the sorption of the tetravalent cation, altering the surface charge of the sediment to a more positive charge. Therefore, the infiltrating basic solution did not cause the same magnitude of repulsive forces between the colloids and the grain surfaces. This effect was also observed in SRS # 5. Although high concentrations of colloids were released once the ionic strength was decreased at the pH of 11, no colloidal front was visibly seen mobilizing through the column like the Th(IV)-free column. In addition, no plugging was observed in SRS # 5.

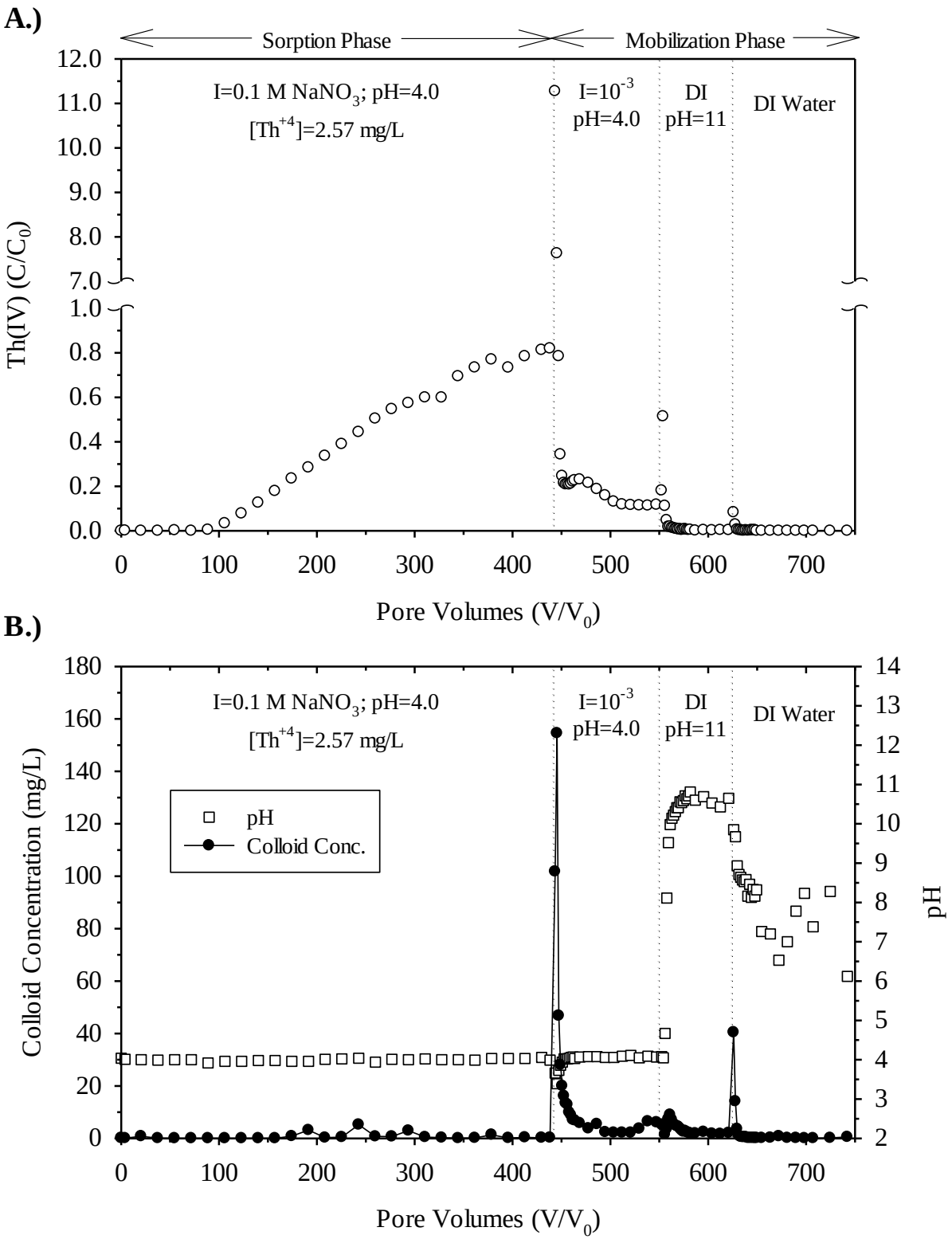

Figure 3.11: Effluent total Th(IV) concentrations (A.), colloid concentrations, and pH (B.) for SRS # 6 (Temp=26±1, Q=6 mL/hr). Dotted lines indicate changes in solution chemistry.

As seen from Figure 3.11, the second mobilization phase of SRS # 6 slightly enhanced the transport of Th(IV) even though low concentrations of colloids were released. This was caused by a slight drop in pH before increasing to 11. The decreased pH front was attributed to the small change in ionic strength, shifting from a solution containing 0.001 M $NaNO_3$ at a pH of 4 (I=0.0011 M) to DI water at a pH of 11 (I=0.001 M). Similar to the first mobilization phase, a slight drop in pH in the second phase desorbed higher concentrations of Th(IV) from the sediment. The third mobilization phase of SRS # 6, further decreased the solution salinity by introducing deionized water. This final phase caused effluent colloid concentrations to peak at 40 mg/L and slightly enhanced Th(IV) transport by colloid-facilitated transport.

3.3.7 Environmental Implications

This study determined the effects of changes in solution chemistry on the transport of Th(IV) through a saturated subsurface sediment collected from the Savannah River Site. In addition, it also simulated realistic scenarios at DOE waste sites, where acidic plumes of actinide waste containing high concentrations of electrolytes are replaced by infiltrating dilute rainwater from the surface. Such salinity fronts are commonly associated with the mobilization of colloids. In many aquifers, this decrease in solution ionic strength can promote the *in situ* mobilization of natural colloids by increasing the electrostatic repulsive forces between colloidal particles and immobile aquifer grains. However, decreases in solution salinity may also be accompanied by pH fronts, as demonstrated in this study. Both of these mechanisms have the potential to enhance the migration of strongly adsorbing contaminants.

After Th(IV) was sorbed to the SRS sediment, column experiments demonstrated that Th(IV) transport was significantly enhanced by decreases in influent solution ionic strength. In

addition, this change in solution salinity also promoted the *in situ* mobilization of natural colloids from the SRS subsurface sediment. However, contrary to the original hypothesis, colloid-facilitated transport played only a minor role in enhancing the transport of Th(IV). Instead, the decreased pH front accompanying the change in solution salinity was primarily responsible for the enhanced the transport of Th(IV), causing higher concentrations of Th(IV) to desorb from the SRS sediment. This phenomenon can drastically affect the mobilization of radionuclides and heavy metals located at contaminated sites, especially if the initial aquifer pH is lower than the PZSE of the sediment.

In addition, this experiment also demonstrated that the sorption of tetravalent cations, such as Th(IV), can impact the aquifer sediment surface charge, significantly affecting the release of colloids. In the absence of Th(IV), colloids were released from the SRS sediment only after increases in influent solution pH, while changes in solution salinity at the lower pH range had no effect in releasing colloids. However, when Th(IV) was adsorbed to the SRS sediment, changes in solution salinity at the lower pH range liberated significant concentrations of colloids. Therefore, contaminated aquifers containing multivalent ions might respond differently to changes in solution chemistry in comparison to uncontaminated aquifers containing the same sediment.

Chapter Four.

Conclusions and Recommendations

4.1 Conclusions

Column Transport Experiments in the Absence of Th(IV)

1. In the absence of Th(IV), decreases in solution ionic strength at a constant pH of 4 were ineffective at mobilizing natural colloidal particles from the SRS sandy sediment. However, changes in solution salinity did induce a pH front, causing a non-retarded decrease in effluent solution pH.

2. Contrary to changes in solution salinity, increases in solution pH promoted the mobilization of natural colloids from the surface of the SRS sediment. This elevation in influent pH from 4 to 11 was consistent with reversing the positive surface charge of the goethite colloidal particles, releasing both goethite and kaolinite colloids from the surface of the SRS sediment as seen from the STXM analysis.

Th(IV) Column Transport Experiments

1. The SRS sandy sediment significantly retarded the migration of Th(IV) through saturated columns during the sorption phases conducted at a pH of 4, taking over 100 pore volumes before detecting any Th(IV) concentrations in the effluent samples.

2. After Th(IV) was adsorbed to the SRS sediment, decreases in solution salinity promoted the *in situ* mobilization of natural colloids from the surface of the SRS sediment.

However, colloid mobilization was not observed until the influent ionic strength was decreased to a critical salt concentration (CSC) of approximately 0.01 M $NaNO_3$. Once the ionic strength was decreased to this point, significant concentrations of colloids (greater than 15 mg/L) were detected in the effluent samples.

3. In addition to the mobilization of colloids, decreases in solution ionic strength also enhanced the transport of Th(IV), causing Th(IV) concentrations in the effluent samples to peak up to 11 times the initial influent concentrations. Contrary to the original hypothesis, the enhanced Th(IV) migration was primarily attributed to the decreased pH front accompanying the change in solution ionic strength instead of colloid-facilitated transport. The decreased pH caused higher concentrations of Th(IV) to desorb from the SRS sediment, enhancing its transport. This result agrees with previous batch studies conducted by Melson et al. (2012), which showed that Th(IV) adsorption onto the SRS sandy sediment is highly pH dependent.

4. Although Th(IV) migration was immediately enhanced after decreases in solution salinity, it was later retarded in comparison to transport experiments that did not initiate changes in solution chemistry.

5. Increases in influent solution pH from 4 to 11 alone were ineffective in releasing colloids from the SRS sediment. However, decreasing the ionic strength once the solution pH reached 11 promoted the release of colloids. The decreased ionic strength further increased the repulsive force between the colloids and immobile grain surfaces, releasing them from the surface of the sediment. This decrease in solution salinity also caused increased concentrations of Th(IV) in the effluent samples, which were oversaturated

with respect to the formation of amorphous thorium hydroxide. Therefore, colloid-facilitated transport was believed to be responsible for the enhanced Th(IV) transport at higher pH values. However, it was much less effective in facilitating the transport of Th(IV) in comparison to the enhanced Th(IV) transport triggered by pH fronts associated with changes in solution salinity at the lower pH range.

6. The sorption of Th(IV) had a significant impact on the surface charge of the SRS sediment, affecting the release of colloids. In the absence of Th(IV), colloids were released from the SRS sediment only after increases in influent solution pH, while changes in solution salinity at the lower pH range were ineffective at releasing colloids. However, when Th(IV) was adsorbed to the SRS sediment, changes in solution salinity alone at the lower pH range liberated significant concentrations of colloids.

4.2 Recommendations for Future Work

1. Future colloid mobilization experiments should use frits with larger pore sizes, such as 100 μm. Although 30 μm frits should allow for the passage of most colloids (typically defined as <10 μm), they can become plugged when very high concentrations of colloids are mobilized, which was observed in column experiment SRS # 1.

2. Along with frits with larger pore sizes, future colloid mobilization experiments need to connect an in-line pressure gauge to the tubing before the packed column. Pressure gauges would allow for the pressure to be monitored within the column to determine if plugging is a factor after colloid mobilization phases are initiated. The use of a pressure monitoring system could have prevented one of the 2.5 cm diameter columns from breaking in this study.

3. In addition to the analysis of uncontaminated colloids mobilized from the SRS sediment, further investigation using STXM combined with XANES spectroscopy could be used to analyze liberated colloids after Th(IV) was adsorbed to the SRS sediment. This would be especially beneficial for the transport experiments releasing colloids at a high pH, where Th(IV) migration was thought to be predominately enhanced by colloid-facilitated transport. Not only would STXM analysis verify Th(IV) adsorption to the colloidal particles, it would also identify which colloidal minerals adsorbed the highest concentrations of Th(IV).

4. In this study, dissolved Th(IV) samples were determined by analyzing with the ICP-OES after filtering with 0.2 μm water-wettable PTFE syringe filters. Although the turbidity was checked after filtration to ensure the removal of colloids, the Zetasizer determined that the size of colloids released from the SRS sediment after elevated pH ranged from 185 to 600 nm. Therefore, there was a possibility that some of the smaller-sized colloids could have penetrated the syringe filters. In order to ensure complete filtration of colloids, future experiments should use smaller pore size filters, if available. However, the type of membrane filter is limited due to the adsorption of Th(IV). Of the membrane filters tested in this study, the PTFE membranes showed the least Th(IV) adsorption, yielding 98 % recovery. While conducting this study, the smallest pore size for this type of membrane filter was 0.2 μm.

5. Although it was evident that Th(IV) impacted the surface charge of the SRS sediment, further investigation should conduct surface charge tests on the bulk SRS sediment in the presence of Th(IV) as a function of pH. In addition, the SRS colloids released after

Th(IV) adsorption should also be tested for ζ-potentials as a function of pH. These results would be very helpful in further explaining how the sorption of Th(IV) impacted the surface charge of the bulk sediment and mobilized colloids.

6. In addition to analyzing turbidity, pH, and Th(IV) concentration, future colloid mobilization experiments could also analyze electrical conductivity (EC) in the effluent samples. Electrical conductivity breakthrough curves would show how the conductivity changes after decreases in solution salinity, giving additional valuable information. A combination pH/EC meter would be helpful for analyzing the effluent samples for both of these parameters.

7. Further investigation is needed to determine whether increases in solution pH at high ionic strength (I=0.1 M $NaNO_3$) promotes in situ mobilization of colloids from the surface of the SRS sediment in the absence of Th(IV). In this study, increases in pH were conducted at low electrolyte concentrations. Therefore, an additional experiment should be conducted to determine whether colloids are mobilized by increases in pH while keeping a constant high ionic strength. These results could then be compared to similar colloid mobilization experiments that were conducted in the presence of Th(IV) to determine if Th(IV) affects the colloid release at high pH values.

References

Abu-Sharar, T. M. and A. S. Salameh (1995). "Reductions in hydraulic conductivity and infiltration rate in relation to aggregate stability and irrigation water turbidity." Agricultural Water Management **29**(1): 53-62.

Ahearne, J. F. (1997). "Radioactive Waste: The Size of the Problem." Physics Today **50**(6): 24-29.

Airey, P. L. (1986). "Radionuclide migration around uranium ore bodies in the Alligator Rivers Region of the Northern Territory of Australia — Analogue of radioactive waste repositories — A review." Chemical Geology **55**(3–4): 255-268.

Alkan, M., Ö. Demirbaş and M. Doğan (2005). "Electrokinetic properties of kaolinite in mono- and multivalent electrolyte solutions." Microporous and Mesoporous Materials **83**(1–3): 51-59.

Allen, S. E. (1989). Analysis of soils. Chemical analysis of ecological materials. Oxford, England, Blackwell Scientific Publications**:** 16-17.

Altmaier, M., V. Neck, M. A. Denecke, R. Yin and T. Fanghänel (2006). "Solubility of ThO2·xH2O(am) and the formation of ternary Th(IV) hydroxide-carbonate complexes in NaHCO3-Na2CO3 solutions containing 0−4 M NaCl." Radiochimica Acta **94**(9-11): 495-500.

Altmaier, M., V. Neck and T. Fanghänel (2004). "Solubility and colloid formation of Th(IV) in concentrated NaCl and MgCl2 solution." Radiochimica Acta **92**(9-11-2004): 537-543.

Altmaier, M., V. Neck, R. Müller and T. Fanghänel (2005). "Solubility of ThO2·xH2O(am) in carbonate solution and the formation of ternary Th(IV) hydroxide-carbonate complexes." Radiochimica Acta **93**(2-2005): 83-92.

Anna-Maria, J. (1999). "Measurement and Modeling of Th Sorption onto TiO2." Journal of Colloid and Interface Science **220**(2): 367-373.

Appel, C., L. Q. Ma, R. Dean Rhue and E. Kennelley (2003). "Point of zero charge determination in soils and minerals via traditional methods and detection of electroacoustic mobility." Geoderma **113**(1–2): 77-93.

ATSDR (1990). Toxicological Profile for Thorium, Agency for Toxic Substances and Disease Registry U.S. Public Health Service.

ATSDR. (2011, November 9, 2011). "Detailed Data Table for the 2011 Priority List of Hazardous Substances." Substance Priority List Retrieved January 19, 2012, from http://www.atsdr.cdc.gov/spl/resources/ATSDR_2011_SPL_Detailed_Data_Table.pdf.

Baes, C. F., N. J. Meyer and C. E. Roberts (1965). "The Hydrolysis of Thorium(IV) at 0 and 95°." Inorganic Chemistry **4**(4): 518-527.

Banik, N. L., R. A. Buda, S. Bürger, J. V. Kratz and N. Trautmann (2007). "Sorption of tetravalent plutonium and humic substances onto kaolinite." Radiochimica Acta **95**(10): 569-575.

Blume, T., N. Weisbrod and J. S. Selker (2005). "On the critical salt concentrations for particle detachment in homogeneous sand and heterogeneous Hanford sediments." Geoderma **124**(1–2): 121-132.

Brown, P. L., J. Ellis and R. N. Sylva (1983). "The hydrolysis of metal ions. Part 5. Thorium(IV)." Journal of the Chemical Society, Dalton Transactions(1): 31-34.

Buddemeier, R. W. and J. R. Hunt (1988). "Transport of colloidal contaminants in groundwater: radionuclide migration at the Nevada test site." Applied Geochemistry **3**(5): 535-548.

Bundschuh, T., R. Knopp, R. Müller, J. I. Kim, V. Neck and T. Fanghänel (2000). "Application of LIBD to the determination of the solubility product of thorium(IV)-colloids." Radiochimica Acta **88**(9-11_2000): 625.

Bunn, R. A., R. D. Magelky, J. N. Ryan and M. Elimelech (2002). "Mobilization of Natural Colloids from an Iron Oxide-Coated Sand Aquifer: Effect of pH and Ionic Strength." Environmental Science & Technology **36**(3): 314-322.

Cantrell, K. J. and R. G. Riley (2008). Subsurface Behavior of Plutonium and Americium at Non-Hanford Sites and Relevance to Hanford, Pacific Northwest National Laboratory**:** PNNL-17386.

Chang, P., S. Yu, T. Chen, A. Ren, C. Chen and X. Wang (2007). "Effect of pH, ionic strength, fulvic acid and humic acid on sorption of Th(IV) on Na-rectorite." Journal of Radioanalytical and Nuclear Chemistry **274**(1): 153-160.

Chen, C. and X. Wang (2007). "Sorption of Th (IV) to silica as a function of pH, humic/fulvic acid, ionic strength, electrolyte type." Applied Radiation and Isotopes **65**(2): 155-163.

Chen, L., X. J. Yu, Z. D. Zhao and Y. H. Dong (2006). "The sorption of Th(IV) ions onto montmorillonite: the effect of pH, ionic strength and fulvic acid." Adsorption Science & Technology **24**(4): 301-310.

Cheng, T. and J. E. Saiers (2010). "Colloid-Facilitated Transport of Cesium in Vadose-Zone Sediments: The Importance of Flow Transients." Environmental Science & Technology **44**(19): 7443-7449.

Choppin, G. (2007). "Actinide speciation in the environment." Journal of Radioanalytical and Nuclear Chemistry **273**(3): 695-703.

Choppin, G. R. (1999). "Utility of oxidation state analogs in the study of plutonium behavior." Radiochimica Acta **85**(3-4): 89-95.

Clark, D. L., D. E. Hobart and M. P. Neu (1995). "Actinide carbonate complexes and their importance in actinide environmental chemistry." Chemical Reviews **95**(1): 25-48.

Crancon, P., E. Pili and L. Charlet (2010). "Uranium facilitated transport by water-dispersible colloids in field and soil columns." Science of the Total Environment **408**(9): 2118-2128.

Cromieres, L., V. Moulin, B. Fourest, R. Guillaumont and E. Giffaut (1998). "Sorption of thorium onto hematite colloids." Radiochimica Acta **82**: 249-255.

Dai, M., J. M. Kelley and K. O. Buesseler (2002). "Sources and Migration of Plutonium in Groundwater at the Savannah River Site." Environmental Science & Technology **36**(17): 3690-3699.

Ekberg, C., Y. Albinsson, M. J. Comarmond and P. L. Brown (2000). "Studies on the Complexation Behavior of Thorium(IV). 1. Hydrolysis Equilibria." Journal of Solution Chemistry **29**(1): 63-86.

Elimelech, M., M. Nagai, C.-H. Ko and J. N. Ryan (2000). "Relative Insignificance of Mineral Grain Zeta Potential to Colloid Transport in Geochemically Heterogeneous Porous Media." Environmental Science & Technology **34**(11): 2143-2148.

EPA (1999). Understanding Variation in Partition Coefficient, Kd, Values. Review of Geochemistry and Available Kd Values for Cadmium, Cesium, Chromium, Lead, Plutonium, Radon, Strontium, Thorium, Tritium, and Uranium. **2**.

EPA. (2011, July 08, 2011). "Thorium." Radiation Protection, from http://www.epa.gov/radiation/radionuclides/thorium.html.

Fanghanel, T. and V. Neck (2002). "Aquatic chemistry and solubility phenomena of actinide oxides/hydroxides." Pure and Applied Chemistry **74**(10): 1895-1907.

Felmy, A., D. Rai, S. Sterner, M. Mason, N. Hess and S. Conradson (1997). "Thermodynamic models for highly charged aqueous species: Solubility of Th(IV) hydrous oxide in concentrated $NaHCO_3$ and Na_2CO_3 solutions." Journal of Solution Chemistry **26**(3): 233-248.

Felmy, A. R. and D. Rai (1999). "Application of Pitzer's Equations for Modeling the Aqueous Thermodynamics of Actinide Species in Natural Waters: A Review." Journal of Solution Chemistry **28**(5): 533-553.

Gephart, R. E. and R. E. Lundgren (1998). Hanford tank cleanup: a guide to understanding the technical issues. Columbus, Ohio, Battelle Press.

Goldenberg, L. C. (1985). "Decrease of hydraulic conductivity in sand at the interface between seawater and dilute clay suspensions." Journal of Hydrology **78**(1–2): 183-199.

Grenthe, I. and B. Lagerman (1991). "Studies on metal carbonate equilibria: 23. Complex formation in the Th(IV)-H_20-CO_2(g) system." Acta Chem. Scand. **45**: 231-238.

Grolimund, D. and M. Borkovec (2005). "Colloid-facilitated transport of strongly sorbing contaminants in natural porous media: Mathematical modeling and laboratory column experiments." Environmental Science & Technology **39**(17): 6378-6386.

Grolimund, D. and M. Borkovec (2006). "Release of colloidal particles in natural porous media by monovalent and divalent cations." Journal of Contaminant Hydrology **87**(3–4): 155-175.

Grolimund, D., M. Elimelech, M. Borkovec, K. Barmettler, R. Kretzschmar and H. Sticher (1998). "Transport of in Situ Mobilized Colloidal Particles in Packed Soil Columns." Environmental Science & Technology **32**(22): 3562-3569.

Guo, Z.-J., X.-M. Yu, F.-H. Guo and Z.-Y. Tao (2005). "Th(IV) adsorption on alumina: Effects of contact time, pH, ionic strength and phosphate." Journal of Colloid and Interface Science **288**(1): 14-20.

Harvey, R. W., L. H. George, R. L. Smith and D. R. LeBlanc (1989). "Transport of microspheres and indigenous bacteria through a sandy aquifer: results of natural- and forced-gradient tracer experiments." Environmental Science & Technology **23**(1): 51-56.

Higashi, S. (1959). "Determination of the solubility of thorium hydroxide." Bull. Inst. Phys. Chem. Res. (Toyko) **37**: 200-206.

Higgo, J. J. W., G. M. Williams, I. Harrison, P. Warwick, M. P. Gardiner and G. Longworth (1993). "Colloid transport in a glacial sand aquifer. Laboratory and field studies." Colloids and Surfaces A: Physicochemical and Engineering Aspects **73**(0): 179-200.

Hongxia, Z., Y. Jieqiong and T. Zuyi (2007). "Effects of phosphate and Cr^{3+} on the sorption and transport of Th(IV) on a silica column." Journal of Radioanalytical and Nuclear Chemistry **273**(2): 465-471.

Hongxia, Z., D. Zheng and T. Zuyi (2006). "Sorption of thorium(IV) ions on gibbsite: Effects of contact time, pH, ionic Strength, concentration, phosphate and fulvic acid." Colloids and Surfaces a-Physicochemical and Engineering Aspects **278**(1-3): 46-52.

Hunter, K. A., D. J. Hawke and C. Lee Kwee (1988). "Equilibrium adsorption of thorium by metal oxides in marine electrolytes." Geochimica et Cosmochimica Acta **52**(3): 627-636.

Kaplan, D. I., P. M. Bertsch, D. C. Adriano and W. P. Miller (1993). "Soil-borne mobile colloids as influenced by water flow and organic carbon." Environmental Science & Technology **27**(6): 1193-1200.

Kaplan, D. I., P. M. Bertsch, D. C. Adriano and K. A. Orlandini (1994). "Actinide association with groudnwater colloids in a coastal-plain aquifer." Radiochimica Acta **66-7**: 181-187.

Kaplan, D. I., M. E. Sumner, P. M. Bertsch and D. C. Adriano (1996). "Chemical conditions conducive to the release of mobile colloids from ultisol profiles." Soil Science Society of America Journal **60**(1): 269-274.

Kersting, A. B., D. W. Efurd, D. L. Finnegan, D. J. Rokop, D. K. Smith and J. L. Thompson (1999). "Migration of plutonium in ground water at the Nevada Test Site." Nature **397**(6714): 56-59.

Khilar, K. C. and H. S. Fogler (1984). "The existence of a critical salt concentration for particle release." Journal of Colloid and Interface Science **101**(1): 214-224.

Kia, S. F., H. S. Fogler and M. G. Reed (1987). "Effect of pH on colloidally induced fines migration." Journal of Colloid and Interface Science **118**(1): 158-168.

Kim, J. I. (1991). "Actinide colloid generation in groundwater." Radiochimica Acta **52-3**: 71-81.

Kretzschmar, R. and T. Schafer (2005). "Metal retention and transport on colloidal particles in the environment." Elements **1**(4): 205-210.

LaFlamme, B. D. and J. W. Murray (1987). "Solidsolution interaction: The effect of carbonate alkalinity on adsorbed thorium." Geochimica et Cosmochimica Acta **51**(2): 243-250.

Lenhart, J. J. and J. E. Saiers (2003). "Colloid Mobilization in Water-Saturated Porous Media under Transient Chemical Conditions." Environmental Science & Technology **37**(12): 2780-2787.

Li, D., D. I. Kaplan, K. A. Roberts and J. C. Seaman (2012). "Mobile Colloid Generation Induced by a Cementitious Plume: Mineral Surface-Charge Controls on Mobilization." Environmental Science & Technology **46**(5): 2755-2763.

Li, W. J. and Z. Y. Tao (2002). "Comparative study on Th(IV) sorption on alumina and silica from aqueous solutions." Journal of Radioanalytical and Nuclear Chemistry **254**(1): 187-192.

Liang, L., A. Hofmann and B. Gu (2000). "Ligand-induced dissolution and release of ferrihydrite colloids." Geochimica et Cosmochimica Acta **64**(12): 2027-2037.

Long, J. C. S. and R. C. Ewing (2004). "Yucca Mountain: Earth-science issues at a geologic repository for high-level nuclear waste." Annual Review of Earth and Planetary Sciences **32**: 363-401.

Loveland, J. P., S. Bhattacharjee, J. N. Ryan and M. Elimelech (2003). "Colloid transport in a geochemically heterogeneous porous medium: aquifer tank experiment and modeling." Journal of Contaminant Hydrology **65**(3–4): 161-182.

Lucian W. Zelazny, Liming He and A. Vanwormhoudt (1996). Charge analysis of soils and anion exchange. Methods of Soil Analysis. Part 3. Chemical Methods. D. L. Sparks, A. L. Page, P. A. Helmkeet al. Madison, WI, Soil Science Society of America and American Society of Agronomy**:** 1245-1248.

McCarthy, J. and J. Zachara (1989). "ES&T Features: Subsurface transport of contaminants." Environmental Science & Technology **23**(5): 496-502.

McCarthy, J. F. and C. Degueldre (1993). Sampling and characterization of groundwater colloids for studying their role in the subsurface transport of contaminants. Environmental Particles. Chelsea, MI, Lewis Publishers. **2:** 247-315.

McCarthy, J. F. and L. D. McKay (2004). "Colloid transport in the subsurface: Past, present, and future challenges." Vadose Zone Journal **3**(2): 326-337.

McCarthy, J. F., W. E. Sanford and P. L. Stafford (1998). "Lanthanide Field Tracers Demonstrate Enhanced Transport of Transuranic Radionuclides by Natural Organic Matter." Environmental Science & Technology **32**(24): 3901-3906.

Melson, N. (2011). Sorption of Thorium onto Subsurface Geomedia. Department of Civil Engineering. Auburn, AL, Auburn University. **Masters of Science:** 72.

Melson, N. H., B. P. Haliena, M. O. Barnett and D. I. Kaplan (2012). "Adsorption of tetravalent thorium by geomedia." Radiochim. Acta **(in press)**.

Milić, N. B. and T. M. Šuranji (1982). "Hydrolysis of the thorium(IV) ion in sodium nitrate medium." Canadian Journal of Chemistry **60**(11): 1298-1303.

Moon, H. C. (1989). "Equilibrium ultrafiltration of hydrolyzed thorium(IV) solutions." Bull. Korean Chem. Soc. **10**: 270-272.

Mori, A., W. R. Alexander, H. Geckeis, W. Hauser, T. Schafer, J. Eikenberg, T. Fierz, C. Degueldre and T. Missana (2003). "The colloid and radionuclide retardation experiment at the Grimsel Test Site: influence of bentonite colloids on radionuclide migration in a fractured rock." Colloids and Surfaces a-Physicochemical and Engineering Aspects **217**(1-3): 33-47.

Murphy, R. J., J. J. Lenhart and B. D. Honeyman (1999). "The sorption of thorium (IV) and uranium (VI) to hematite in the presence of natural organic matter." Colloids and Surfaces A: Physicochemical and Engineering Aspects **157**(1–3): 47-62.

Neck, V., M. Altmaier, R. Müller, A. Bauer, T. Fanghänel and J.-I. Kim (2003). "Solubility of crystalline thorium dioxide." Radiochimica Acta **91**(5-2003): 253-262.

Neck, V. and J. I. Kim (2001). "Solubility and hydrolysis of tetravalent actinides." Radiochimica Acta **89**(1): 1-16.

Neck, V., R. Müller, M. Bouby, M. Altmaier, J. Rothe, M. A. Denecke and J.-I. Kim (2002). "Solubility of Amorphous Th(IV) Hydroxide – Application of LIBD to Determine the Solubility Product and EXAFS for Aqueous Speciation." Radiochimica Acta **90**(9-11_2002): 485-494.

Nightingale, H. I. and W. C. Bianchi (1977). "Ground-Water Turbidity Resulting from Artificial Recharge." Ground Water **15**(2): 146-152.

Novikov, A. P., S. N. Kalmykov, S. Utsunomiya, R. C. Ewing, F. Horreard, A. Merkulov, S. B. Clark, V. V. Tkachev and B. F. Myasoedov (2006). "Colloid transport of plutonium in the far-field of the Mayak Production Association, Russia." Science **314**(5799): 638-641.

Omenyi, S. N., B. J. Herren, R. S. Snyder and G. V. F. Seaman (1986). "Comparative isosteric ion adsorption for minerals." Journal of Colloid and Interface Science **110**(1): 130-136.

Östhols, E. (1995). "Thorium sorption on amorphous silica." Geochimica et Cosmochimica Acta **59**(7): 1235-1249.

Östhols, E., J. Bruno and I. Grenthe (1994). "On the influence of carbonate on mineral dissolution: III. The solubility of microcrystalline ThO2 in CO2-H2O media." Geochimica et Cosmochimica Acta **58**(2): 613-623.

Östhols, E., A. Manceau, F. Farges and L. Charlet (1997). "Adsorption of Thorium on Amorphous Silica: An EXAFS Study." Journal of Colloid and Interface Science **194**(1): 10-21.

Penrose, W. R., W. L. Polzer, E. H. Essington, D. M. Nelson and K. A. Orlandini (1990). "Mobility of plutonium and americium through a shallow aquifer in a semiarid region." Environmental Science & Technology **24**(2): 228-234.

Peterson, J., M. MacDonell, L. Haroun, F. Monette, D. Hildebrand and A. Taboas (2007). Radiological and Chemical Fact Sheets to Support Health Risk Analyses for Contaminated Areas, Argonne National Laboratory Environmental Science Division**:** 133.

Pitts, M. M. (1995). "Fouling mitigation in aqueous systems using electrochemical water treatment." Retrieved January 24, 2012, from http://www.zetacorp.com/fouling_mitigation.shtml.

Povetko, O. G. (2008). "An analysis of external radiation dose fields in an underground facility at the potential HLW geologic repository at Yucca Mountain, Nevada." Nuclear Technology **163**(1): 31-37.

Prasad, R., M. L. Beasley and W. O. Milligan (1967). "Aging of Hydrous Thoria Gels." Journal of Electron Microscopy **16**(2): 101-119.

Priesing, C. P. (1962). "A theory of coagulation useful for design." Industrial & Engineering Chemistry **54**(8): 38-45.

Pshinko, G., T. Timoshenko and A. Bogolepov (2009). "Effect of fulvic acids on Th(IV) sorption on montmorillonite." Radiochemistry **51**(1): 91-95.

Puls, R. W. and R. M. Powell (1992). "Transport of inorganic colloids through natural aquifer material: implications for contaminant transport." Environmental Science & Technology **26**(3): 614-621.

Quirk, J. P. and R. K. Schofield (1955). "The effect of electrolyte concentration on soil permeability." Journal of Soil Science **6**(2): 163-178.

Rai, D., D. A. Moore, C. S. Oakes and M. Yui (2000). "Thermodynamic model for the solubility of thorium dioxide in the Na+-Cl--OH--H2O system at 23 degrees C and 90 degrees C." Radiochimica Acta **88**(5): 297-306.

Rand, M., J. Fuger, V. Neck, I. Grenthe and D. Rai (2008). Chemical Thermodynamics of Thorium. Paris, France, OECD Publishing.

Reiller, P., F. Casanova and V. Moulin (2005). "Influence of Addition Order and Contact Time on Thorium(IV) Retention by Hematite in the Presence of Humic Acids." Environmental Science & Technology **39**(6): 1641-1648.

Reiller, P., V. Moulin, F. Casanova and C. Dautel (2002). "Retention behaviour of humic substances onto mineral surfaces and consequences upon thorium (IV) mobility: case of iron oxides." Applied Geochemistry **17**(12): 1551-1562.

Reiller, P., V. Moulin, F. Casanova and C. Dautel (2003). "On the study of Th(IV)-humic acid interactions by competition sorption studies with silica and determination of global interaction constants." Radiochimica Acta **91**(9-2003): 513-524.

Reynolds, T. D. and P. A. Richards (1996). Unit Operations and Processes in Environmental Engineering Boston, MA, PWS Publishing Company.

Rojo, I., F. Seco, M. Rovira, J. Giménez, G. Cervantes, V. Martí and J. de Pablo (2009). "Thorium sorption onto magnetite and ferrihydrite in acidic conditions." Journal of Nuclear Materials **385**(2): 474-478.

Roy, S. B. and D. A. Dzombak (1996). "Colloid release and transport processes in natural and model porous media." Colloids and Surfaces a-Physicochemical and Engineering Aspects **107**: 245-262.

Roy, S. B. and D. A. Dzombak (1997). "Chemical factors influencing colloid-facilitated transport of contaminants in porous media." Environmental Science & Technology **31**(3): 656-664.

Runde, W. (2000). "The Chemical Interactions of Actinides in the Environment." Los Alamos Science **26**: 392-411.

Runde, W., S. D. Conradson, D. Wes Efurd, N. Lu, C. E. VanPelt and C. D. Tait (2002). "Solubility and sorption of redox-sensitive radionuclides (Np, Pu) in J-13 water from the Yucca Mountain site: comparison between experiment and theory." Applied Geochemistry **17**(6): 837-853.

Ryan, J. N. and M. Elimelech (1996). "Colloid mobilization and transport in groundwater." Colloids and Surfaces A: Physicochemical and Engineering Aspects **107**(0): 1-56.

Ryan, J. N. and P. M. Gschwend (1994). "Effect of solution chemistry on clay colloid release from an iron oxide-coated aquifer sand." Environmental Science & Technology **28**(9): 1717-1726.

Ryan, J. N. and P. M. Gschwend (1994). "Effects of ionic strength and flow rate on colloid release: Relating kinetics to intersurface potential energy." Journal of Colloid and Interface Science **165**(2): 536-536.

Schapira, J. P. and R. K. Singhal (1999). "Radiological impact at the extraction stage of the thorium fuel cycle." Nuclear Technology **128**(1): 25-34.

Scheidegger, A., C. S. Bürgisser, M. Borkovec, H. Sticher, H. Meeussen and W. van Riemsdijk (1994). "Convective transport of acids and bases in porous media." Water Resour. Res. **30**(11): 2937-2944.

Schindler, P. W. (1967). Heterogeneous Equilibria Involving Oxides, Hydroxides, Carbonates, and Hydroxide Carbonates. Equilibrium Concepts in Natural Water Systems, AMERICAN CHEMICAL SOCIETY. **67:** 196-221.

Schramm, L. L., K. Mannhardt and J. J. Novosad (1991). "Electrokinetic properties of reservoir rock particles." Colloids and Surfaces **55**: 309-331.

Seaman, J. C., P. M. Bertsch and W. P. Miller (1995). "Chemical Controls on Colloid Generation and Transport in a Sandy Aquifer." Environmental Science & Technology **29**(7): 1808-1815.

Seaman, J. C., B. B. Looney and M. K. Harris (2007). "Research in support of remediation activities at the Savannah River Site." Vadose Zone Journal **6**(2): 316-326.

Seco, F., C. Hennig, J. d. Pablo, M. Rovira, I. Rojo, V. Martí, J. Giménez, L. Duro, M. Grivé and J. Bruno (2009). "Sorption of Th(IV) onto Iron Corrosion Products: EXAFS Study." Environmental Science & Technology **43**(8): 2825-2830.

Sen, T. K. and K. C. Khilar (2006). "Review on subsurface colloids and colloid-associated contaminant transport in saturated porous media." Advances in Colloid and Interface Science **119**(2–3): 71-96.

Sen, T. K., S. P. Mahajan and K. C. Khilar (2002). "Colloid-Associated contaminant transport in porous media: 1. Experimental studies." AIChE Journal **48**(10): 2366-2374.

Sharma, M. M., H. Chamoun, D. S. H. S. R. Sarma and R. S. Schechter (1992). "Factors controlling the hydrodynamic detachment of particles from surfaces." Journal of Colloid and Interface Science **149**(1): 121-134.

Short, S. A., R. T. Lowson and J. Ellis (1988). "$^{234}U/^{238}U$ and $^{230}Th/^{234}U$ activity ratios in the colloidal phases of aquifers in lateritic weathered zones." Geochimica et Cosmochimica Acta **52**(11): 2555-2563.

Sirivithayapakorn, S. and A. Keller (2003). "Transport of colloids in saturated porous media: A pore-scale observation of the size exclusion effect and colloid acceleration." Water Resources Research **39**(4): 1109.

Snoeyink, V. L. and D. Jenkins (1980). Water chemistry. New York, NY, Wiley.

Šuranji, T. M. and N. B. Milić (1981). "Hydrolysis of thorium(IV) ions in lithium and potassium chloride media." Glas. Hem. Drus. Beograd **46**: 657-661.

Tan, X., X. Wang, C. Chen and A. Sun (2007). "Effect of soil humic and fulvic acids, pH and ionic strength on Th(IV) sorption to TiO2 nanoparticles." Applied Radiation and Isotopes **65**(4): 375-381.

Taubaso, C., M. Dos Santos Afonso and R. M. Torres Sánchez (2004). "Modelling soil surface charge density using mineral composition." Geoderma **121**(1–2): 123-133.

Um, W. and C. Papelis (2002). "Geochemical effects on colloid-facilitated metal transport through zeolitized tuffs from the Nevada Test Site." Environmental Geology **43**(1-2): 209-218.

Vašíček, R. and J. Svoboda (2011). "Long-term lining performance – Civil engineering problem of potential retrieval of buried spent nuclear fuel." Nuclear Engineering and Design **241**(4): 1233-1237.

Wan, J. M., T. K. Tokunaga, E. Saiz, J. T. Larsen, Z. P. Zheng and R. A. Couture (2004). "Colloid formation at waste plume fronts." Environmental Science & Technology **38**(22): 6066-6073.

Yan, L., F. Qiaohui and W. Wangsuo (2011). "Sorption of Th(IV) on goethite: effects of pH, ionic strength, FA and phosphate." Journal of Radioanalytical and Nuclear Chemistry **289**(3): 865-871.

Zhang, H. and H. M. Selim (2007). "Colloid mobilization and arsenite transport in soil columns: Effect of ionic strength." Journal of Environmental Quality **36**(5): 1273-1280.

Zhao, D. L., S. J. Feng, C. L. Chen, S. H. Chen, D. Xu and X. K. Wang (2008). "Adsorption of thorium(IV) on MX-80 bentonite: Effect of pH, ionic strength and temperature." Applied Clay Science **41**(1–2): 17-23.

Zhijun, G., N. Lijun and T. Zuyi (2005). "Sorption of Th(IV) ions onto TiO_2: Effects of contact time, ionic strength, thorium concentration and phosphate." Journal of Radioanalytical and Nuclear Chemistry **266**(2): 333-338.

Zhou, D. M., D. J. Wang, L. Cang, X. Z. Hao and L. Y. Chu (2011). "Transport and re-entrainment of soil colloids in saturated packed column: effects of pH and ionic strength." Journal of Soils and Sediments **11**(3): 491-503.

Zhuang, J., M. Flury and Y. Jin (2003). "Colloid-facilitated Cs transport through water-saturated Hanford sediment and Ottawa sand." Environmental Science & Technology **37**(21): 4905-4911.

Appendices

Appendix A. Column Characteristics and Setup

Table A.1: Column transport experiment characteristics

Column ID	SRS # 1	SRS # 2	SRS # 3	SRS # 4	SRS # 5	SRS # 6
Height (cm)	7.00	6.70	6.90	7.05	6.85	6.85
Diameter (cm)	1	1	1	2.5	1	1
Total Column Volume V_t (mL)	5.50	5.26	5.42	34.61	5.38	5.38
Flow Q (mL/hr)	6	6	6	36.6	6	6
Specific Discharge q (cm/hr)	7.64	7.64	7.64	7.46	7.64	7.64
Bulk Density ρ_b (g/cm^3)	1.56	1.57	1.53	1.58	1.62	1.62
Porosity φ	0.412	0.409	0.422	0.405	0.390	0.389
Soil Pore Volume V_0 (mL)	2.27	2.15	2.28	14.03	2.10	2.09
Average Flow Velocity *v* (cm/hr)	18.52	18.67	18.12	18.40	19.58	19.65
Retention Time θ (hr)	0.38	0.36	0.38	0.38	0.35	0.35
Dispersion Coefficient D (cm^2/hr)	N/A	2.69	2.61	2.9	5.44	8.34
Column Peclet Number N_{pe}	N/A	46.44	47.82	44.70	24.66	16.14
Th (IV) Influent Concentration (mg/L)	N/A	2.64	2.61	2.64	2.55	2.57
Th (IV) Influent Concentration (M)	N/A	1.14E-05	1.12E-05	1.14E-05	1.10E-05	1.11E-05
Mass of SRS Sediment (g)	8.5601	8.2387	8.3059	54.54	8.6931	8.7137

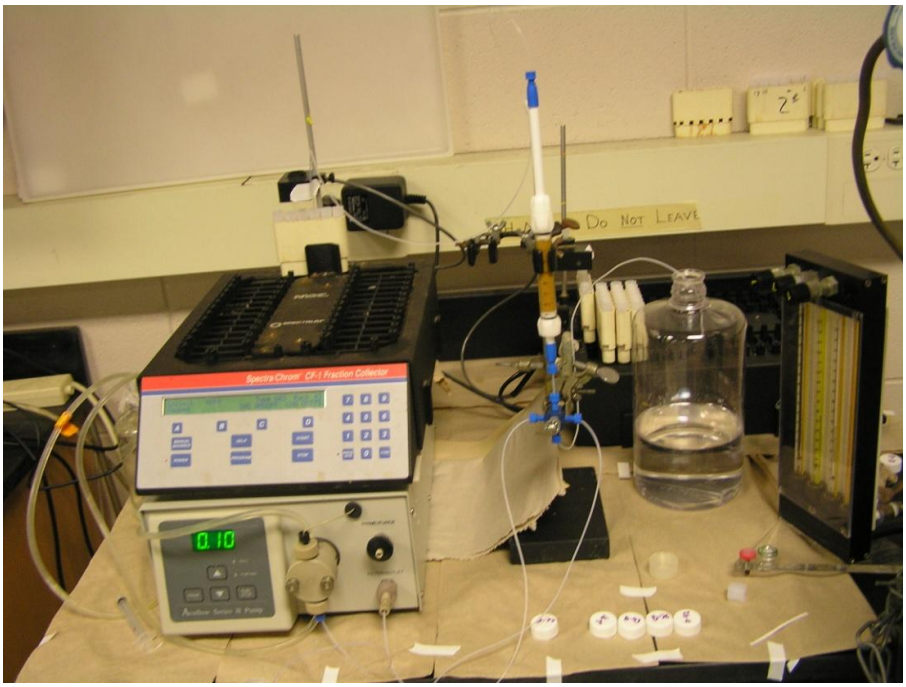

Figure A.1: Image of column experiment setup.

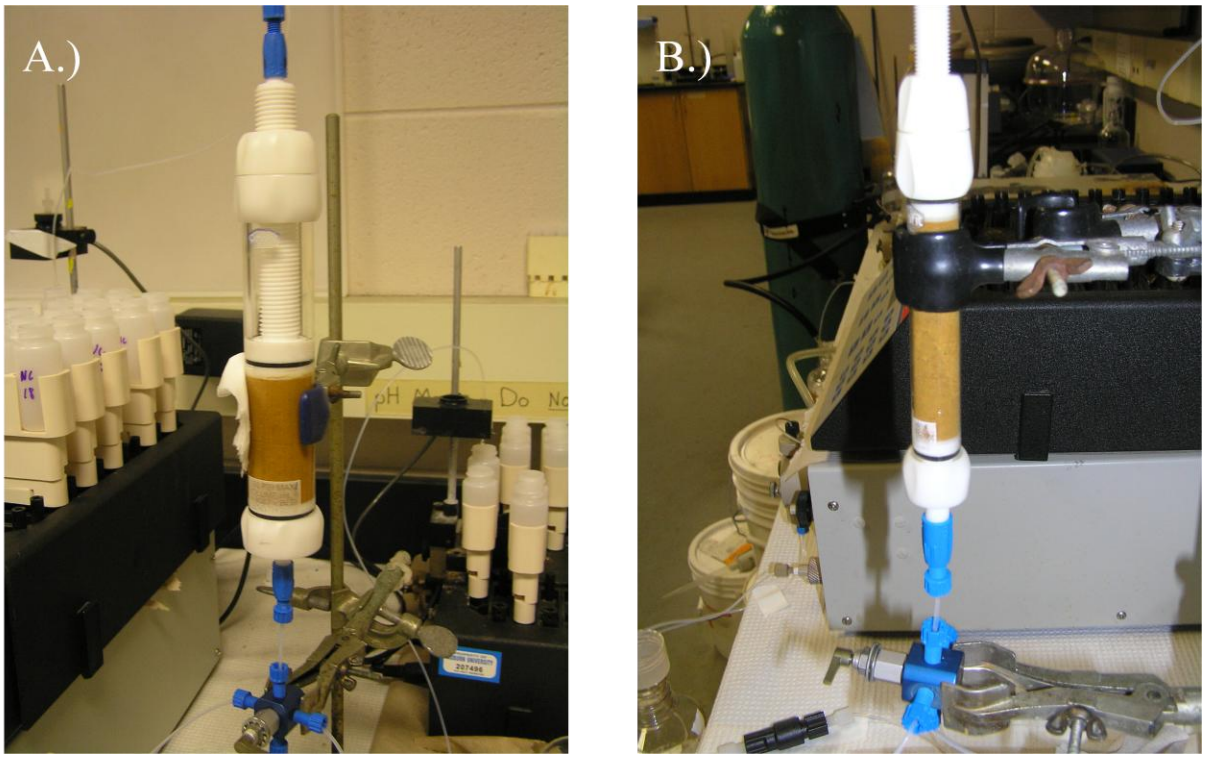

Figure A.2: Images of sand-packed Omnifit glass columns – (A) 2.5 cm diameter and (B) 1 cm diameter.

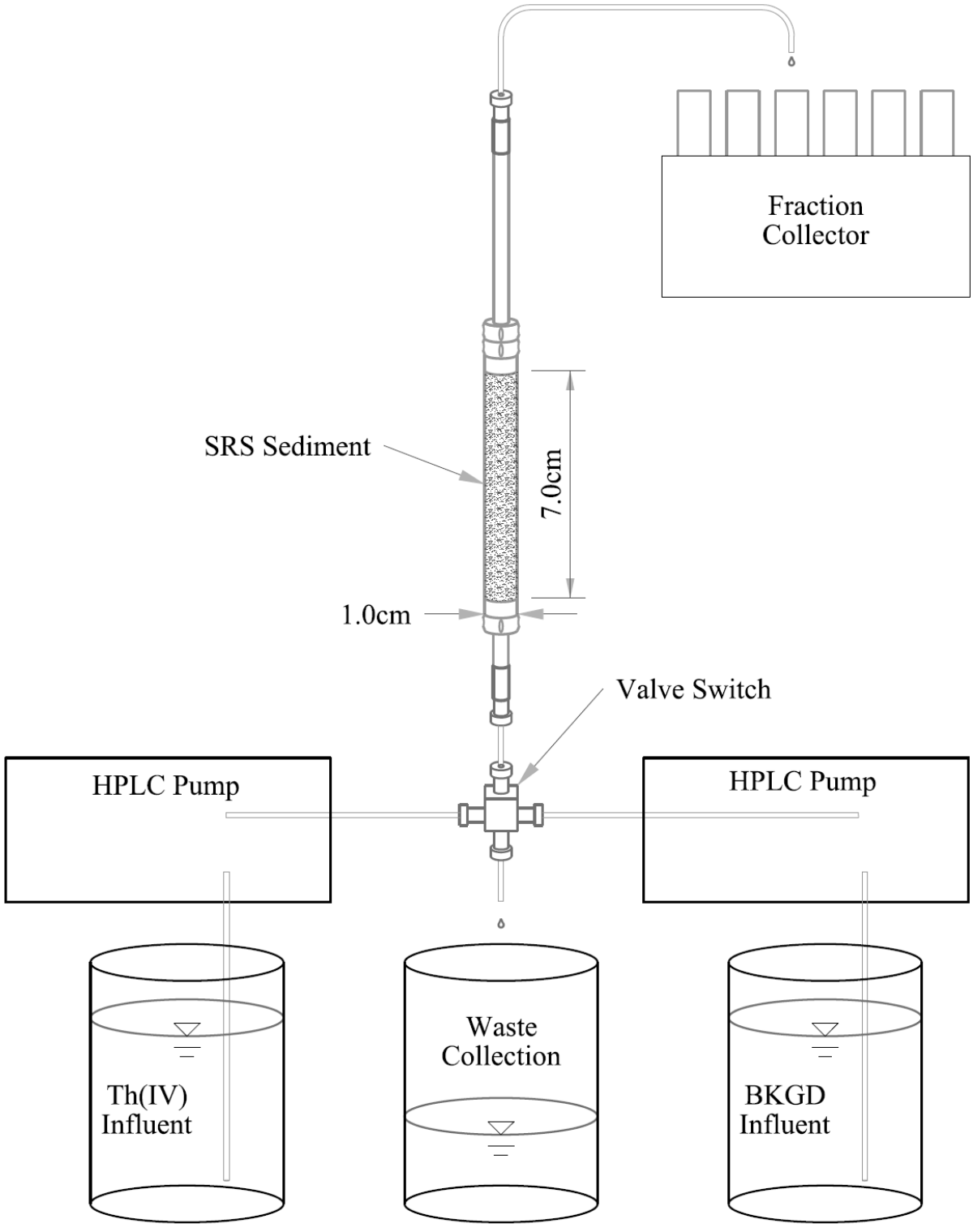

Figure A.3: Schematic of column experiment setup.

Appendix B. SRS Colloid Concentration Calibration Curves

The following calibration curves were used to correlate measured effluent turbidity to colloid concentration. The calibration curves were developed by measuring the turbidity and colloid concentration (by gravimetric analysis) of SRS colloids released from column experiments. The colloids were released from the SRS sediment by elevating the influent pH. Large (15mL) and small (3.5mL) sized turbidity cells were used to measure the turbidity of the effluent samples. This allowed smaller effluent sample sizes to be measured for colloid concentration.

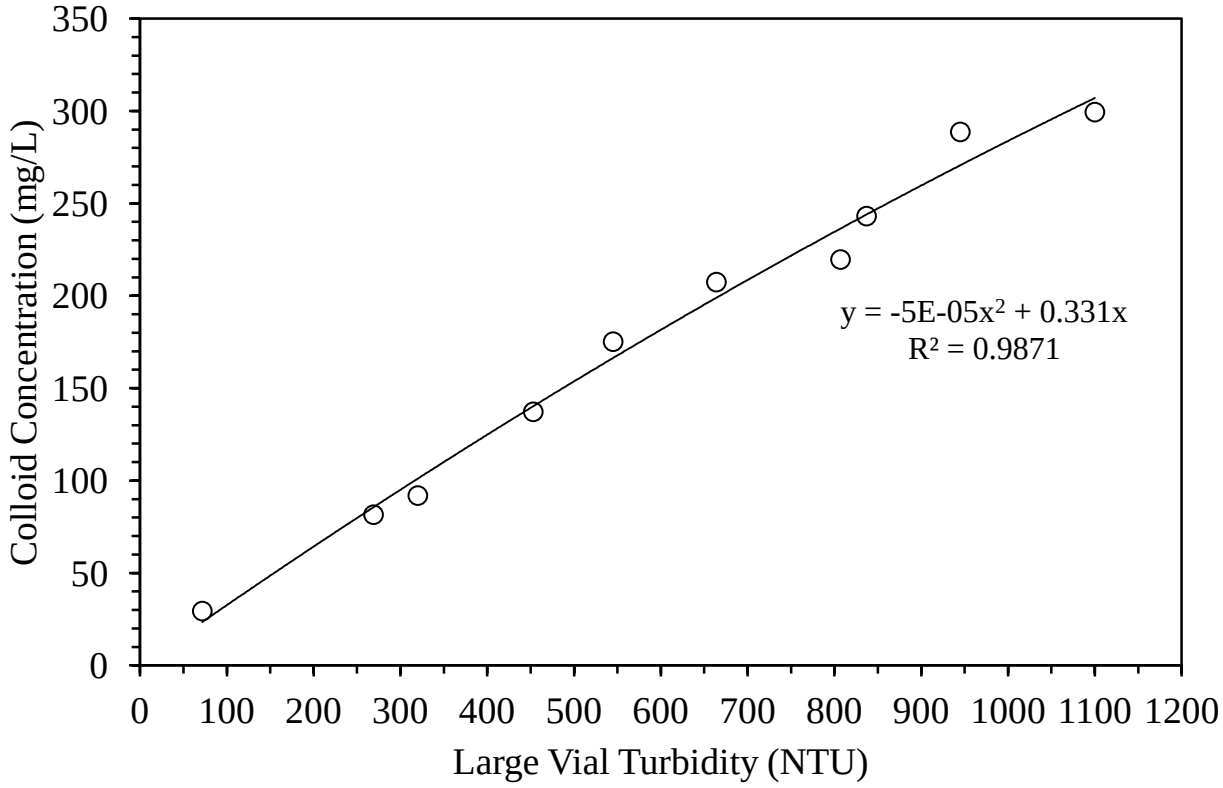

Figure B.1: Correlation curve between colloid concentration and large vial turbidity of SRS colloid suspensions mobilized by elevated pH from SRS sandy subsurface sediment. (Correlation curve was fitted with a polynomial equation for calculation of colloid concentration.)

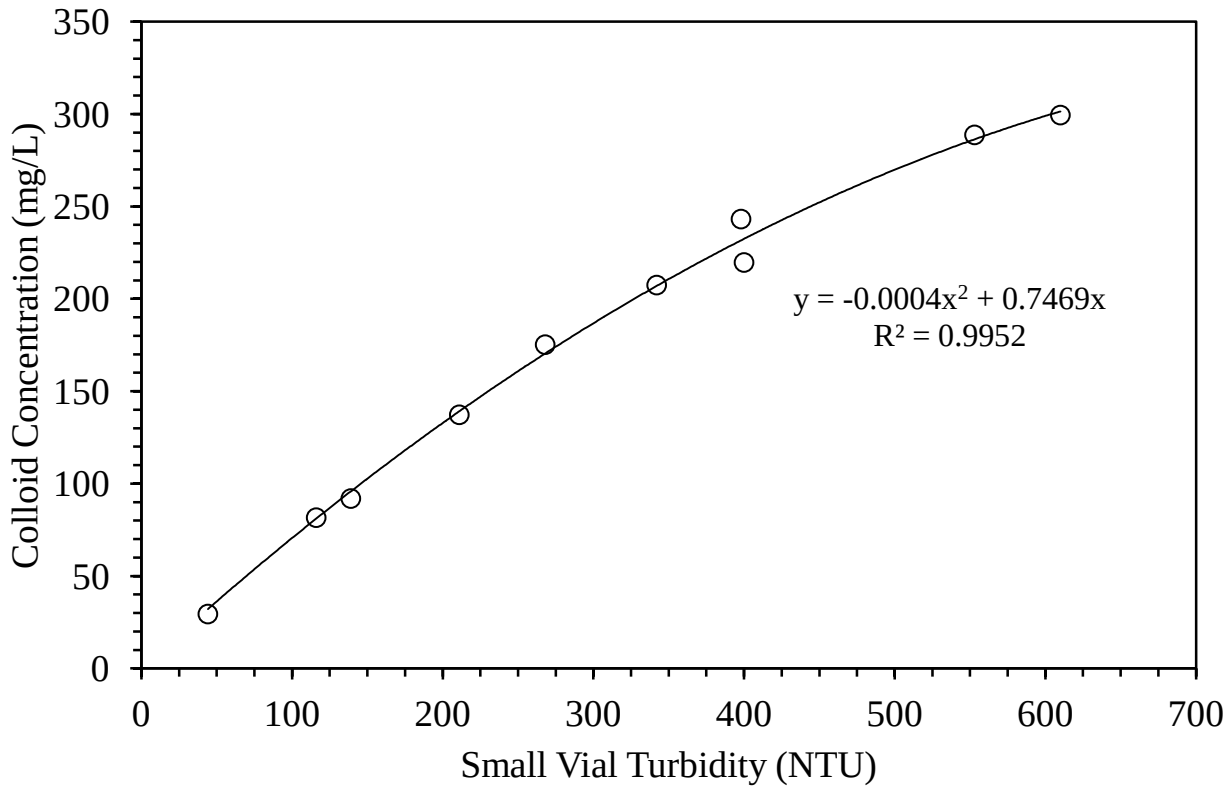

Figure B.2: Correlation curve between colloid concentration and small vial turbidity of SRS colloid suspensions mobilized by elevated pH from SRS sandy subsurface sediment. (Correlation curve was fitted with a polynomial equation for calculation of colloid concentration.)

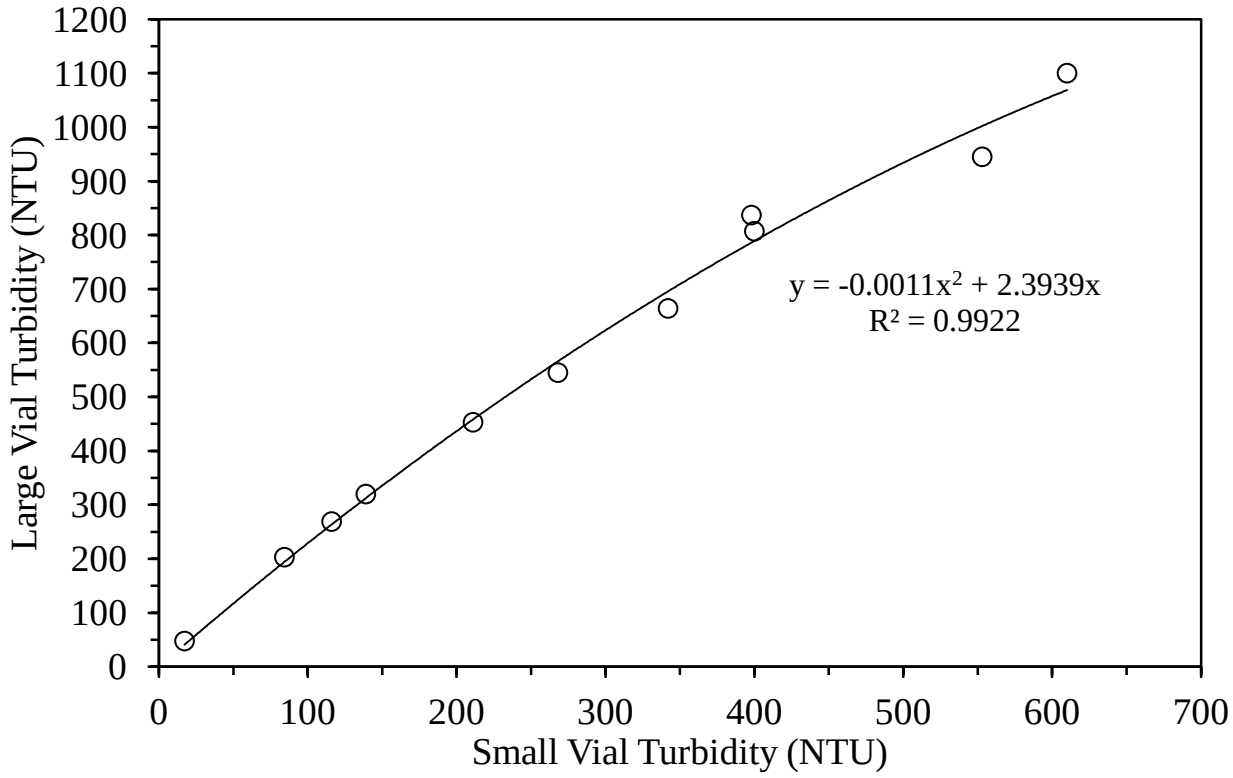

Figure B.3: Correlation curve between large vial turbidity and small vial turbidity of SRS colloid suspensions mobilized by elevated pH from SRS sandy subsurface sediment. (Correlation curve was fitted with a polynomial equation for calculation of large vial turbidity.)

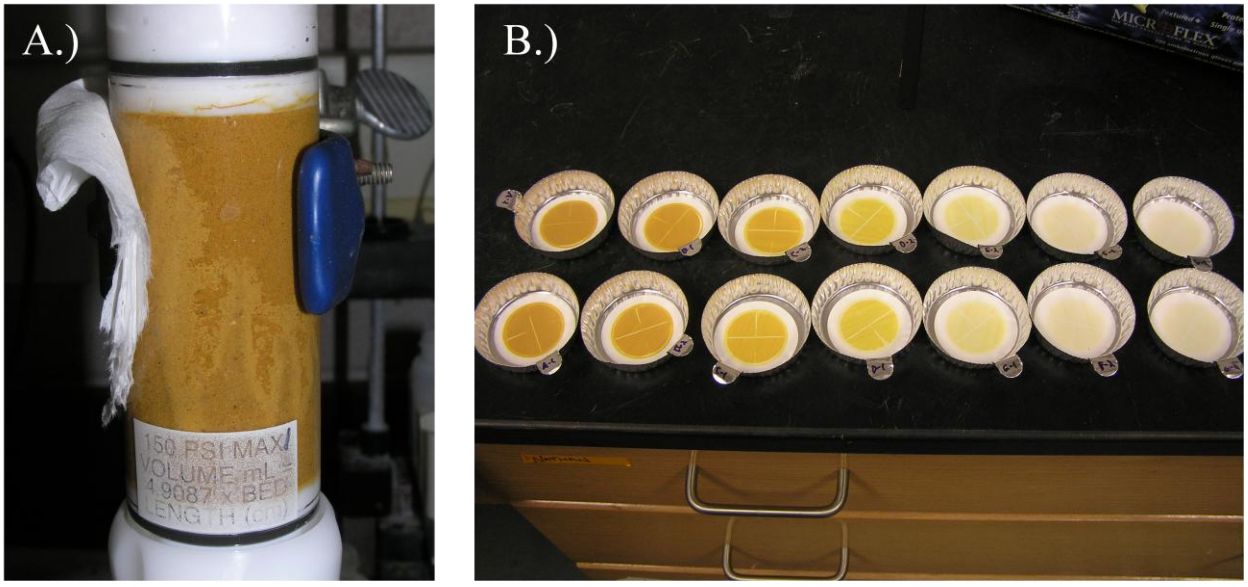

Figure B.4: Colloid mobilization from SRS sediment after increasing influent pH (A) and filtrated effluent colloid samples after gravimetric analysis (B).

Appendix C. Bromide Tracer Tests

The following bromide tracer breakthrough curves (BTCs) were fitted with CXTFIT to determine the hydrodynamic properties of each column.

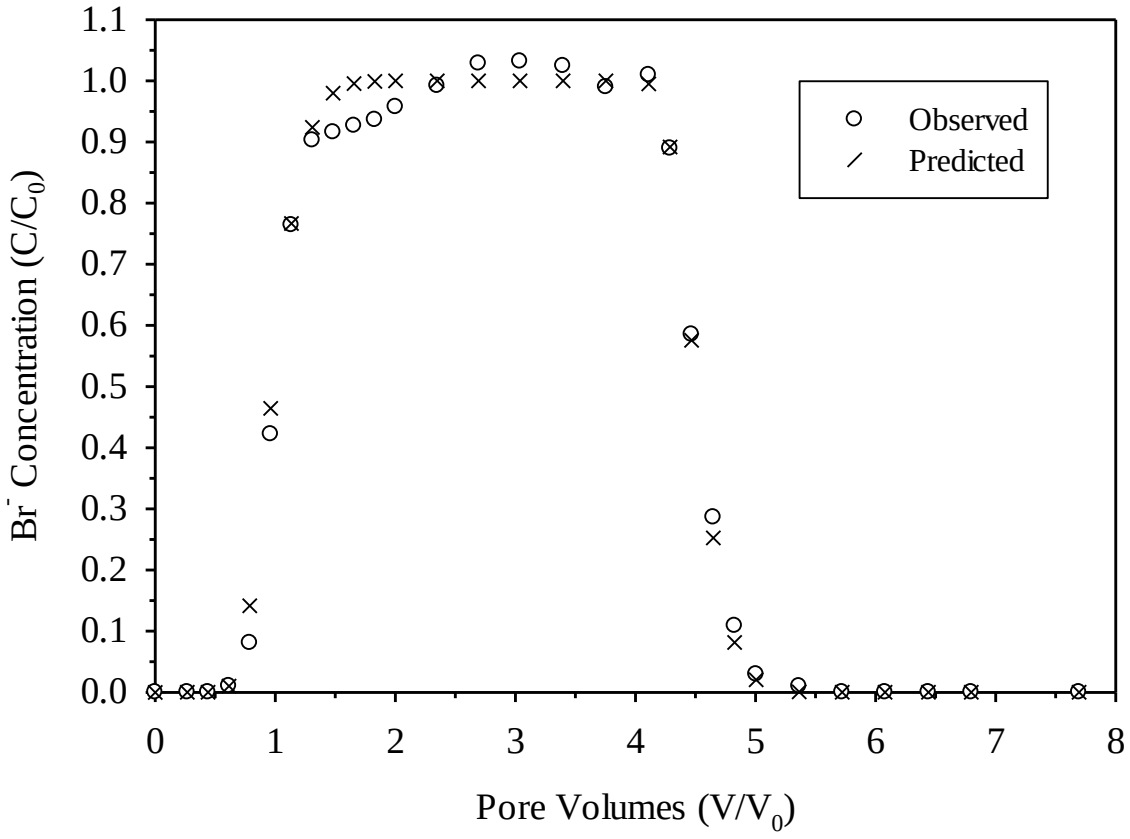

Figure C.1: SRS # 3 Br^- tracer BTC fitted with CXTFIT (C_0=25.7 ppm, Q=6 mL/hr, Temp=26±1°C, λ=0.1443 cm, R^2=0.995, D=2.61 cm^2/hr, N_{pe}=47.82).

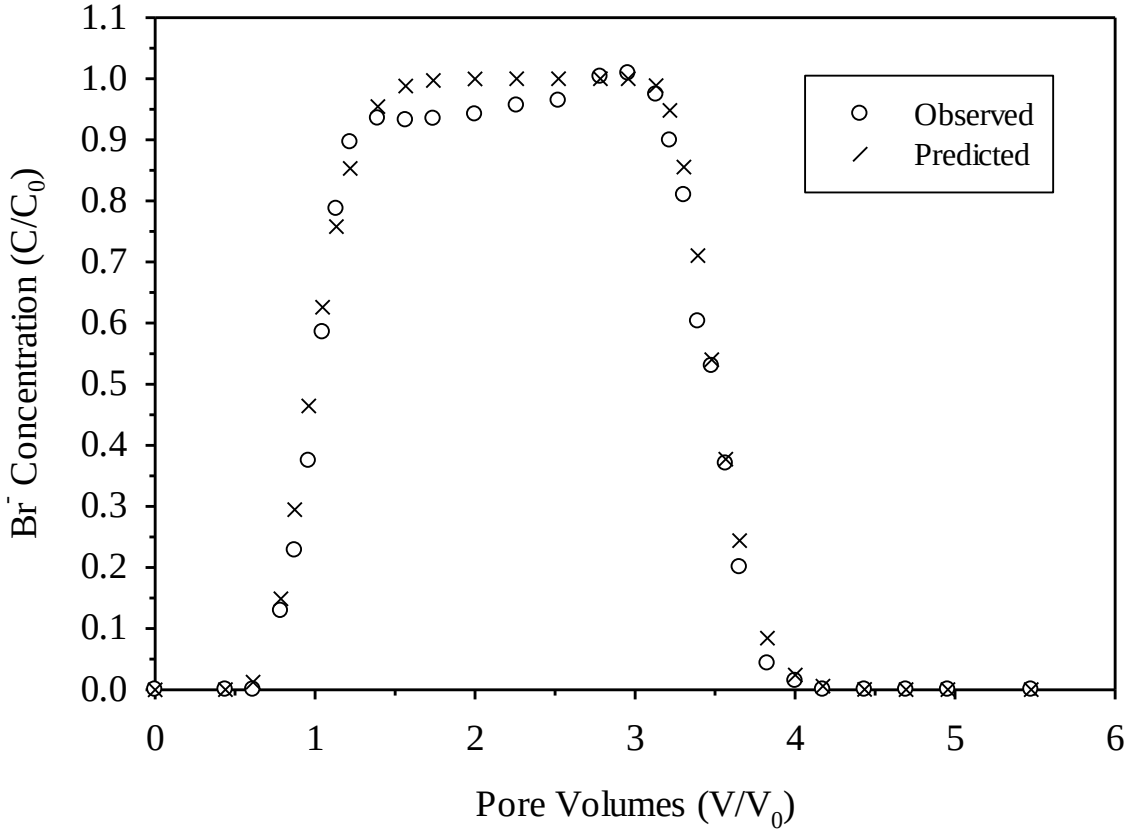

Figure C.2: SRS # 4 Br^- tracer BTC fitted with CXTFIT (C_0=21.8 ppm, Q=36.6 mL/hr, Temp=26±1°C, λ=0.1577 cm, R^2=0.99, D=2.90 cm^2/hr, N_{pe}=44.70).

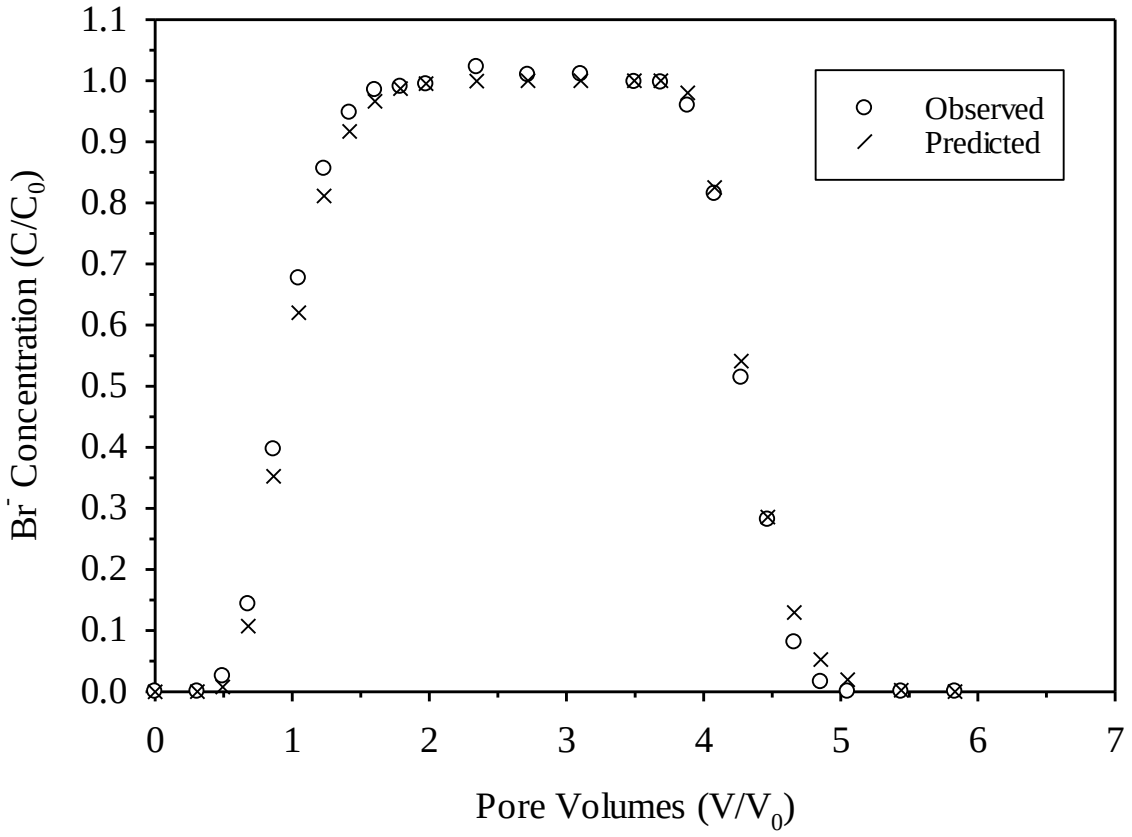

Figure C.3: SRS # 5 Br^- tracer BTC fitted with CXTFIT (C_0=29.76 ppm, Q=6 mL/hr, Temp=26±1°C, λ=0.2778 cm, R^2=0.997, D=5.44 cm^2/hr, N_{pe}=24.66).

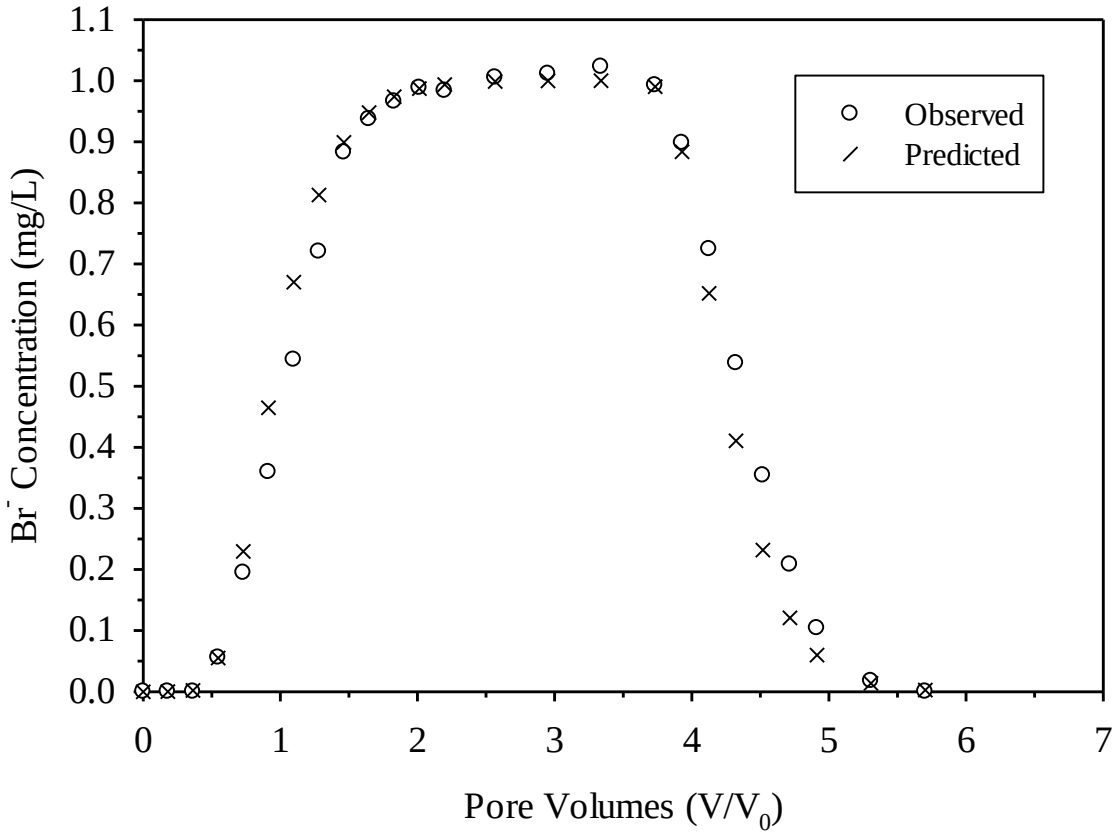

Figure C.4: SRS # 6 Br^- tracer BTC fitted with CXTFIT (C_0=28.40 ppm, Q=6 mL/hr, Temp=26±1°C, λ=0.4245 cm, R^2=0.979, D=8.34 cm^2/hr, N_{pe}=16.14).

Appendix D. Preliminary Column Transport Experiments

D.1 Th(IV) Adsorption to the HPLC Pump System

Preliminary transport experiments examined the adsorption of Th(IV) to the HPLC pump system at a pH of 4 (Figure D.1). Results showed that Th(IV) significantly adsorbed to the pump system. Therefore, before each column transport experiment, Th(IV) influent solution was run through the pump for at least 1 day before entering the packed columns, allowing Th(IV) to be fully adsorbed to the pump system. After one day, the effluent Th(IV) concentration leaving the pump system was analyzed to ensure it was the same as the influent concentration. At this point, Th(IV) influent solutions were allowed to infiltrate the sand-packed columns.

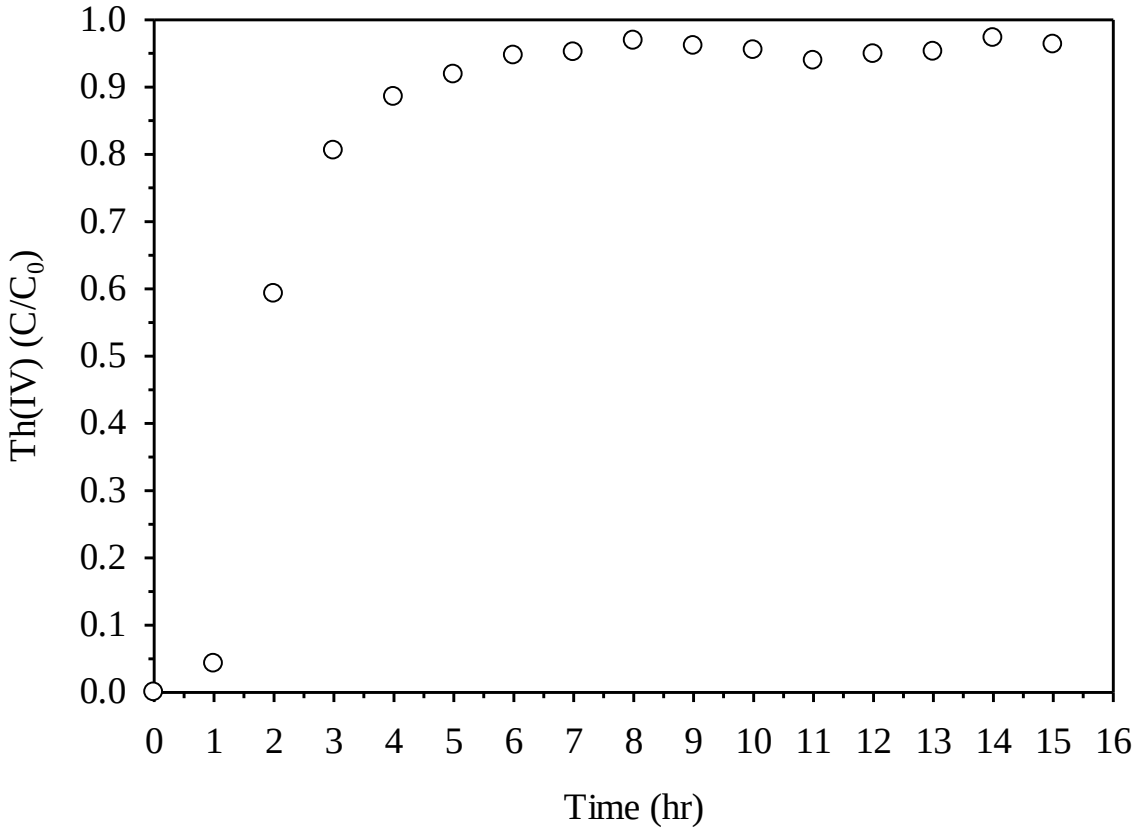

Figure D.1: Effluent Th(IV) concentration BTC through HPLC pump (C_0=2.54 mg/L, I=0.1 M $NaNO_3$, pH=4.02, Temp=26±1˚C, Q=4.2 mL/hr).

D.2 Th(IV) Adsorption to Empty Glass Column

Preliminary transport experiments also examined the adsorption of Th(IV) to empty glass columns at a pH of 4 (Figure D.2). Results showed that Th(IV) adsorption to the walls of the glass column was insignificant in comparison to the adsorption by the SRS sediment.

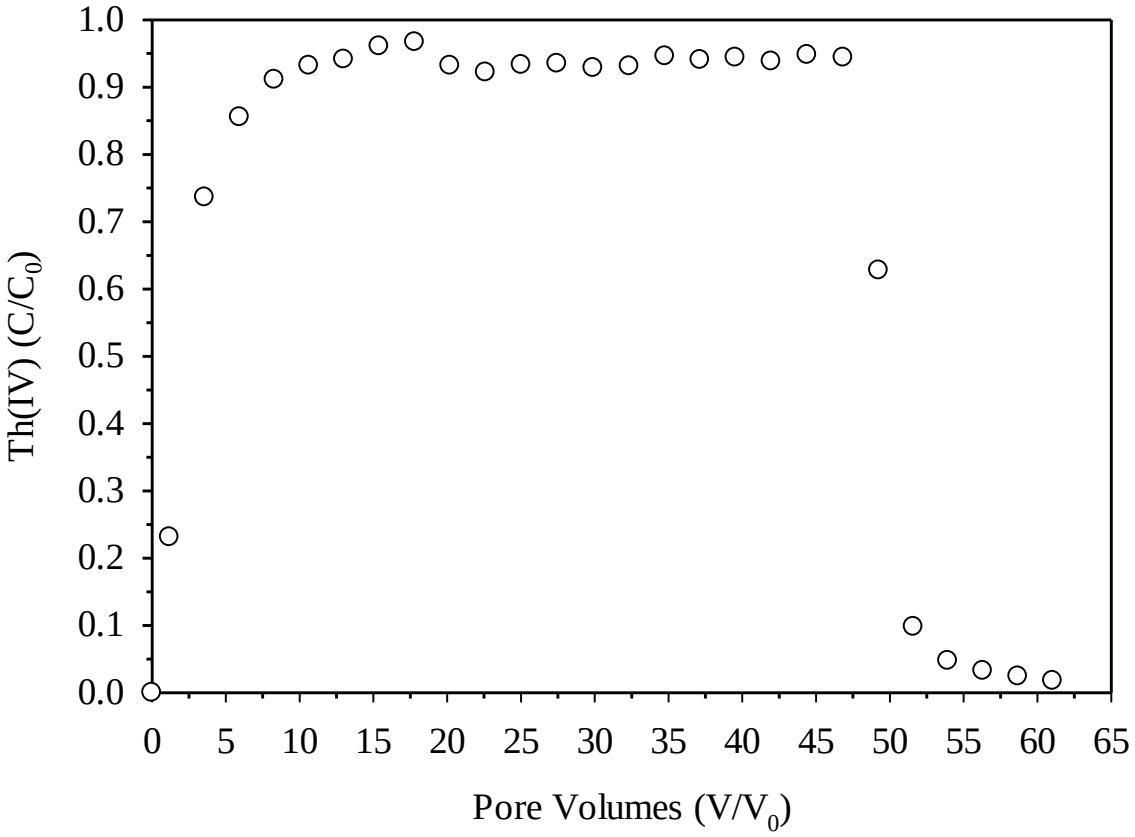

Figure D.2: Effluent Th(IV) concentration BTC through empty glass column (C_0=2.54 mg/L, I=0.1 M $NaNO_3$, pH=4.02, Temp=26±1˚C, Q=4.2 mL/hr).

Appendix E. Sample Calculations

The following calculations were used to determine the results shown in Chapter 3.

1.) <u>Davies Equation – Single ion activity coefficient, γ</u>

$$Equation: \quad \log\gamma = -0.513(Z)^2 \cdot \left[\frac{\sqrt{I}}{1+\sqrt{I}} - 0.2(I)\right]$$

Where:

γ	=	Single ion activity coefficient,
Z	=	Charge of ions, and
I	=	Ionic strength of solution (M)

Example:
Given: Z = 1, I = 0.005 M $NaNO_3$

$$Step\ 1: \quad \log\gamma = -0.513(1)^2 \cdot \left[\frac{\sqrt{0.005\ M}}{1+\sqrt{0.005\ M}} - 0.2(0.005\ M)\right] = -0.0334$$

$$Step\ 2: \quad \gamma = 10^{-0.0334} = 0.926$$

2.) <u>Surface charge density modified from Zelazny *et al.* (1996)</u>

$$Equation: \quad \Delta H - \Delta OH = \frac{\left[10^{-pH(B)} - 10^{-pH(S)}\right] - \left[10^{-[14-pH(B)]} - 10^{-[14-pH(S)]}\right]}{\gamma} \cdot \left(\frac{V}{W}\right) \cdot (100)$$

Where:

ΔH-ΔOH	=	Apparent proton surface charge density calculated by titration at a given ionic strength and pH ($cmol_c/kg$),
pH(B)	=	pH of the blank solution,
pH(S)	=	pH of the sediment suspension,
14	=	Conditional dissociation product of water,
γ	=	Single ion activity coefficient calculated with the Davies equation,
V	=	Total solution volume in each sample (L),
W	=	Oven-dried sediment sample weight (kg), and
100	=	Conversion factor for moles to centimoles.

Example:
Given: pH(B) = 2.62, pH(S) = 2.68, γ = 0.926, V = 0.03 L, and W = 0.005 kg

$$\Delta H - \Delta OH = \frac{[10^{-2.62} - 10^{-2.68}] - \left[10^{-[14-2.62]} - 10^{-[14-2.68]}\right]}{0.926} \cdot \left(\frac{0.03\ L}{0.003\ kg}\right) \cdot (100) = 0.334\ \frac{cmol}{kg}$$

3.) <u>Total empty column volume, V_t</u>

$$Equation: \qquad V_t = \pi \cdot \left(\frac{d}{2}\right)^2 \cdot H$$

Where:

V_t	=	Total empty column volume (cm^3),
d	=	Inside diameter of column (cm), and
H	=	Height of soil inside column (cm)

Example: Column SRS # 3
Given: d = 1 cm, H = 6.90 cm

$$V_t = \pi \cdot \left(\frac{1\ cm}{2}\right)^2 \cdot 6.90\ cm = 5.42\ cm^3$$

4.) <u>Specific discharge, q</u>

$$Equation: \quad q = \frac{Q}{A} = \frac{Q}{\pi\left(\frac{d}{2}\right)^2}$$

Where:

q	=	Specific discharge (cm/hr),
Q	=	Pump flow rate (cm^3/hr),
A	=	Cross sectional area of column (cm^2), and
d	=	Inside diameter of column (cm)

Example: Column SRS # 3
Given: Q = 6 mL/hr, d = 1 cm

$$q = \frac{Q}{A} = \frac{6\ \frac{cm^3}{hr}}{\pi\left(\frac{1\ cm}{2}\right)^2} = 7.64\ \frac{cm}{hr}$$

5.) <u>Bulk density, ρ_b</u>

$$Equation: \quad \rho_b = \frac{m}{V_t}$$

Where:

ρ_b	=	Bulk density (g/cm^3),
m	=	Dry packed soil mass (g), and
Vt	=	Total empty column volume (cm^3)

Example: Column SRS # 3
Given: m = 8.3059 g, V_t = 5.42 cm^3

$$\rho_b = \frac{8.3059\ g}{5.42\ cm^3} = 1.53\ \frac{g}{cm^3}$$

6.) <u>Porosity, φ</u>

$$Equation: \quad \varphi = 1 - \frac{\rho_b}{\rho_p}$$

Where:

φ	=	Porosity,
ρ_b	=	Bulk density (g/cm^3), and
ρ_p	=	Particle density (assume quartz = 2.65 g/cm^3)

Example: Column SRS # 3
Given: ρ_b = 1.53 g/cm^3, ρ_p = 2.65 g/cm^3

$$\varphi = 1 - \frac{1.53\ \frac{g}{cm^3}}{2.65\ \frac{g}{cm^3}} = 0.422$$

7.) <u>Column pore volume, V_0</u>

$$Equation: \quad V_0 = V_t \varphi$$

Where:

V_0	=	Column pore volume (mL)
V_t	=	Total empty column volume (mL), and
φ	=	Porosity

Example: Column SRS # 3
Given: V_t = 5.42 cm^3, φ = 0.42

$$V_0 = 5.42\ cm^3(0.42) = 2.28\ cm^3$$

8.) Average flow velocity, *v*

$$Equation: \quad v = \frac{Q}{A \cdot \varphi} = \frac{Q}{\pi \cdot \left(\frac{d}{2}\right)^2 \cdot \varphi}$$

Where:

v	=	Average flow velocity (cm/hr),
Q	=	Pump flow rate (cm^3/hr),
A	=	Cross sectional area of column (cm^2),
d	=	Inside diameter of column (cm), and
φ	=	Porosity

Example: Column SRS # 3
Given: Q = 6 cm^3/hr, d = 1 cm, φ = 0.42

$$v = \frac{Q}{A \cdot \varphi} = \frac{6\ \frac{cm^3}{hr}}{\pi \cdot \left(\frac{1\ cm}{2}\right)^2 \cdot (0.42)} = 18.12\ \frac{cm}{hr}$$

9.) Retention time, θ

$$Equation: \quad \theta = \frac{H}{v} = \frac{V_0}{Q}$$

Where:

H	=	Height of soil inside column (cm),
v	=	Average flow velocity (cm/hr),
V_0	=	Column pore volume (cm^3), and
Q	=	Pump flow rate (cm^3/hr)

Example: Column SRS # 3
Given: H = 6.90 cm, v = 18.12 cm/hr, V_0 = 2.28 mL, Q = 6 cm^3/hr

$$\theta = \frac{H}{v} = \frac{6.90\ cm}{18.12\ \frac{cm}{hr}} = 0.38\ hr = \frac{V_0}{Q} = \frac{2.28\ cm^3}{6\ \frac{cm^3}{hr}} = 0.38\ hr$$

10.) <u>Dispersion coefficient, D</u>

$Equation$: $D = \lambda \cdot v$

Where:

D	=	Dispersion coefficient (cm^2/hr),
λ	=	Dispersivity coefficient from Br^- tracer test (cm), and
v	=	Average flow velocity (cm/hr)

Example: Column SRS # 4
Given: λ = 0.1443 cm, 18.12 cm/hr

$$D = (0.1443\ cm) \cdot \left(18.12\ \frac{cm}{hr}\right) = 2.61\ \frac{cm^2}{hr}$$

11.) <u>Peclet Number, N_{pe}</u>

$Equation$: $N_{pe} = \frac{H \cdot v}{D}$

Where:

H	=	Height of soil inside column (cm)
v	=	Average flow velocity (cm/hr)
D	=	Dispersion coefficient (cm^2/hr), and

Example: Column SRS # 3
Given: H = 6.90 cm, v = 18.12 cm/hr, D = 2.61cm^2/hr

$$\frac{(6.90\ cm)(18.12\ \frac{cm}{hr})}{2.61\ \frac{cm^2}{hr}} = 47.82$$

12.) Percent recovery

$$Equation: \quad \% \, Recovery = \frac{Mass_{out} + Mass_{desorbed}}{Mass_{in}} \cdot 100$$

Where:

$Mass_{out}$	=	Cumulative mass of Th(IV) in the effluent solutions during the sorption phase calculated by trapezoidal rule,
$Mass_{desorbed}$	=	Cumulative mass of Th(IV) in the effluent solutions during the desorption phase calculated by trapezoidal rule, and
$Mass_{in}$	=	Cumulative mass of Th(IV) introduced to the column in the influent solution during the sorption phase

Example: Column SRS # 3

Given: Average Th(IV) influent concentration, C_0 = 2.64 mg/L; cumulative volume of the influent Th(IV) solution introduced to the column, V = 1907.46 mL; Th(IV) concentrations measured in effluent samples, C_i (mg/L); cumulative volume of effluent samples, V_i (mL)

$$Step\ 1: \quad Mass_{out} = \sum_{i=1}^{n} \left(\frac{C_i + C_{i+1}}{2} \right) \cdot \frac{(V_{i+1} - V_i)}{1000 \ \frac{mL}{L}} = 2.9309 \ mg \ Th(IV)$$

$$Step\ 2: \quad Mass_{desorbed} = \sum_{i=D1}^{n} \left(\frac{C_i + C_{i+1}}{2} \right) \cdot \frac{(V_{i+1} - V_i)}{1000 \ \frac{mL}{L}} = 1.0585 \ mg \ Th(IV)$$

$$Step\ 3: \quad Mass_{in} = C_0 \cdot \left(\frac{V}{1000 \ \frac{mL}{L}} \right) = \left(2.64 \ \frac{mg}{L} \right) \cdot \left(\frac{1907.46 \ mL}{1000 \ \frac{mL}{L}} \right) = 4.978 \ mg \ Th(IV)$$

$$Step\ 4: \quad \% \, Recovery = \frac{2.9309 \ mg + 1.0585 \ mg}{4.978 \ mg} \cdot 100 = 80.14 \ \%$$

13.) <u>Colloid concentration from turbidity calibration curve equations</u>

a.) From large vial turbidity cells

$Equation$: $C = -0.00005(T_L)^2 + 0.331(T_L)$

Where:
C = Colloid concentration (mg/L), and
T_L = Measured turbidity in effluent samples using large vial cells (NTU)

Example: Column SRS # 4 effluent sample D-21
Given: Measured large vial turbidity, T = 25.2 NTU

$$C = -0.00005(25.2\ NTU)^2 + 0.331(25.2\ NTU) = 8.31\ \frac{mg}{L}$$

b.) From small vial turbidity cells

$Equation$: $C = -0.0004(T_S)^2 + 0.7469(T_S)$

Where:
C = Colloid concentration (mg/L), and
T_S = Measured turbidity in effluent samples using small vial cells (NTU)

Example: Column SRS # 4 effluent sample D-3
Given: Measured small vial turbidity, T_s = 421 NTU

$$C = -0.0004(421\ NTU)^2 + 0.7469(421\ NTU) = 243.55\ \frac{mg}{L}$$

14.) <u>Actual turbidity from small vial turbidity measurement</u>

$Equation$: $T = -0.0011(T_S)^2 + 2.3939(T_S)$

Where:
T = Actual turbidity (NTU), and
T_S = Measured turbidity in effluent samples using small vial cells (NTU)

Example: Column SRS # 4 effluent sample D-3
Given: Measured small vial turbidity, T_s = 421 NTU

$$T = -0.0011(421\ NTU)^2 + 2.3939(421\ NTU) = 813\ NTU$$

15. Th(IV) uptake, q, by mobilized SRS colloids

$$Equation: \quad q = \frac{C_{Th(IV)}}{C_{Colloids}}$$

Where:

q	=	Concentration of Th(IV) sorbed by SRS colloids (mg/mg),
$C_{Th(IV)}$	=	Concentration of Th(IV) in effluent sample (mg/L), and
$C_{Colloids}$	=	Concentration of SRS colloids in effluent sample (mg/L)

Example: Column SRS # 5 Sample D-2 Mobilization Phase 2

Given: Concentration of Th(IV) in effluent sample, $C_{Th(IV)}$ = 2.72 mg/L, Concentration of SRS colloids in effluent sample = 307 mg/L

$$Step\ 1: \quad q = \frac{2.72\frac{mg}{L}}{307\frac{mg}{L}} = 0.00886\ \frac{mg\ Th(IV)}{mg\ Colloids}$$

$$Step\ 2: \quad q = \left(0.00886\frac{mg\ Th(IV)}{mg\ Colloids}\right)\cdot\left(\frac{1000\ mg\ Colloids}{1g\ Colloids}\right) = 8.86\ \frac{mg\ Th(IV)}{g\ Colloids}$$

$$Step\ 3: \quad q = \left(8.86\frac{mg\ Th(IV)}{g\ Colloids}\right)\cdot\left(\frac{1\ g\ Th(IV)}{1000\ mg\ Th(IV)}\right)\cdot\left(\frac{1\ mol\ Th(IV)}{232\ g\ Th(IV)}\right)$$

$$\cdot\left(\frac{10^6 \mu mol\ Th(IV)}{1\ mol\ Th(IV)}\right) = 38.2\frac{\mu mol\ Th(IV)}{g\ Colloids}$$